Conceptual Design Report for the PHENIX Nosecone Calorimeter

December, 2005

December 4, 2005

Conceptual Design Report for the PHENIX Nosecone Calorimeter: Nov 2005

S. Boose, J.S. Haggerty, E.P.Kistenev, D. Lynch, S.P. Stoll, C.L. Woody
Brookhaven National Laboratory, Physics Department, Upton, NY 11973-5000, USA

K. Barish, S. Bathe, V. Dzordzhadze, O. Eyser, T. Hester, A. Moreale, Ken Sedgewick,
R. Seto, Z. Yasin
University of California, Riverside, CA 92521, USA

Z. Li, V. Radeka, S. Rescia
Brookhaven National Laboratory, Instrumentation Department, Upton, NY 11973-5000, USA

R. Pak, A. Sukhanov
Brookhaven National Laboratory, Chemistry Department, Upton, NY 11973-5000, USA

J.C. Hill, J.L. Lajoie, F. Wei
Iowa State University, Iowa, USA

A. Deshpande
State University of New York, Stony Brook, USA

M. Chiu, M. Grosse-Perdekamp, J. Koster, J.C. Peng
University of Illinois Urbana-Champaign, Illinois, USA

C.Y. Chi
Nevis Laboratories, Columbia University, USA

J.H. Kang, D.J. Kim, S. Kim
Yonsei University, Seoul, Korea

J. Nagle, E. Kinney
University of Colorado, Boulder, USA

I. Park, S.Nam
Ewha Women's University, Seoul, Korea

B. Hong, K.S. Sim, B.I. Kim
Korea University, Seoul, Korea

I. Nakagawa, A. Taketani
Riken, Japan

S. Esumi
Tsukuba University, Japan

Michael Finger, Miroslav Finger, P, Mikes
Charles University, Faculty of Mathematics and Physics, Prague, Czech Republic

J. Popule, L. Tomasek, M. Tomasek, V. Vrba
Institute of Physics, Academy of Sciences of Czech Republic, Prague, Czech Republic

M. Virius, J. Klaus, T. Liska
Czech Technical University, Faculty of Nuclear Sciences and Physical Engineering, Prague, Czech Republic

D.Karmanov, M.Merkin, A.Voronin
Moscow State University, Moscow, Russia

S. Afanasiev, S. Basilev, A. Baskakov, A. Bychkov, A. Isupov, N. Kotsev, A. Litvinenko,
A. Malakhov, V. Peresedov, P. Rukoyatkin, V. Slepnev, I. Slepnev, L. Zolin
Joint Institute for Nuclear Research - Dubna, Moscow Region

E. Atkin
MEPHI (front end electronics) , Russia

???????
SENS: company, Korea

??????
ERTI:company, Korea

???????
ON semiconductor:company, Czech Republic

A. Vlasov
Ekaterinbourg (company- board assembly), Russia

Igor Ilyushchenko
RIMST-ELMA (company-Si construction), Russia

Abstract

Contents

I. INTRODUCTION AND EXECUTIVE SUMMARY

The RHIC program is progressing beyond the discovery phase to the precision measurement phase. This is being made possible by the upgrade of the machine luminosity (RHIC II). The demands of the program require that the unique capabilities of PHENIX - that is the ability to make precision measurements of leptons and photons - be extended to a large coverage. We propose the construction of a pair of Nosecone Calorimeters (NCC) the the PHENIX experiment at RHIC. The NCC will significantly enhance the physics capabilities of the PHENIX detector by extending calorimetric coverage to forward rapidities expanding the calorimetric coverage of the detector by more than a factor of 10. One of its key advantages is the presence of the muon spectrometer in the forward (and backward) regions. Together with the Forward Silicon vertex Detector - the NCC will make PHENIX a nearly 4π spectrometer, capable of detecting photons, electrons, muons, and hadrons. Our prime motivation is to provide precision measurements of direct photons, π^0's and dielectrons in A+A, p(d)+A, and polarized pp collisions. The upgrade will provide us the access to the physics observables that are to date not accessible to PHENIX or available only indirectly with very limited accuracy. The primary measurements addressed by the NCC are

1. The Strongly Interacting Quark Gluon Plasma - Heavy Ion Collisions
   (a) The opacity of the sQGP via studies of γ-jet events
   (b) The suppression of the charmonium and botomoiun states due to screening via measurements of the χ_c and χ_b states
2. The structure of very high energy density cold nuclear matter - p(d)+A Collisions and the fate of the gluon structure function over a large x-range via
   (a) direct photons and jets
   (b) hadrons (particularly pi^0's and eta's)
   (c) dielectrons
3. The spin structure of the nucleon - polarized pp collisions via
   (a) Direct photons and jets
   (b) hadrons (particularly pi^0's and eta's)

(c) W isolation

The main benefits are in the following areas. Firstly, by correctly identifying multiphoton showers in the high position resolution layers built into the calorimeters we will measure π^0 yields at large rapidities thus extending the PHENIX sensitivity to jet quenching studies. Secondly by increasing acceptance for the direct photons and introducing the capability to recognize and measure jets in the forward direction we will make possible the section of correlated photon-jet production – critical process for understanding Color Glass Condensate and its relevance to initial state modifications in heavy ion collisions. Finally by providing the energy measurements withing the cone around lepton candidate NCC will dramatically improve background conditions for identification of muons from decays of W bosons which are supposed to carry basic information on the spin dependent quark structure functions in protons.

The NCC is to be installed on both the North and South sides and replaces the present Copper Nosecones in front of the muon spectrometer. The structure is a silicon-tungsten sandwich sampling calorimeter. Each side is longitudinally composed of 3 calorimeter sections read out by Si pads $2.22^2 cm^2$ In addition there are two precision readout sections readout by strip-pixels at pitch. These are located at a depth of 2 and 7 radiation lengths and enable us to identify, and measure π^0's to high energy even when there is an overlap of showers in the main calorimeter. This also allows the separation of direct photons and high energy π^0's.

The proposed calorimeters are both energy measuring and tracking devices. Energy is measured in three calorimeter segments (two fine or electromagnetic and one leakage or hadronic), coordinates are measured in calorimeter segments and two high resolution layers of pixilated strips with 2-D sensitivity. To avoid cost intensive and time consuming R&D, we relied heavily on established technologies and expertise already available in collaborating laboratories. For the calorimeter we propose to use silicon sensors closely resembling those currently in use for prototyping future calorimeter for ILC and b the number of cosmic ray experiments, for coordinate detectors we follow the lead of the PHENIX Silicon Vertex Tracker and use pixilated strips with 2-D sensitivity. As a backup to this latter solution we work in collaboration with NUCLON experiment in Russia on implementing standard one-coordinate strip detectors with identical strip width of 0.5 mm.

We plan to use hybrid preamplifier chips developed at BNL for ATLAS experiment at CERN as a base solution for signal conditioning in calorimeter and the SVX4 readout chip developed at FNAL to readout the strip detectors.

With the help of institutional contributions, PHENIX was able to maintain a small but well focused effort over the past two years to aid in the design of the detector, and to establish expertise in the relevant technologies.

A collaboration of about 60 members and 20 institutions has formed to construct, install and operate the Nosecone Calorimeter. Among the members are experts with deep experience in calorimetry, in silicon detector technology, the design, fabrication and operations of modern readout electronics, mechanical and integration issues, software experts as well as physicists who are well versed in the different aspects of analysis necessary to extract physics from this detector.

We anticipate that the bulk of the project will be funded by two agencies, the DOE Office of Nuclear Physics and the RIKEN Institute of Japan. There demarcated clearly the scope of deliverables for both agencies. In addition we expect smaller contributions from the Czech Republic and Russia. A preliminary management plan of the project, which discusses the roles and responsibilities of the participating institutions is included in this document.

We propose to construct the NCC detector over a period of three years, US FY07, FY08 and FY09. To carry out this project we seek funding of a total of $3M through DOE. These funds would be supplemented with deliverables equivalent to about $3M US dollar provided by the RIKEN Institute during calendar years 2007 to 2009.

This document has the following structure. The physics motivation for the upgrade is given in section 2. The capabilities of the proposed detector and its impact on the aforementioned physics goals is discussed in section 3. Section 4 gives a detailed description of the NCC and the technical aspects of the project. The management plan is given and section 6, which specify the deliverables and institutional responsibilities. Section 7 lays out the budget request and the proposed schedule. Appendices cover addition technical details of the proposal, not covered in the main document.

II. PHYSICS OVERVIEW

The Nosecone calorimeter increases the calorimetric coverage of the PHENIX detector to forward and backward rapidities so that the the total coverage is increased by more than an order of magnitude. This impacts the entire PHENIX physics program - AA collisions, pA collisions, and polarized p-p collisions. This section gives an overview of the physics program relevant to the NCC in each of these three areas. For the study of heavy-ion collisions - the essential questions revolve around our understanding of the state of matter which has been created - called the sQGP - or strongly interacting Quark Gluon Plasma. High $p_\perp$ photons opposite a jet can be used as a calibrated probe to measure the energy loss of quarks or gluons in the plasma. The yield of charmonium and bottomoniunm states - particularly the χ_c measured in conjunction with the muon spectrometer, will give information on the deconfinement temperatures. The NCC can be used to find the reaction plane with great accuracy, all such signatures can be studied as a function of the geometry of the colliding system. This should lead to very accurate measurements of the energy loss of high momentum partons in the plasma. In pA collisions, direct photons, di-electrons, and one or more high $p_\perp$ π^0's can be used to study what has traditionally been called shadowing in nuclei. Recently new interpretations of shadowing has emerged - the Colored Glass Condensate, which in itself is an exciting field of study. Finally, direct photons, jets, and high momentum particles in polarized pp collisions are an effective way to make measurements of the gluon spin contribution. Transversely polarized protons will give access to the transverse structure functions in of the nucleon. In conjunction with the muon spectrometer the NCC will allow us to make isolation cuts for the study of W's to measure anti-quark spin structure functions.

A. HEAVY ION PHYSICS

1. Hard Scattering

Hard scattered partons are an important probe of the matter created in heavy-ion collisions. Because the hard scattering event occurs early in the evolution of the collisions ($\tau < 1$ fm/c), the scattered partons can be affected by the evolution of the surrounding QCD matter, particularly if this matter passes through a deconfined phase. The scattered partons

will be sensitive to the medium primarily through the mechanism of energy loss through medium-induced gluon radiation (Bjorken, 1982)(Gyulassy and Plumer, 1990) (Wang *et al.*, 1995)(Wang and Gyulassy, 1992)(Baier *et al.*, 1995) (Baier *et al.*, 1998)(Gyulassy *et al.*, 2000)(Gyulassy *et al.*, 2001), resulting in a reduction of the energy available to the parton when it fragments into hadrons. This phenomenon was predicted to lead to a suppression of particles with large transverse momentum in heavy-ion collisions at RHIC and this suppression has been quantified by excellent measurements from the first RHIC runs (Adcox *et al.*, 2002)(Adcox *et al.*, 2003)(Adler *et al.*, 2003c)(Adler, 2003). Measurements in d+Au collisions have demonstrated that the suppression is not due to initial state effects (Adler *et al.*, 2003a).

The four RHIC experiments have measured charged particle spectra from Au+Au collisions at $\sqrt{s_{NN}} = 130$ and 200 GeV, with measurements for unidentified hadrons extending out to $p_T \sim 12$ GeV/c. All of these measurements show a suppression of high transverse momentum hadrons in central collisions when compared to data from p+p collisions (suitably scaled by the number of binary collisions and the energy difference). The PHENIX detector is also capable of reconstructing the decay of the π^0 meson to two photons using the electromagnetic calorimeter in both central arms. Using the measured production of π^0 mesons in both p+p and Au+Au collisions, we can construct a ratio known as the nuclear modification factor R_{AA}:

$$R_{AA} = \frac{dN_{AA}}{< N_{coll} > \times dN_{pp}} \tag{1}$$

where dN_{AA} is the differential yield for a point-like process in an AA collision, and dN_{pp} is the differential yield for the same process in nucleon-nucleon collisions. The number of binary collisions for a given centrality class N_{coll} is estimated using a Glauber model of the nuclear overlap. In the naive limit that a nucleus-nucleus collision can be though of as a superposition of independent nucleon-nucleon collisions, the nuclear modification faction at high p_T should be unity. The measured nuclear modification factor for charged hadrons and neutral pions as measured by the PHENIX collaboration is shown in Figure 1. There is a significant suppression of high transverse momentum hadrons observed in Au+Au collisions, consistent with substantial energy loss of the scattered partons. A similar suppression was observed in data taken at $\sqrt{s_{NN}} = 130$ GeV (Adcox *et al.*, 2002). Models of energy loss that incorporate the expansion of the system indicate the energy loss in the matter created in heavy-ion collisions at RHIC may be as much as fifteen times larger than the energy loss of

a comparable parton in ordinary nuclear matter (Wang and Wang, 2002). Since the energy loss is proportional to the gluon density, this implies the gluon density created in a heavy ion collision is more than an order of magnitude larger than in cold nuclei.

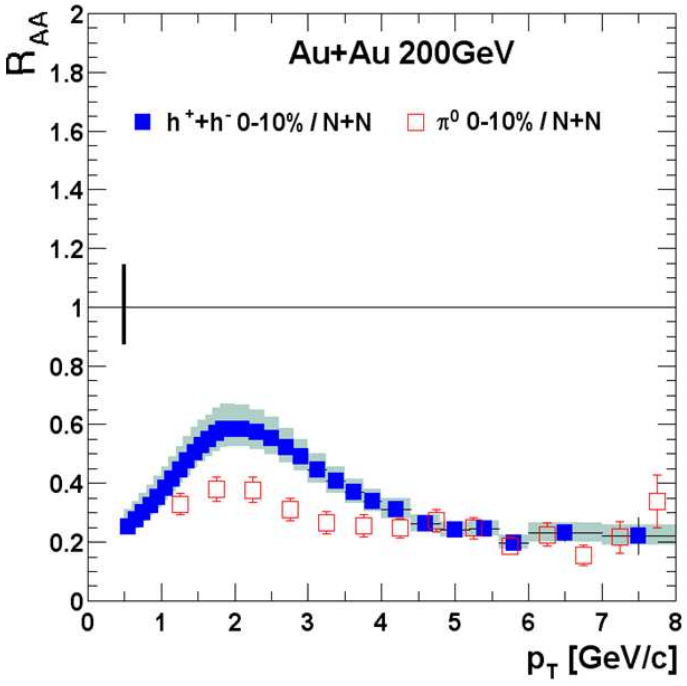

FIG. 1 (left) $R_A A$ for π_0 mesons and inclusive charged particles from as measured by PHENIX. The difference in the observed suppression for charged hadrons and neutral pions between 1-4 GeV/c is due to the changing particle composition of the charged hadrons, highlighting the importance of pi^0 measurement.

It is important to remember that direct detection of jets is not possible in heavy-ion collisions due to the large combinatoric background from particles in the underlying event. Jets of hadrons can still be identified, however, using two-particle correlation techniques that take advantage of the fact that hadrons resulting from a parton cascade will be correlated in azimuthal angle and pseudorapidity. Such techniques make use of the "leading hadron" effect in jet fragmentation, where a single hadron often ends up with a large fraction of the parton momentum. By selecting high transverse momentum hadrons one has a good proxy for the jet direction and momentum. At high-p_T inclusive charged particles can often be subject to background processes that result in a low-p_T particle being reconstructed at high momentum. In contrast, the measurement of π^0 mesons becomes essentially background-free at high-p_T. In addition, at RHIC the particle composition of the inclusive charged

measurements change dramatically for transverse momenta between 2 and 5 GeV/c (Adler *et al.*, 2003b), further complicating the physics interpretation.

The PHENIX experiment has made use of the central arm electromagnetic calorimeters (EMCal) to measure π^0 production to very high transverse momentum in a variety of colliding systems. These measurements demonstrate the power of exploiting the measurement of π^0 mesons with an electromagnetic calorimeter in relativistic heavy-ion collisions.

a. Photon-Tagged Jets The suppression of high-p_T hadrons seen at RHIC is a complicated interplay between the density and time evolution of the created matter, the collision geometry, and the transverse momentum of the probe. Disentangling these effects in such a way as to allow detailed comparisons between theoretical models of energy loss is complicated by the number of factors that affect the suppression observed in the final state. One way to simply the observables is to use jets that are produced in coincidence with photons via a QCD-Compton process (see Figure 2). The photon escapes the colored medium essentially unmodified and without undergoing energy loss, and therefore provides a measure of the total energy of its partner jet. The cross-section for such a process is substantially smaller than the full dijet cross section, however, and the detection of direct photons in such an environment is difficult.

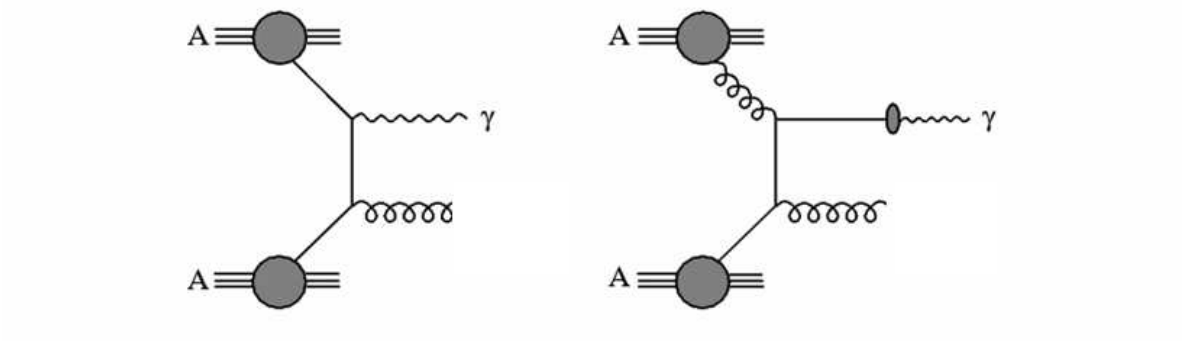

FIG. 2 Tree level diagrams for the production of direct photons by QCD-Compton processes. The photon produced in the hard scattering only interacts electromagnetically and will escape the surrounding medium produced in nucleus-nucleus collisions without interacting. The jet produced by the partner parton in the interaction will, however, interact and suffer energy loss. Measuring both the photon and jet in the final state allows for a calibration of the energy loss.

Direct photons at mid-rapidity in AuAu collisions at $\sqrt{s_{NN}} = 200$ GeV have already been

measured by the PHENIX collaboration, as shown in Figure 3. These initial measurements demonstrate not only the feasibility of measuring direct photons in a heavy-ion environment but the observed scaling with the number of binary collisions indicates that the photons do indeed survive unmodified to the final state. Future studies with photon-tagged jets will allow a detailed, quantitative study of the energy loss suffered by the partner jet, further elucidating the nature of the matter created at RHIC.

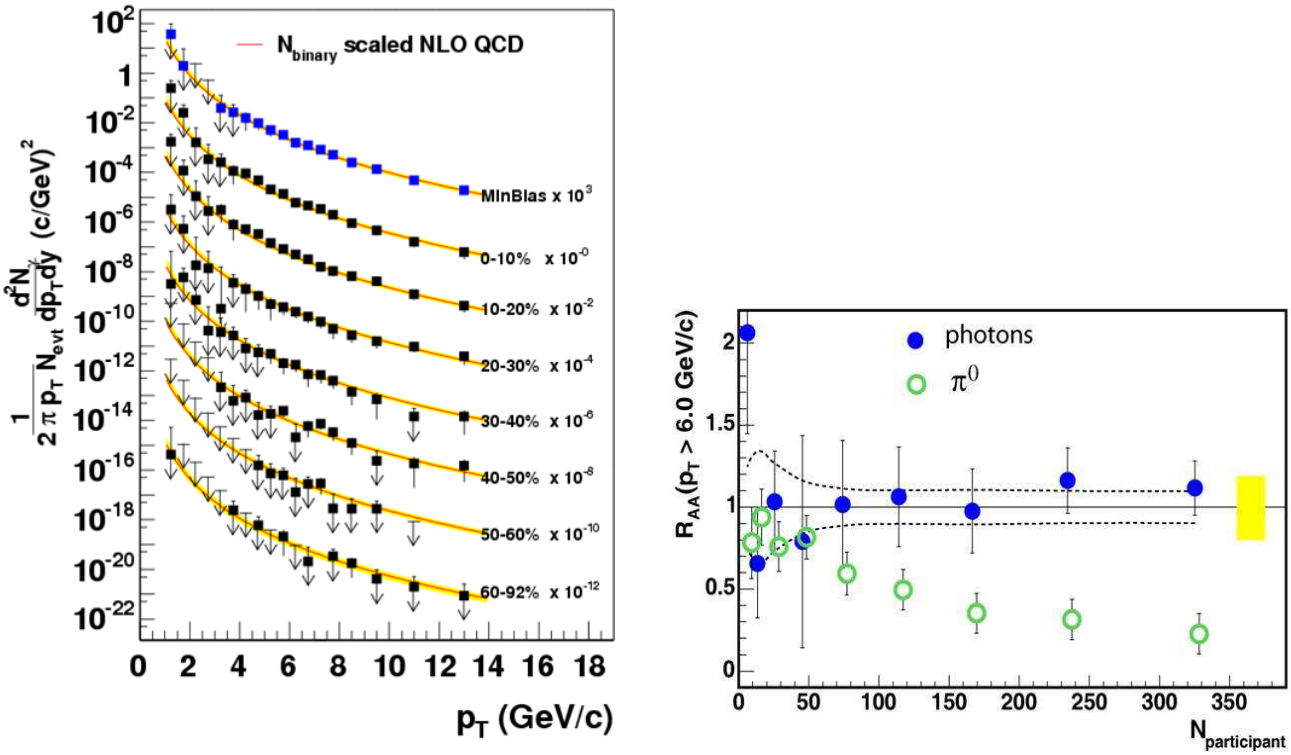

FIG. 3 Measured direct photon invariant multiplicity at mid-rapidity as a function of centrality in AuAu collisions (left) and the R_{AA} for direct photons as a function of transverse momentum (right). The agreement of the data with the scaled NLO calculation as well as the agreement of R_{AA} with unity for direct photons is an indication of the fact the photons escape the medium without interacting.

b. Contribution of the NCC The NCC would add substantial rapidity coverage to the PHENIX detector for the detection of photons and π_0 mesons, covering $1 < |\eta| < 3$, and increasing the overall coverage PHENIX acceptance about a factor of 10. Jet physics and energy loss studies using both photon-tagged jets as well as leading π_0 mesons will be possible

with the NCC. This additional pseudorapidity coverage will allow for the study of physics observables away from central rapidity. Because the effective energy density of the created matter decreases as a function of pseudorapidity, when combined with measurements in the central arms, the NCC observables will provide a robust picture of the created matter for a variety of energy densities within a single colliding system.

2. Importance of Measuring χ_c

Heavy quarkonia states are amongst the best probes of the medium created in heavy ion collisions for understanding modifications in the strong interactions in the quark gluon plasma. The formation of charm-anticharm and beauty-antibeauty quark pairs occurs on very short time scales given the inverse mass or of order 0.1 fm/c. A small fraction of the time the pair evolves into a physical quarkonia state with a time scale given by the relative momentum of the heavy quarks in the bound state or of order 1 fm/c. Since charm and beauty quarks have a mass much larger than the expected temperature of the medium, they are only abundantly created in the earliest stage of the nuclear collision. Thus, we can unambiguously ascribe the final yield of heavy quarkonia to how the quarks and antiquarks interact with the surrounding cold and hot nuclear medium between their creation time 0.1 fm/c and the final freeze-out of the system 10 fm/c.

The original suggestion that color screening in a deconfined medium should lead to a suppression of heavy quarkonia states has evolved significantly over the past 20 years. Now evidence from studies of lattice QCD reveal that many of the quarkonia states continue to exist, in modified form, inside the deconfined medium of a quark gluon plasma up to temperatures well beyond the expected 170 MeV transition value. The current state of the art in lattice results yields a somewhat ambiguous picture where considerations of free energy give a different melting point for quarkonia than studies of the spectral functions. However, it is common amongst the pictures that the most loosely bound psi' and χ_c should be modified and melt at a lower temperature compared with the jpsi.

Include spectral function figure...

The first statistically significant results on heavy quarkonia in heavy ion collisions at RHIC come from the PHENIX experiment. Although the results are currently in preliminary form, a very striking and perhaps surprising observation has been made. As shown in the

state	J/ψ	χ_c	ψ'	Υ	χ_b	Υ'	χ_b'	Υ"
E_s^i [GeV]	0.64	0.20	0.05	1.10	0.67	0.54	0.31	0.20
T_d/T_c [from F_1]	1.1	0.74	0.1 - 0.2	2.31	1.13	1.1	0.83	0.74
T_d/T_c [from U_1]	~ 2.0	~ 1.1	~ 1.1	~ 4.5	~ 2.0	~ 2.0	–	–

TABLE I Dissociation temperatures in the charmonium and bottomonium system obtained by using pure gauge theory results for singlet free energies (**?**) (third row) and energies (**?**) (last row).

figure below, the nuclear suppression factor is quite similar at RHIC energies as the results from the NA50 and NA60 experiments at the CERN-SPS, almost an order of magnitude lower in collision energy. Most model calculations of expected jpsi production, whether via color screening or co-mover absorption, predicted a substantially larger suppression at RHIC due to the higher energy density and also higher temperature. In fact, there were many predictions that the Jpsi might be so suppressed as to make any observation difficult, and thus turning the focus to the more tightly bound and thus less suppression Upsilon (1s) state. However, this new experimental information, drives us to make precision measurements not just of the more tightly bound states, but the less tightly bound χ_c and ψ'.

This reasoning is threefold - χ_c near transition temperature, feed-down effect. Recombination or detailed balance.

There are three P wave quarkonia states ($\chi_{c1}, \chi_{c2}, \chi_{c3}$ all of which can decay via $\chi_c \longrightarrow \gamma J/\psi$, though only the first two have appreciable branching fractions (0.27 and 0.17 respectively). PHENIX can currently measure the J/ψ via reconstruction of the two decay muons, and needs to add the capability to measure the associated photon. The photon from the radiative decay of the χ_c has a small relative momentum to that of its parent and therefore the proposed nosecone calorimeter has good acceptance (58%) for γ when the J/ψ is accepted into the existing PHENIX forward spectrometer. In addition, due to the forward rapidity of these χ_c, the photon is boosted and can have an appreciable momentum, making the measurement ...

Effect of suppression already seen in CuCu and .....reasonable signal to background.

a. Charm via Electrons Further PHENIX upgrades include a silicon vertex detector with coverage matching that of the forward muon spectrometer. With the additional capability

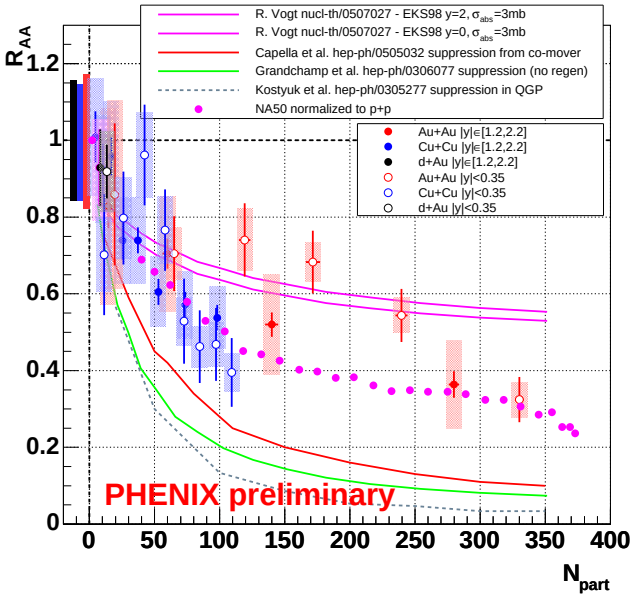

FIG. 4 PHENIX Preliminary R_{AA} for J/ψ in $Au + Au$ and $Cu + Cu$ 200 GeV reactions.

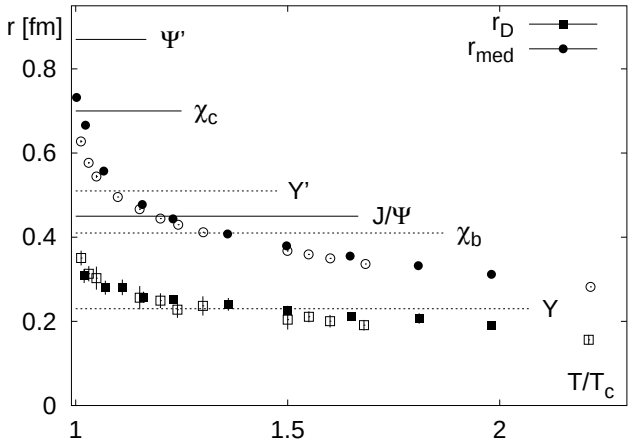

FIG. 5 PHENIX Preliminary R_{AA} for J/ψ in $Au + Au$ and $Cu + Cu$ 200 GeV reactions.

to statistically tag displaced vertices's, we greatly extend our ability to measure charm and beauty via single muon semi-leptonic decays by rejecting much longer lifetime muon backgrounds from pion and kaons decays. Additionally, one can then separate J/ψ contributions from B meson decay. Putting this information fro the forward silicon detector with the nosecone calorimeter, may allow for the tagging of forward rapidity electrons which has a displaced vertex. In principle, one can then separate the charm and beauty semi-leptonic decay electrons from the very prompt Dalitz decays and conversions (?). This could be complementary to the single muon program. In reality the kinematic coverage for both is

limited by the coverage of the silicon detector and both measure essentially the same thing with quite different kinematics.

We note that with a limited number of layers in the silicon detector, significant detailed studies on whether a clean electron sample can be obtained in proton-proton or heavy ion reactions must be completed.

B. pA PHYSICS, NUCLEON STRUCTURE AND SATURATION

NOTE TO RKS: add some stuff on the CGC

The NCC upgrade will offer many exciting new opportunities for p-A (d-A) physics at PHENIX. A major justification for a p-A (d-A) program at RHIC is to provide baseline measurements for understanding the A-A collision. This was beautifully demonstrated in the first d-Au run at RHIC which clearly showed the absence of jet-quenching in d+Au collision. Another major objective for a p-A program has to do with p-A physics in its own right. It is important to note that the c.m. energy at RHIC is more than a factor of 5 greater than any existing fixed-target experiments. This makes it possible to reach kinematic regions not accessible before. Moreover, the collider environment and the large-acceptance detectors at RHIC allow qualitatively different measurements which were not possible or difficult to perform in fixed-target experiments (i.e. access to negative rapidity region, multi-particle coincidence, etc.).

In the following we discuss several p-A physics topics which would benefit from the installation of the Nosecone Calorimeters in the North and South arms. Some specific measurements using the NCC are also presented.

1. Gluon distribution in nuclei at small x

Strong suppression of hadron productions at forward rapidity region in d-Au collision have been observed at RHIC (**?**). Since the forward rapidity region corresponds to small x, these data suggest that the gluon distributions in nuclei are significantly reduced. Various interpretations of these data, including gluon shadowing (**?**), Color-Glass Condensate (**?**), and x_F scaling (**?**), have been put forward. Measurements at PHENIX via the punch-through hadrons have also contributed to this subject. To understand the physics origin of

this suppression, it is crucial to measure the nuclear effects of a variety of particles produced in p-A collisions over a wide kinematic range. In particular, the NCC will make it possible to access many interesting channels in the forward rapidity regions which are sensitive to gluon distributions. These channels include:

1. Single hadron production. Several hadrons can be readily detected by NCC via their decays to lepton/photon channels. The hadrons and their relevant decay channels include $\pi^0 \to \gamma\gamma$, $\eta \to \gamma\gamma$, $\omega \to \pi^0\gamma$, $\phi \to e^+e^-$, $J/\Psi \to e^+e^-$, $\Psi' \to e^+e^-$, $\chi_c \to \gamma J/\Psi$ followed by $J/\Psi \to e^+e^-$, and $\Upsilon \to e^+e^-$. The p-A data at forward rapidity region on the production of these particles would significantly enhance the physics reach of PHENIX which is currently limited to heavy quarkonium and punch-through hadrons.

2. Direct photon and jet production. The inclusive production of direct photon at forward rapidity is sensitive to gluon distribution. Moreover, a measurement of direct photon in coincidence with a jet would be very valuable since the kinematic variables of the gluons can be readily reconstructed.

3. Dihadron production. The nosecone calorimeters will greatly extend the kinematic coverage for detecting dihadrons. A hadron such as π^0 or η could be detected in the NCC, while the other hadron could be measured by the barrel detectors. Energetic dihadrons would correspond largely to leading particles from dijet events, and can provide independent information on the gluon distributions in nuclei at small x.

4. Open charm and beauty production. In conjunction with the Forward Silicon Tracker, the NCC can be used to measure D and B meson productions via their semi-leptonic decays ($D \to eX$ and $B \to eX$). These heavy-quark productions are sensitive to gluon distributions. Furthermore, the acceptance for detecting a pair of charmed particle through their semileptonic decays is significantly enhanced when the NCC is combined with the muon spectrometers ($D \to eX$ in coincidence with $D \to \mu X$).

2. Antiquark distribution in nuclei at small x

In the past decade, nuclear shadowing at small x – has been very well characterized experimentally in DIS (**?**). The experimental signature is that the DIS cross section ratio

falls below unity for $x \leq 0.08$. Theoretically, shadowing has been studied extensively in the past 10 years (**?**).

Shadowing is also expected in hadronic processes. To date, the only experimental evidence for shadowing in hadronic reactions is the reduction in the nuclear dependence seen in the Drell-Yan experiments E772 (**?**) and E866 (**?**). The lowest x covered in these experiments is $x = 0.04$, just below the onset of shadowing effect.

Shadowing in the $p + A$ Drell-Yan process is largely due to antiquarks in the nucleus, unlike in DIS, where quarks dominate for most of the explored region. Although shadowing effects are expected for antiquarks and gluons, there is no known requirement that they be identical (**?**) to those for quarks. There exists no experimental information on the antiquark shadowing at small x ($x < 0.04$). The coverage in x_2 will be significantly extended at RHIC. In particular, the lowest x_2 reachable at RHIC is around 10^{-3}, a factor of 40 lower than in E772. Therefore, nuclear shadowing effect of antiquarks can be well studied at PHENIX using the muon arms and the NCC to detect Drell-Yan events via the $\mu^+\mu^-$ and e^+e^- channels.

An important role of the NCC in the Drell-Yan measurement is that it will allow a realistic determination of the contribution of open-charm background to the dimuon (or di-electron) events. The $e\mu$ pair events from the NCC and muon arm would lead to a direct measurement of the charm background. This would enable a reliable Drell-Yan measurement down to the smallest possible x values.

3. Cronin effect and x_F-scaling

Cronin effect, first observed in fixed-target experiments, has also been seen in d+Au data at mid-rapidity. The mechanisms for the nuclear enhancement of large p_T events are still poorly understood. In particular, the dependencies of the Cronin effect on the hadron species and on the hadron rapidity (particularly the negative rapidity region) remain to be measured at RHIC energies. A universal x_F-scaling behavior (**?**) has been noted for hadron productions in p-A collisions. The ability to measure a variety of hadrons at the forward and backward rapidity region with the NCC would shed much light on the origin of the Cronin effect, as well as the validity of the x_F-scaling.

C. The Colored Glass Condensate

Recently, Mclerran(**?**) and his collaborators have used a classical approximation for the initial stage of the collision, arguing that the occupation numbers at low x where much of the particle production occurs are rather high. This model - which they have named the "Colored Glass Condensate"- shows the phenomenon of gluon saturation and makes predictions which can be used to calculate the initial conditions in a heavy ion collision which in turn can then be used as input to the hydrodynamical calculations. This calculation relies on the fact that very early in the collision, gluon saturation effects at low x set a value of Q$\sim$Q$_S$ where α_S can be considered small but the occupation numbers are high. The value of Q_S at RHIC is 1-2 GeV so $\alpha_S^2 \sim \frac{1}{10}$. The saturation assumed by these authors is present in the initial state before the nuclei collide. This fact will be important in distinguishing these effects, from final state effects such as the formation of a quark-gluon plasma.

Such an effect is consistent with ep collisions at HERA (reference). In a heavy ion collision, the nucleas acts as an amplifier of the effect because of the the thickness of the nucleas. Saturation effects which in a proton would be at x 10^{-4} would show up in pA collisions at x 10^{-2}.

A striking of evidence for the CGC relies on the fact that in going to forward rapidities, one begins to sample a lower range in x in the nucleus. The ratio $R_{CP} = \frac{Yield(central)/N_{coll}(Central)}{Yield(peripheral)/N_{coll}(Peripheral)}$ is a measure of the yield per collision from hard processes coming from central as compared to peripheral collisions, where the peripheral collisions are taken as a baseline. If pp data is available, it is often used as the baseline as will be done later in the definition of R$_{AA}$. Using hadrons identified in the muon spectrometer PHENIX looked at this ratio in deuteron-nucleus collisions. For a given p_T, a lower and lower value of x is sampled as one moves to higher rapidity. Since the gluon structure function increases at low x one would see a stronger suppression as one moves to higher rapidity. Fig. **??** shows just this effect, with the more central collisions showing a larger suppression. The NCC will be directly sensitive to the gluon structure function (or what is taken for a structure function in the CGC model). One interesting fact is that in the backward rapidity region, a strong enhancement is shown. For just such studies, it is important that both the north and sound NCC's are installed.

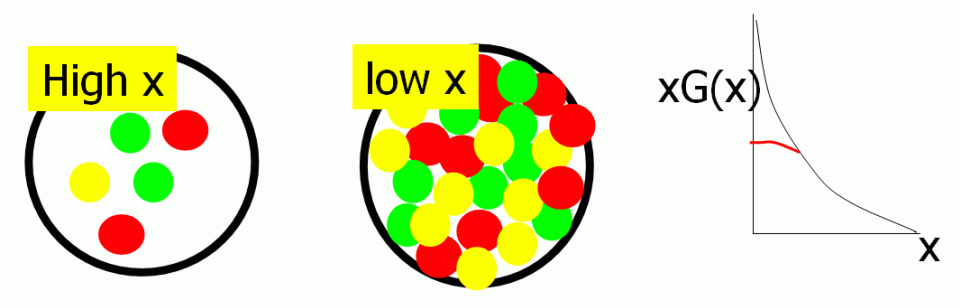

FIG. 6 A schematic showing the saturation of the gluons at low-x. This has the effect of suppressing very low x gluons and pushing them to higher-x

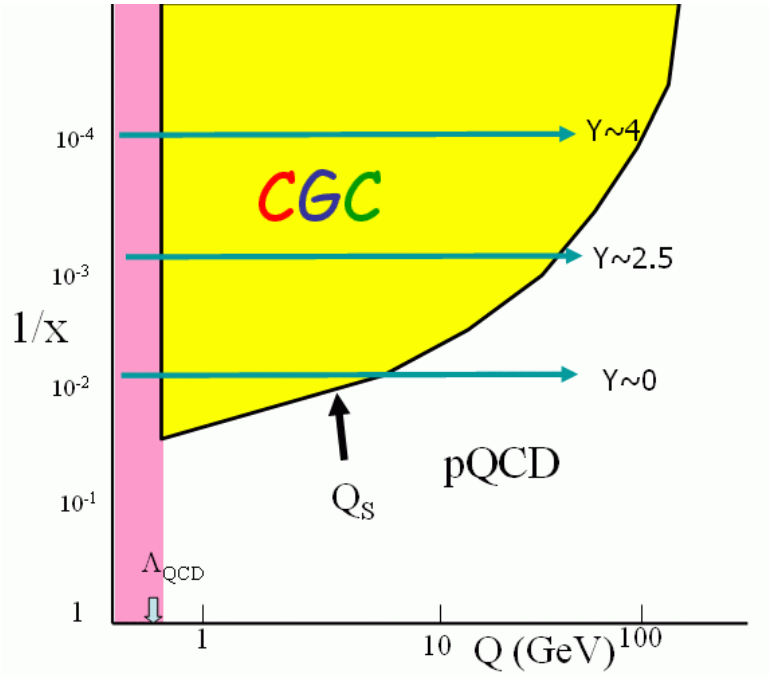

FIG. 7 Regions of the nucleas showing the CGC region bordered by a line representing Q_S. As one goes forward in rapidity, one goes deeper into the CGC region.

D. SPIN STRUCTURE OF THE NUCLEON

1. Physics Motivation

What carries the spin of the proton? Is QCD the correct theory of the strong interaction?

The advent of RHIC has given us an unprecedented tool to examine the characteristics of the strong interaction. At high energies and small distance scales, asymptotic freedom permits the use of a perturbative expansion in α_s, the strong coupling constant, to perform precise computations. In this regime, the QCD evolution of several observables has been

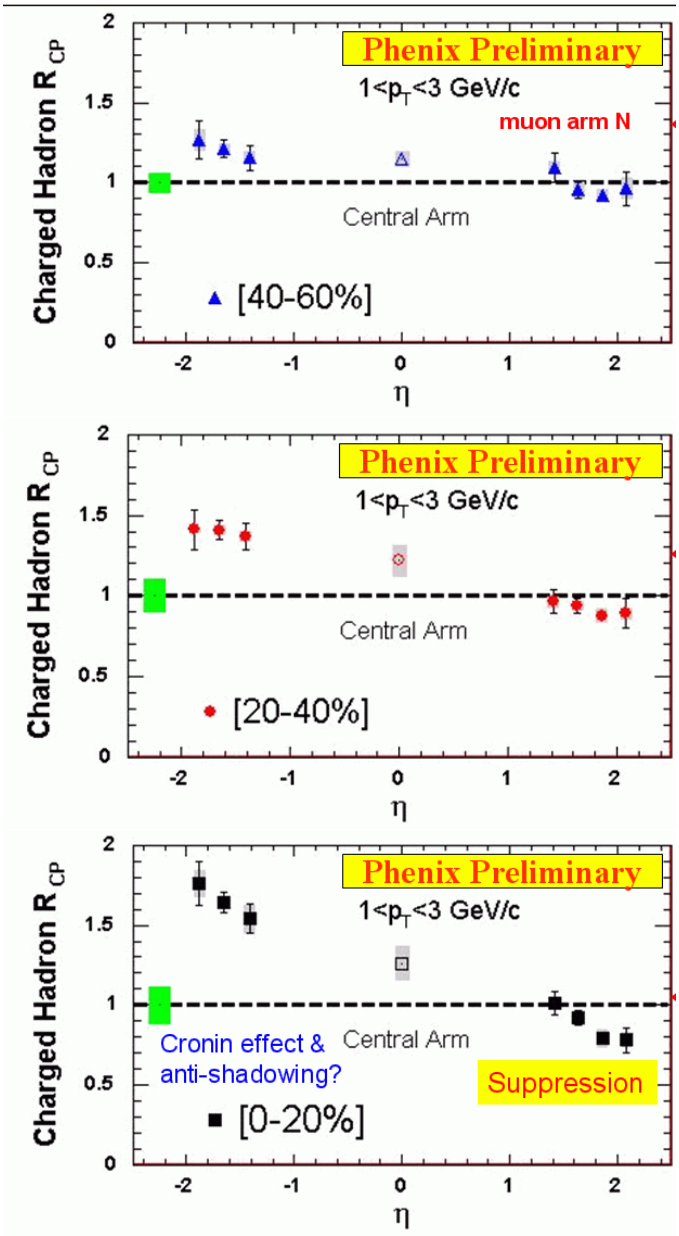

FIG. 8 R_{CP} for charged hadrons as measured in by the PHENIX muon arms for different centrailites.

carefully tested over many orders of magnitude in energy scale. However, the most important manifestation of the strong interaction in nature—the formation of protons and neutrons from their quark and gluon constituents—lies at the low-energy and long-distance scale where confinement sets in and perturbative QCD is not a viable option, although recent theoretical advances in lattice QCD suggest that accurate, non-perturbative calculations may be on the horizon. Accurate experimental data in conjunction with theoretical development is needed for our understanding of QCD to progress. Spin measurements have historically yielded

surprising results and are a stringent test to theories as spin is an intrinsically relativistic and quantum mechanical aspect of particle interactions.

Experiments with high-energy probes are able to take detailed "snapshots" of the nucleon at various levels of resolution, providing information on the structure of the nucleon in terms of their constituents, quarks and gluons. These experiments have now determined the unpolarized parton distribution functions (PDFs) with considerable precision. The PDFs, denoted $q(x)$, describe the probability that a quark of flavor q (or gluon) carries a fraction x of the nucleon's overall momentum.

The situation is much less clear when *spin* degrees of freedom are considered. From where does the proton get its angular momentum $\hbar/2$? Polarized deep inelastic lepton nucleon scattering experiments carried out at SLAC, CERN, and DESY over the past 20 years have provided information on the spin-dependent quark PDFs $\Delta q(x) = q^{\uparrow}(x) - q^{\downarrow}(x)$, where $q^{\uparrow}$ ($q^{\downarrow}$) denote quarks whose spin is aligned (anti-aligned) with the spin of the proton. These measurements have revealed the originally surprising result that the quark spins account for only a small fraction of the proton's spin [1]. Where else can the proton get its spin? There are two possibilities: polarization of the spin-1 gluons and/or orbital angular momentum of the quarks and gluons. We will answer this question with polarized proton collisions at RHIC, where we have access to the portion of the proton spin carried by gluons, ΔG or Δg

2. Nucleon Structure: Gluon Polarization

Spin-dependent DIS experiments have revealed that the quarks only carry a small fraction of the proton's spin. As gluons are responsible for half of the proton's momentum, it is natural to expect that they play a role of similar importance in the spin sector. However, this must be determined experimentally. The results of a recent QCD analysis of the available polarized DIS data (from SLAC, CERN, and DESY) are displayed in Fig.1 and show that the present uncertainties on ΔG are so large that even the sign of the gluon polarization is barely constrained.

The RHIC spin program will provide the first precise measurement of the x-dependence of gluon polarization ΔG(x). The PHENIX experiment, which has excellent particle identification and high rate capabilities, is well suited to this measurement as we are sensitive to ΔG through multiple channels and each of these channels has independent experimental

and theoretical uncertainties. Our main sensitivity is through inclusive hadron production, prompt photon production, and heavy quark production.

Prompt photon production provides the most direct access to the gluon polarization. In unpolarized p+p and e+p experiments the gluon distribution function has been measured using single- and di-jet events as well as from direct photon events. In both cases, jets or high p_t photons carry information directly from the underlying hard scattering process which can be calculated using perturbative QCD. As the cross sections factorize into a hard scattering and a proton structure part a measurement determines the parton distribution functions connected to the processes, schematically

$$\sigma \sim q\left(x_A\right) \otimes G\left(x_B\right) \otimes \left|\mathcal{M}_{\mathrm{pQCD}}\right|^2$$

where x_A and x_B are the fraction of proton momentum carried by the partons entering the hard scattering process. The theoretical problems present in the interpretation of fixed-target data have been largely resolved for the collider environment [3]. PHENIX's first prompt γ cross-section measurement indicates that these calculations are valid at RHIC.

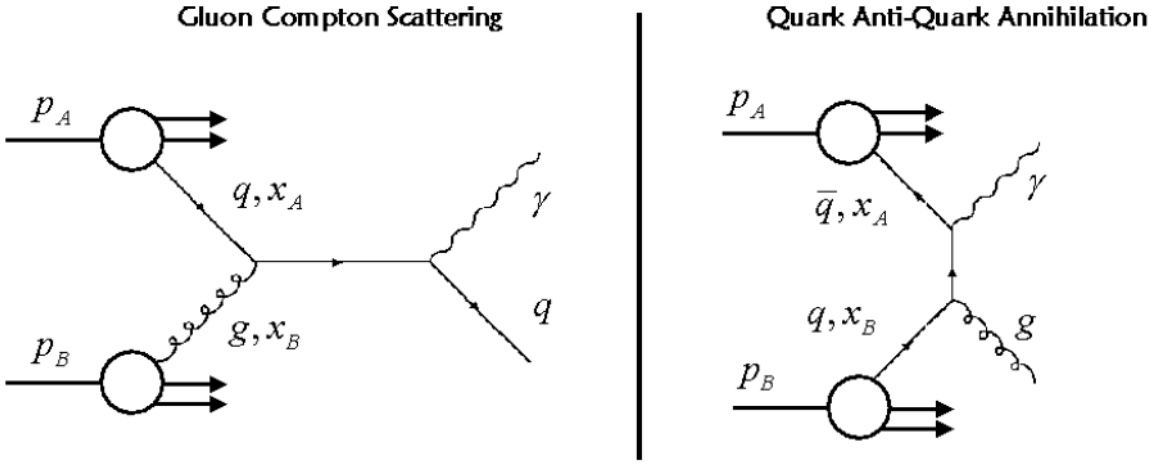

FIG. 9 Figure 1. Direct photon production in the gluon compton and quark anti-quark annihilation processes. The ratio of the two processes has been studied using PYTHIA and was found to be about 9:1.

In PHENIX direct photon production, which is dominated by quark-gluon Compton scattering (see Fig.1), will be used to measure the proton gluon polarization. Helicity conservation at the quark gluon vertex gives rise to a double spin asymmetry

$$A_{LL} \sim \frac{\Delta q\left(x_A\right)}{q\left(x_A\right)} \otimes \frac{\Delta q\left(x_B\right)}{q\left(x_B\right)} \otimes a_{LL}^{qg \rightarrow q\gamma}$$

from which ΔG/G can be extracted. $a_{LL}^{qg\rightarrow q\gamma}$is the spin asymmetry of the underlying quark-gluon Compton diagram. Background from the quark anti-quark annihilation process has been studied using the event generator PYTHIA and was found to be small.

One of the cleanest signals for measuring the gluon contribution to the proton spin is the photon-jet signature. However, the limited acceptance, $|\eta|$g $\leq$ g.35, of the current PHENIX detector and the absence of hadronic calorimetry presently make it impossible for us to reconstruct jets.

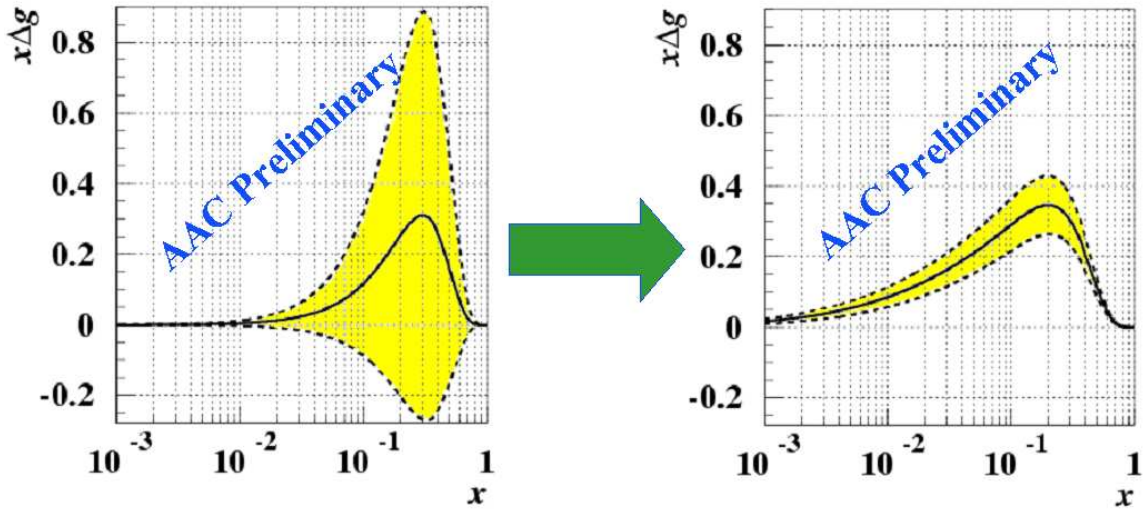

FIG. 10 Figure 2. (left) NLO-QCD analysis of existing DIS data do not constrain the knowledge of the gluon polarization significantly as indicated by the dashed error envelope [2]. (right) Including the prompt γganticipated from PHENIX data from one year at design luminosity in the same NLO-QCD global analysis [2]. [RICH will provide replacement Fig]

The NCC allows us to greatly extend the x-range of PHENIX's measurement. The x-dependence is essentially unconstrained, as suggested by the three very different parameterizations in Fig 2. Despite the fact that the gluon polarization appears best constrained and falls off with decreasing x, the integral of ΔG is dominated by contributions from x<0.1 since this is the regions where gluons are most abundant [note that ΔG is multiplied by x]. It is thus important to measure ΔG to values of$x$ as far below 0.1 as feasible. Historically it is interesting to note that the quark spin crisis only arose when EMC extended the measurement of quark spin contributions to low-x. Extrapolations of the SLAC data alone led to results for the quark spin contribution consistent with expectations from naive quark models. The additional geometric acceptance in the forward direction extends the measure-

ment of the gluon polarization from $0.01 < \quad x \quad < 0.3$ down to about $x = 0.001$. Further, in combination with the new PHENIX inner tracker detectors, which will allow crude jet-reconstruction in the PHENIX central arm, the calorimeter makes it possible to obtain a rough measurement of x on an event-by-event basis by detecting the away-side jet associated with the recoiling quark. The x measurement allows for a leading-order determination of ΔG, which will be particularly valuable in constraining ΔG at low-x and complimenting the NLO determination that will utilize the inclusive measurement. A rough jet measurement can also be made with the NCC making possible a full range of measurements. [**Need some kinematics from Rich to quantify**]

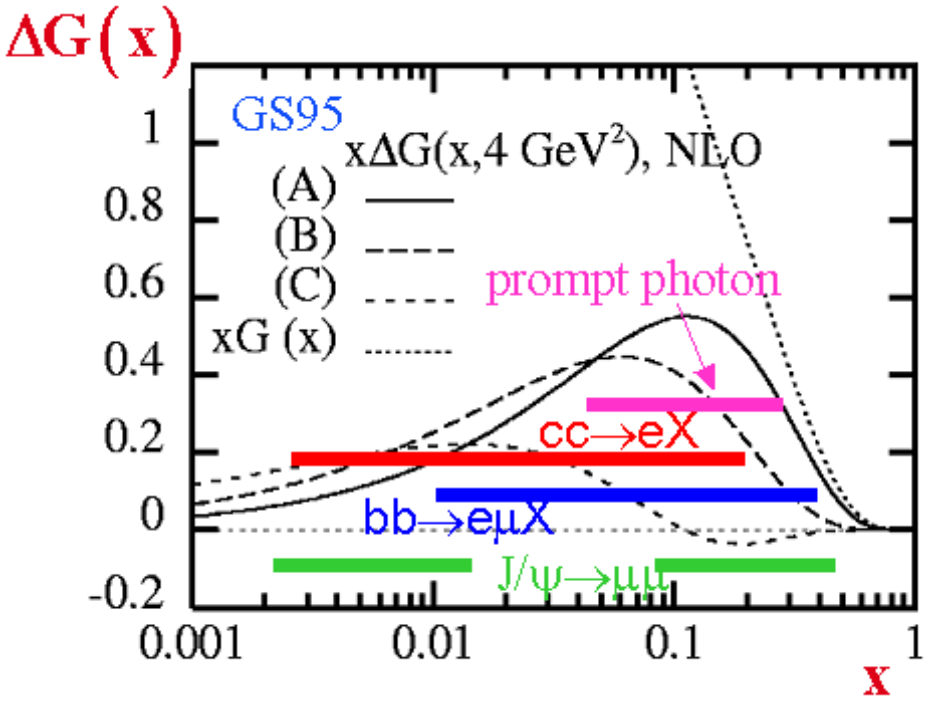

FIG. 11 Figure 3. Kinematic coverage for PHENIX measurements that are sensitive to ΔG. (left) x_{Bj} range shown on-top parameterization of ΔG [14]. (right) Kinematic coverage in relation to SLAC, Hermes, and Hera measurements (unfortunately, Hera does not have polarized beams). [RICH will provide replacement Fig with NCC channels]

Thus, PHENIX is sensitive to ΔG through multiple channels. The kinematic coverage for various channels within PHENIX are shown in Fig. 3. The complementary measurements cover slightly different kinematic ranges, and most importantly provide alternative ways to the gluon polarization with different systematic and theoretical uncertainties.

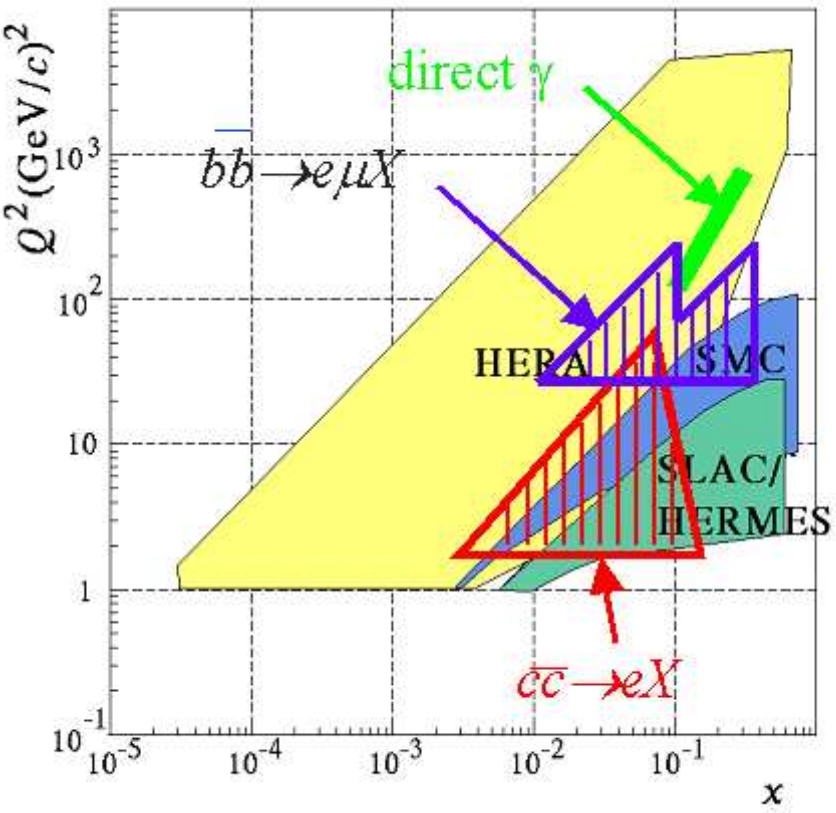
direct γ
$b\bar{b} \to e\mu X$
HERA
SMC
SLAC/
HERMES
$c\bar{c} \to eX$
Q^2(GeV/c)^2
x

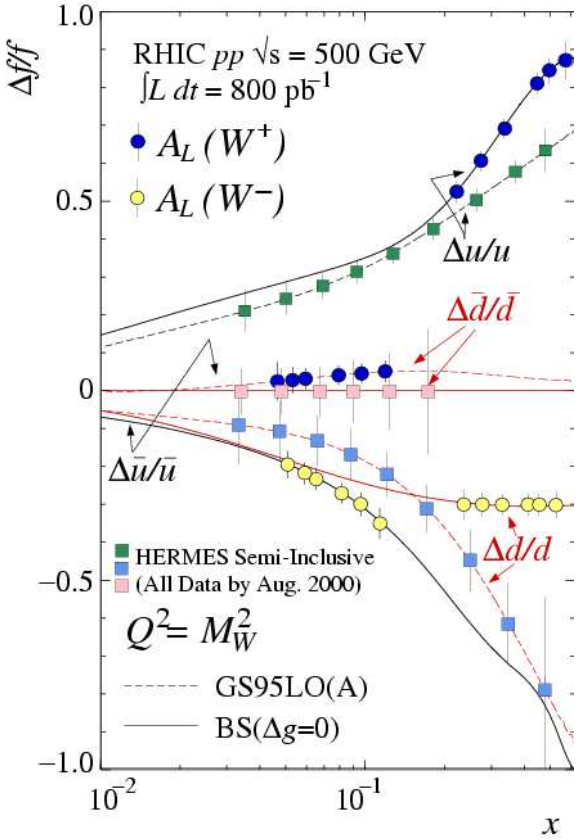
RHIC pp √s = 500 GeV
$\int L\,dt$ = 800 pb^{-1}
$A_L\,(W^+)$
$A_L\,(W^-)$
$\Delta u/u$
$\Delta\bar{d}/\bar{d}$
$\Delta\bar{u}/\bar{u}$
$\Delta d/d$
HERMES Semi-Inclusive
(All Data by Aug. 2000)
$Q^2 = M_W^2$
GS95LO(A)
BS(Δg=0)
$\Delta f/f$
x

While Δq has been fairly well measured, the anti-quark's contribution to Δq is not well known.

The high-energy polarized proton beams at RHIC provide copious yields of W bosons, and the parity-violating nature of the weak interaction permits the extraction of light quark and anti-quark polarizations through measurements of longitudinal single spin asymmetries in W^+ and W^- production. Bourrely and Soffer first discussed this idea using QCD at leading order perturbation theory [4]. Recently Yuan and Nadolsky presented a next-to-leading-order QCD analysis based on modern resummation techniques [5]. This work leads to a robust interpretation from first principles in QCD of the PHENIX quark polarization measurement in W production. In PHENIX, W production is characterized either by detecting high-energy electrons in the two central spectrometer arms or by reconstructing high-p_T muons in the two muon spectrometers. Due to their eight–times-larger acceptances, the PHENIX muon spectrometers will dominate the measurement statistically. The anticipated integrated luminosity of 800 pb^{-1} will yield approximately 10^4 detected W^+ and W^- events. However, before a successful measurement can be carried out, the event selection electronics must be improved significantly. The muon trigger was designed for heavy ion running and low-luminosity proton collisions; an upgrade is required to record selectively energetic muons from W decay during the high-rate spin running.

Some information has come recently from the first measurement from the HERMES collaboration. They have released results for the polarized parton distributions $\Delta q(x)$ for five separate flavors: $\Delta u(x)$, $\Delta d(x)$, $\Delta \bar{u}(x)$, $\Delta \bar{d}(x)$, and $\Delta s(x)$ [6], and the isospin asymmetry of the light-quark sea polarization predicted by several models is not observed in the data. The HERMES results, however, are accompanied by a substantial systematic error as their method of "flavor tagging" relies heavily on understanding the fragmentation process. The PHENIX measurement, thus, will provide an important second measurement an experimental approach completely different from that of HERMES.

Fig.4 shows the projected precision of PHENIX on the light quark polarizations in the proton. Superimposed on the plot are projections of the accuracy achievable by HERMES (the figure has not yet been updated with the actual results released). The anticipated measurements are highly complementary in nature. The HERMES results feature more complete

kinematic coverage, while the PHENIX results are of greater precision. The PHENIX technique distinguishes cleanly between the light quark flavors in a model-independent way, while the HERMES kaon asymmetries are able to probe the strange quark polarization. Finally, the systematic uncertainties in the two experiments are of completely different origin.

The measurement of the anti-quark spin contribution to the spin of the proton will be via the measurement of high p_t leptons coming from W's – a rather rare process. The NCC upgrade will extend this measurement both by allowing the detection of electrons in the forward region – in addition to the muons, and in reducing the backgrounds. One of the major backgrounds to is the decay of high momentum pions or kaons. Such background events can be reduces by requiring a separation between the lepton- detected by either the muon spectrometer (muons) or the calorimeter (electrons) and the jet, as detected by the calorimeter.

4. Transversity

Transverse spin asymmetries of hadron production at high-pt in nucleon-nucleon collisions has become unusually interesting since it is predicted by pQCD at leading twist to be vanishingly small due to the chiral dynamics of QCD. It was therefore a surprise when E704 discovered very large asymmetries in pion production from polarized p+p collisions at $\sqrt{(s)}$ = 20 GeV [6]. It was even more surprising when STAR discovered that these effects persisted to the much higher $\sqrt{(s)}$ of 200 GeV [4], since it was thought that any power corrections should be suppressed at higher energies, despite the fact that the predictions of unpolarized cross-sections agree very well with the data.

The existence of large single spin asymmetries at RHIC, along with the good agreement of the unpolarized cross-sections, means that RHIC exists in a regime where pQCD applies and works well, but fails once goes to transversely polarized proton collisions. This gives hope that transverse spin effects can be used as a tool to probe the transverse structure of protons.

There have been three primary explanations for the single spin asymmetries observed so far:

1. Higher Twist effects, either in the initial state or the final state. [7]

2. Sivers function, a kT dependent modification to the parton distribution functions [8]

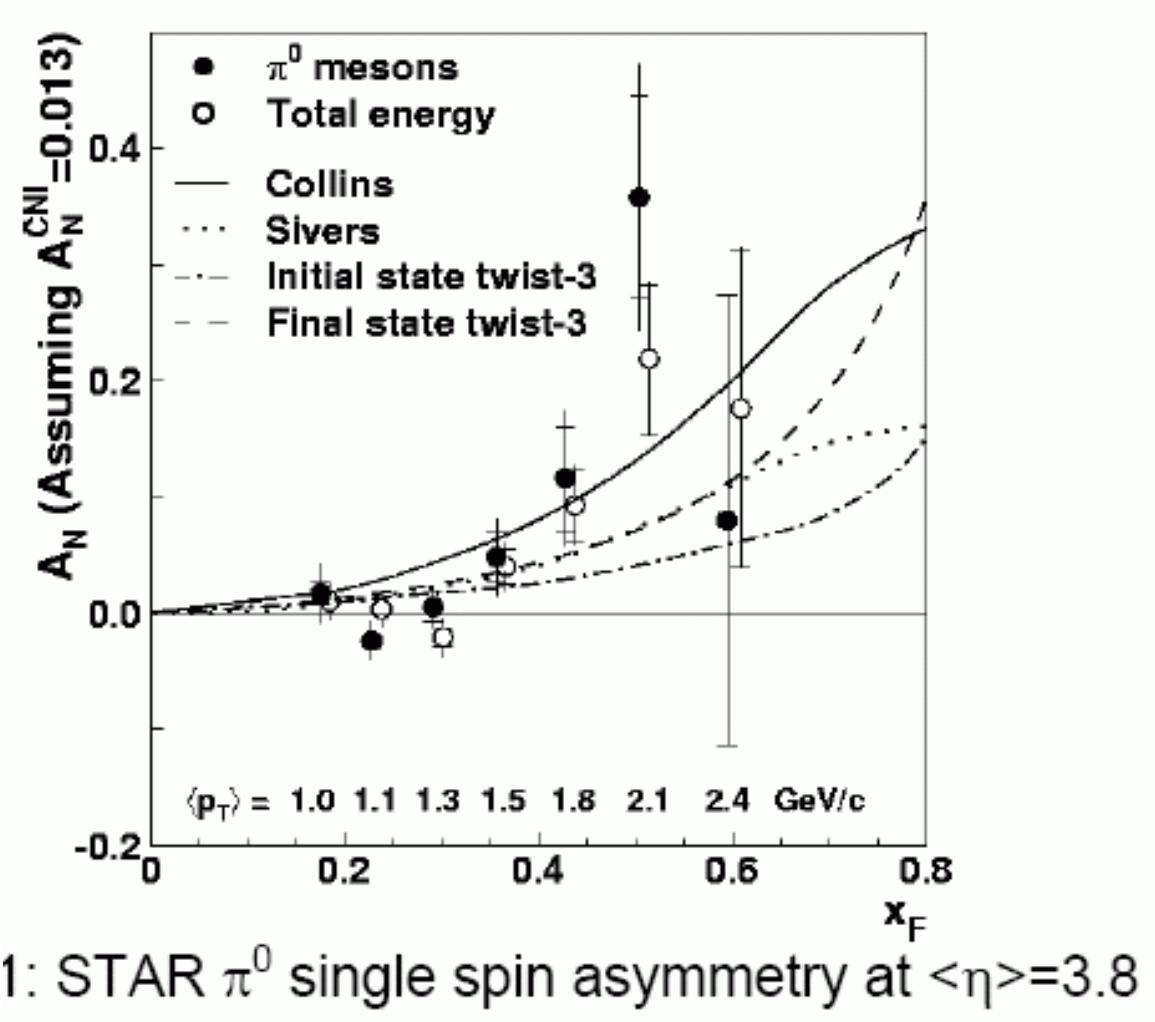

FIG. 12 this is the caption

3. Collins [9] or interference fragmentation function [10] plus tranversity

The calorimeters will be able to measure this asymmetry - they also allow PHENIX to separate out all of the different possible effects, and for the first time systematically deduce the mechanisms behind these single spin asymmetries. The Sivers effect can be measured in the azimuthal asymmetry of back-to-back di-hadrons or di-jets, where one of the hadrons is the forward pi0 or jet. The Collins FF can be measured in the hadron distribution around a jet axis.

The Interference FF can be measured by di-hadron correlations in the near side of a jet. Whatever is left over might then be attributed to higher twist effects. d by s stated by A complete QCD description of the proton structure requires the explicit inclusion of transverse motion, which is essential for spin effects. A measurement of transverse single

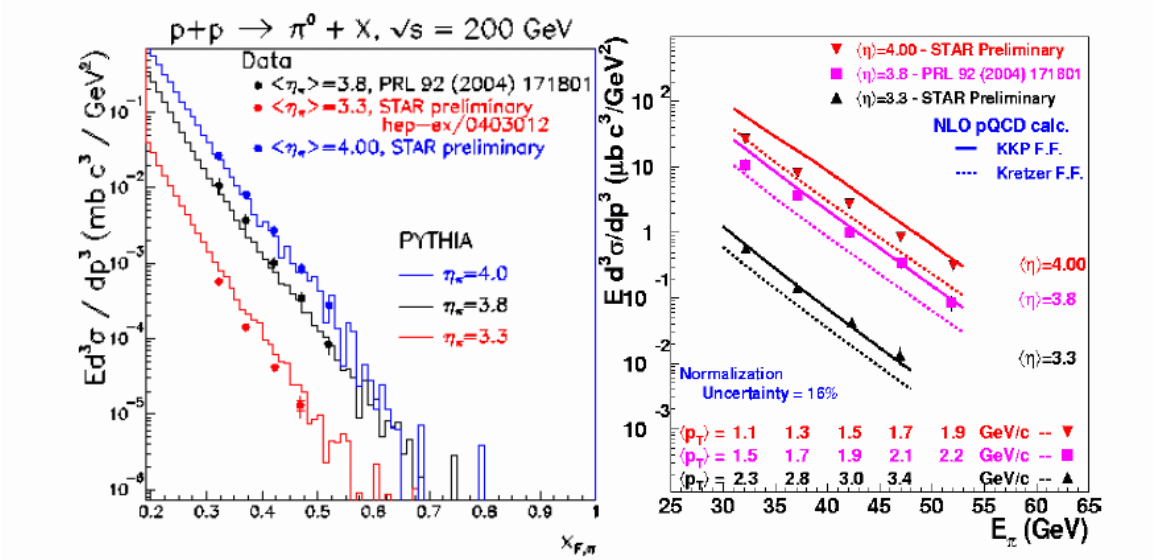

Fig 2.2: Agreement between STAR's forward π0 cross-section and NLO as well as PYTHIA calculations are excellent

FIG. 13 this is the caption

spin asymmetries will tallow us to reach and perhaps understand the transverse motion of quarks in the nucleon, a long-standing problem which has defied a quantitative physical understanding despite decades of research. Any progress in this area will certainly lead to a deeper understand of proton structure, including transversity, orbital angular momentum of partons, and the color Lorentz force inside a polarized nucleon.

1. J. Ashman *et al.*, "A Measurement of the Spin Asymmetry and Determination of the Structure Function g_1 in Deep Inelastic Muon-Proton Scattering", *Phys. Lett.* **B206**, 364 (1988).

2. Y. Goto *et al.*, "Polarized Parton Distribution Functions in the Nucleon", *Phys. Rev.* **D62**, 034017 (2000).

3. E. Laenen, G. Sterman, and W. Vogelsang, "Higher Order QCD Corrections in Prompt Photon Production," *Phys. Rev. Lett.* **84**, 4296-4299 (2000); "Recoil and Threshold Corrections in Short Distance Cross-Sections," *Phys. Rev.* **D63**, 114018 (2001).

4. C. Bourrely and J. Soffer, "Parton Distributions and Parity Violating Asymmetries in $W^{\pm}$ And Z Production at RHIC," *Phys. Lett.* **B314**, 132-138 (1993).

5. P.M. Nadolsky and C.-P. Yuan, "Single spin asymmetries with weak bosons at RHIC", *Nucl. Phys.* **B666**, 31 (2003).

6. A. Airapetian *et al* [HERMES collaboration], "Flavor Decomposition of the Sea Quark Helicity Distribution from Semi-inclusive Deep-inelastic Scattering", *Phys. Rev. Lett.* **92,** 012005 (2004).

III. PHYSICS MEASUREMENTS WITH THE NOSECONE CALORIMETER

A. PERFORMANCE

Above it was shown that constrains driving the design of NCC are mostly related to he goal of correctly separating single showers from the multiple shower overlaps. If this goal is reached the identification of direct photons will still stay partially compromised by the inability of calorimeter to measure charge of the impinging objects although some statistical tools are still available: photon showers are 1 Lrad delayed compared to those due electrons. In the calorimeter fine segmented longitudinally this maybe valuable piece of information although its use will require some creativity in the analysis.

There is only one solution which allows to separate close showers in calorimeters - building it of material with minimal Molier radius. Technology sets the limit to the minimal thickness of readout layers (2.5 mm). The similar thickness of W plates allows keeping Molier radius under control but places a severe burden on the calorimeter resolution. The back of the envelope estimates used above to justify the concept certainly needs further investigation; we also need to propagate performance estimates into physics observables to reach certainty that accepted performance compromises would not compromise the physics.

In our simulation effort the calorimeter as described above was simulated using GEANT to produce libraries of electromagnetic and hadronic showers. The calorimeter was located 40cm away from production vertex, the whole active area of the calorimeter was uniformly illuminated, the data presented below are integrated over all impact angles (0 to 45 degrees).

B. Energy resolution and linearity

It is rather well known that in a longitudinally segmented calorimeter the sampling fraction (which is a calibration coefficient if electronics gains are ignored) depends on the depth along the shower axis (interplay between photon and electron spectra shapes and critical energy). The data in Fig. **??** are for the sampling fraction in four longitudinal segments of NCC (converter, two em and one leakage segments), they clearly show the energy dependence which needs to be corrected for the calorimeter response to be linear.

A simple functional form was used to describe the behavior observed in the data. When energy dependent calibration coefficients were applied to the data the calorimeter response

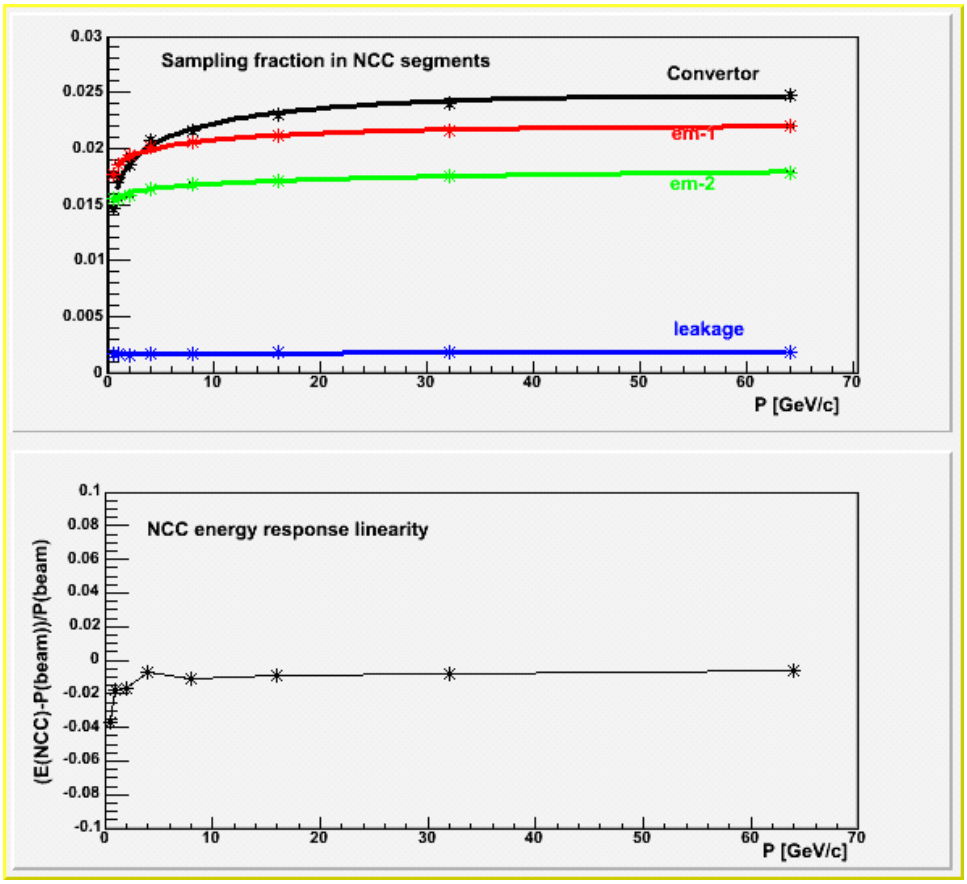

FIG. 14 captoion

was found to be linear within 1(Fig. **??** and its energy resolution matching our expectations in the range of electron momenta below 15 GeV/c and degrading compared to those expectations at larger momenta (developing substantial constant term).

C. Overlapping showers

The π^0 events were simulated with uniform momentum distribution between 1 and 30 GeV/c. Checks were made that only those events with both photons inside NCC aperture are retained. At this time the pattern recognition algorithms we were able to concoct on a very short time scale are rather rudimentary and intended to answer a very simple question if data actually show the features required for our ideas about handling overlapping showers to work. In the detector with molier radius 18mm and tower size 15 mm there should be substantial fraction of π^0's with two photons clearly separated (drops down with π^0 momenta) even this close to the production vertex. Similar to the central calorimeter we

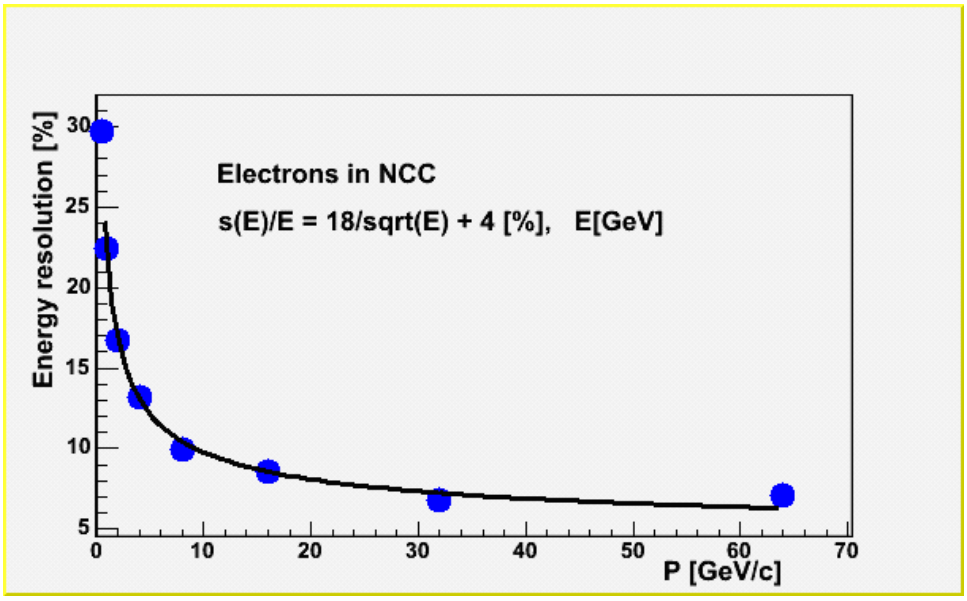

FIG. 15 captoion

consider two showers distinct if their maxima are separated by at least one counter (visible valley). The probability to find two distinct showers in the event with both photons from π^0 decay in the detector aperture thus computed is shown in Fig. ??.

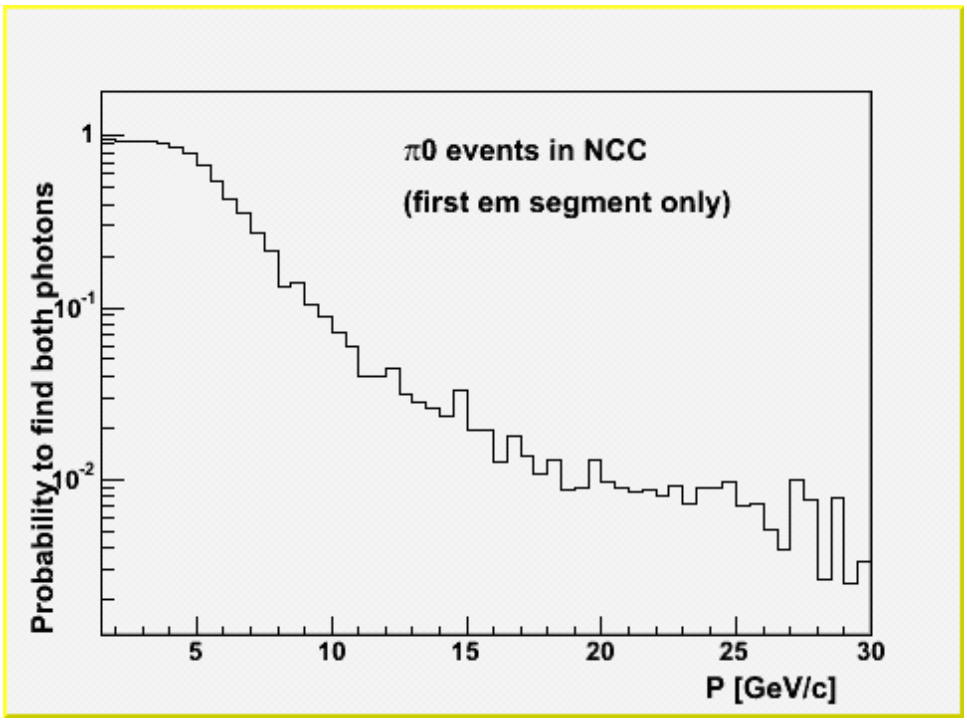

FIG. 16 captoion

Note that the data used in pattern recognition are from the first electromagnetic segment. There is an advantage and disadvantage in this approach which needs further studies: showers are still narrow, angular dependent corrections to shower shape are minimal, the drawback is due to enhanced fluctuations (only about 25energy is in the first em segment). It is clear that measuring π^0's as a peak in effective mass distribution ends around 10 GeV/c where the probability to see two distinct showers stays still close to 10approaches. The most important tool helping to extend the π^0 reconstruction range is preshower detector built of 0.5 mm wide pixilated strips and installed at a depth of 2 Lrad in the calorimeter. It is expected that it will have a S/N ratio 5 for a single MIP and will have a dynamic range up to 15 MIPs (limitations are due to limited dynamic range of SVX4 chips we are planning to use in this detector). The average multiplicity of the fired strips in PS detector when crossed by electron or electron pairs from π^0 decays is shown in Fig. **??**. Asymptotically he ratio of the two is about 4 as expected from the number of charged crossings, low energy photons which (effect of the simulation) are mostly on detector periphery have more strips fired (effect of the impact angle). Two cases are clearly distinct although the fluctuations are enormous (soft Compton photons could travel long distances and convert well away from the shower core).

Next picture is to confirm that even when fluctuations are accounted for the separation between single and multiple showers in PS detector is really possible up to the kinematical limit in π^0 production at RHIC. The pattern recognition algorithm used to interpret PS data was similar to used in the calorimeter segments but applied to the linear structure of strips in X and Y directions separately. Clusters of hits with clearly separated maxima were counted in both planes and simply added together. The pattern recognition was limited to "regions of interest 30 mm wide around expected crossing as predicted from calorimeter segments. The same procedure was applied to electron and π^0 data, only more energetic photon was subjected to the treatment in case if maxima in em segment 1 were distinct. The two pictures are combined in Fig. **??**. Electrons at all momenta have only a small tail above two clusters (one per X and Y plane),. Picture for π^0's is more complicated. There is a substantial population in 2 cluster bin due to both - decision to limit this analysis to highest photon only (low energy enhancement) and loss of conversions due to relatively shallow converter (easy to estimate and correct). The remaining distribution is centered around 4 clusters as expected and extends both way to lower (projection overlaps) and higher (effect

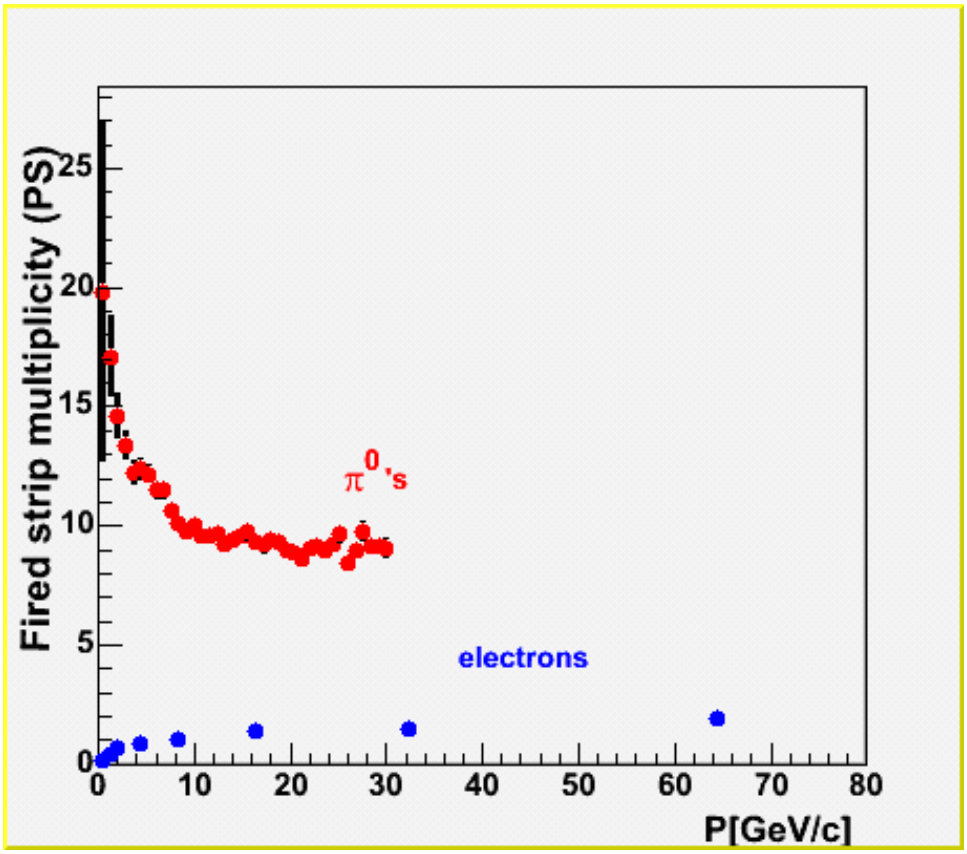

FIG. 17 captoion

of impact angle and fluctuations) cluster multiplicities. It is very important to note that the distinctions between electrons and π^0's persist till maximum considered π^0 momentum of 30 GeV/c where the two-photon separation is only 5 mm in the detector.

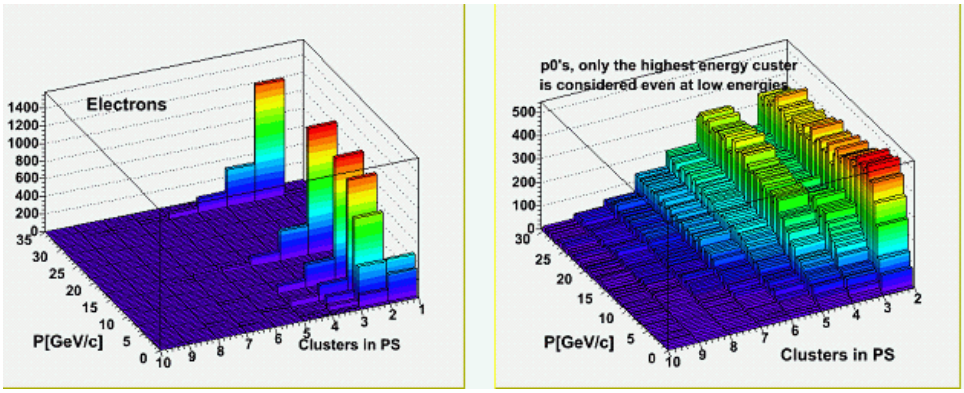

FIG. 18 captoion

While these results are preliminary they clearly indicate that at least in the simulation

NCC performs as expected. Following considerations above one can suggest the following approach to π^0 extraction in NCC:

- - use classic effective mass method to 10 GeV/c momenta. Use PS to identify multi-component showers;
- build an algorithm which will use measured impact positions in PS detector, total shower energy from calorimeter and estimates for the decay asymmetry from shower max detector to further extend effective mass reach;
- use statistical approach (assume that high energy multicomponent showers are due toπ^0's);
- use MonteCarlo to estimate losses and backgrounds.

Now when we reached a certain understanding that data are reach enough to allow for extraction of appropriate primitives it is only a question of time and effort to finalize the strategy and develop software which will do the π^0 reconstruction job.

D. PHYSICS REACH

One of the priciple problems for the NCC is the occupancy, particularly in central heavy ion collisions at high rapidity. In fact in the most central collisions, pads at $\eta > 2.75$ have an average occupancy of $\tilde{1}00\%$. For the signals we are interested in for heavy ion collisions, namely the χ_c, high momentum direct photons, π_0's we have some tools we can use to isolate the signal. In what follows, unless indicated, we assume RHIC II statistics, in particular we assume AuAu-1.5 nb^{-1}, dAu-100/A pb^{-1}=0.5pb^{-1}, pp-76pb^{-1}.

E. The χ_c

The χ_c decays into a J/ψ and a photon. We first identify the J/ψ via its di-muon decay - it may also be possible to use the di-electron channel as well. For χ_c's in which the muons are detected in the muon arms - the photon is seen in the NCC more than 60% of the time Fig. **??**. In order to see the χ_c one reconstucts the $\mu^+\mu^-\gamma$ invariant mass and subtracts off the $\mu^+\mu^-$ invariant mass where the dimuon mass is required to be in the J/ψ peak. The χ_c

should show up as a peak at the χ_c-J/ψ mass difference of about 400-500 MeV. There are actually 2 χ_c states which decay with large branching ratios to the Jψ with masses 3511 and 3556 MeV. As one can see in Fig. 20, for central events, often times the photon is smeared out because of background. However the photon is required to be isolated in a module, that is there is now background, (blue line) the peak shows up nicely. Note that the resolution is now primarily due to the resolution of the photon and not the resolution of the muon spectrometer.

Fig. 21 shows the invariant mass difference for simulated full events where a background subtraction has been done using mixed events, for as assumed run of 1.5 nb^{-1}. The χ_c shows up clearly in all but the most forward rapidity. This is for the top 10% central Au-Au events. In more peripheral events, of course, the signal is cleaner. Figures 22 and 23 are for dAu and pp events respectivly.

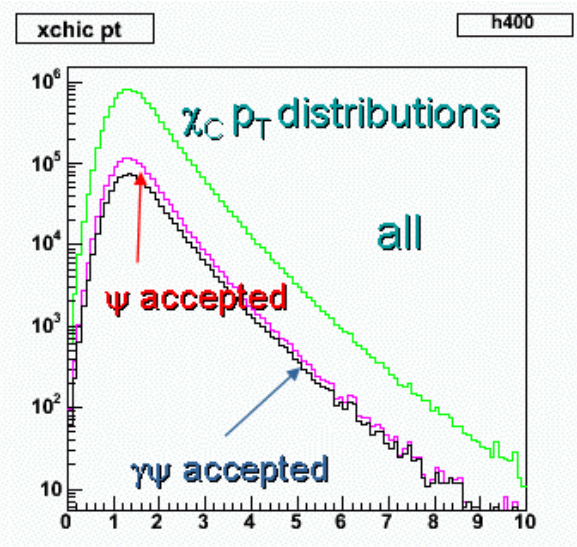

FIG. 19 p_t distributions for the χ_c. Green-all, red-J/ψ accepted in the muon spectrometer, blue-χ_c accepted in NCC.

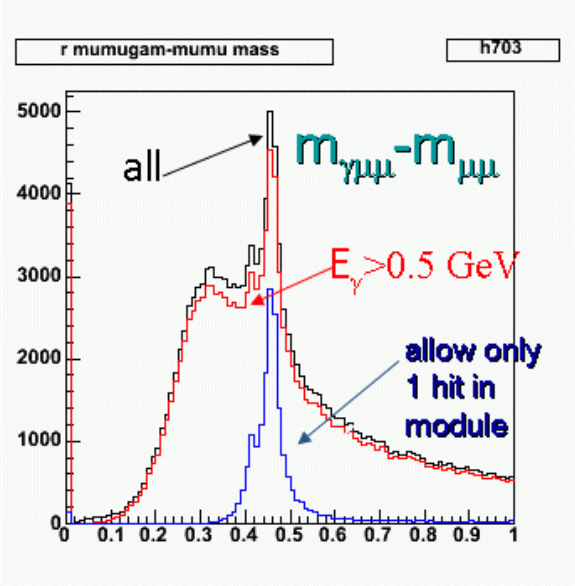

FIG. 20 The $M_{\gamma\mu\mu} - M_{\mu\mu}$ invariant mass distribution in central 10% Au-Au events where we require that the three particles come from a χ_c. Red- all events; red-$E_\gamma > 0.5$ GeV; blue-γ is required to be isolated in a module.

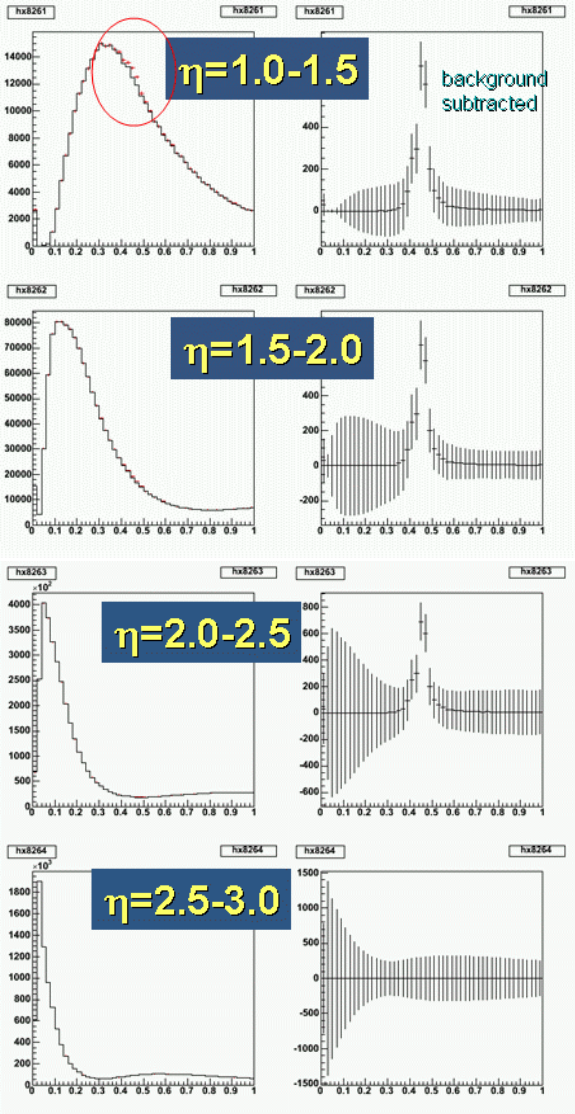

FIG. 21 Central 10% Au-Au events at various rapidities. The left plot of each pair show the raw mass difference, the right plot shows a background subtracted distribution using mixed events. The statistics shown are for

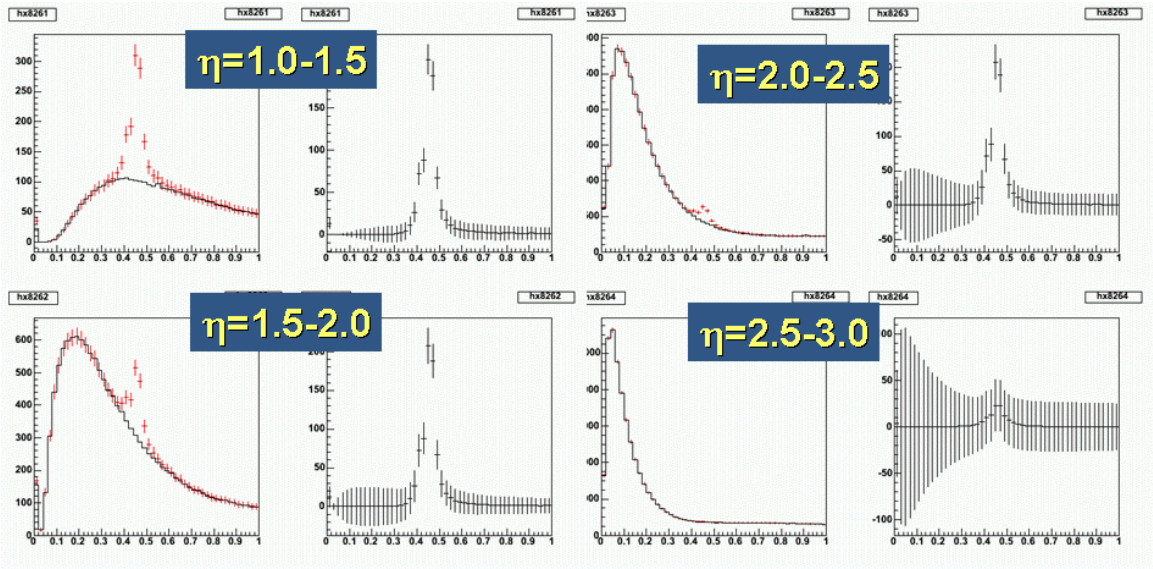

FIG. 22 Same as Fig. 21 for the top 20% central dAu events.

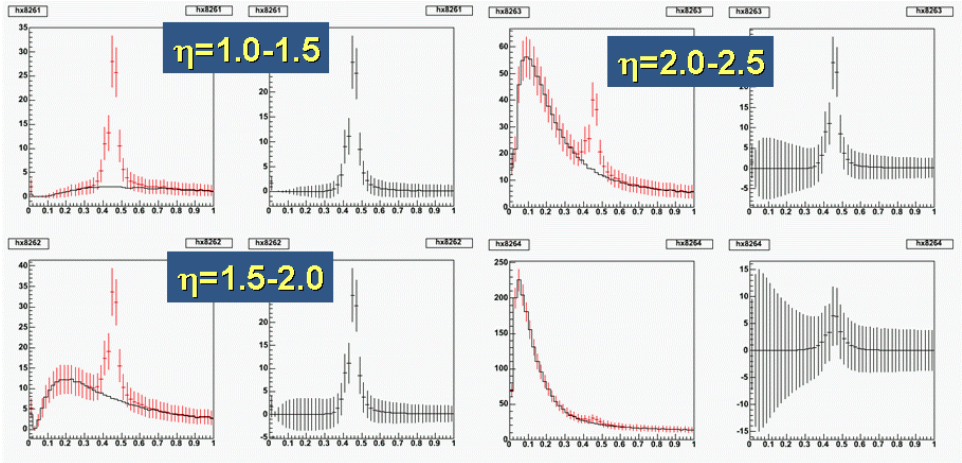

FIG. 23 Same as Fig. 21 for pp events.

FIG. 24 figure caption

FIG. 25 figure caption

FIG. 26 figure caption

$$x_T = \frac{2p_T}{\sqrt{s}}$$

use γ to get p_T

$$x_1 = \frac{x_T}{2}\left(e^{+\eta_\gamma} + e^{+\eta_{Jet}}\right)$$

$$x_2 = \frac{x_T}{2}\left(e^{-\eta_\gamma} + e^{-\eta_{Jet}}\right)$$

FIG. 27 figure caption

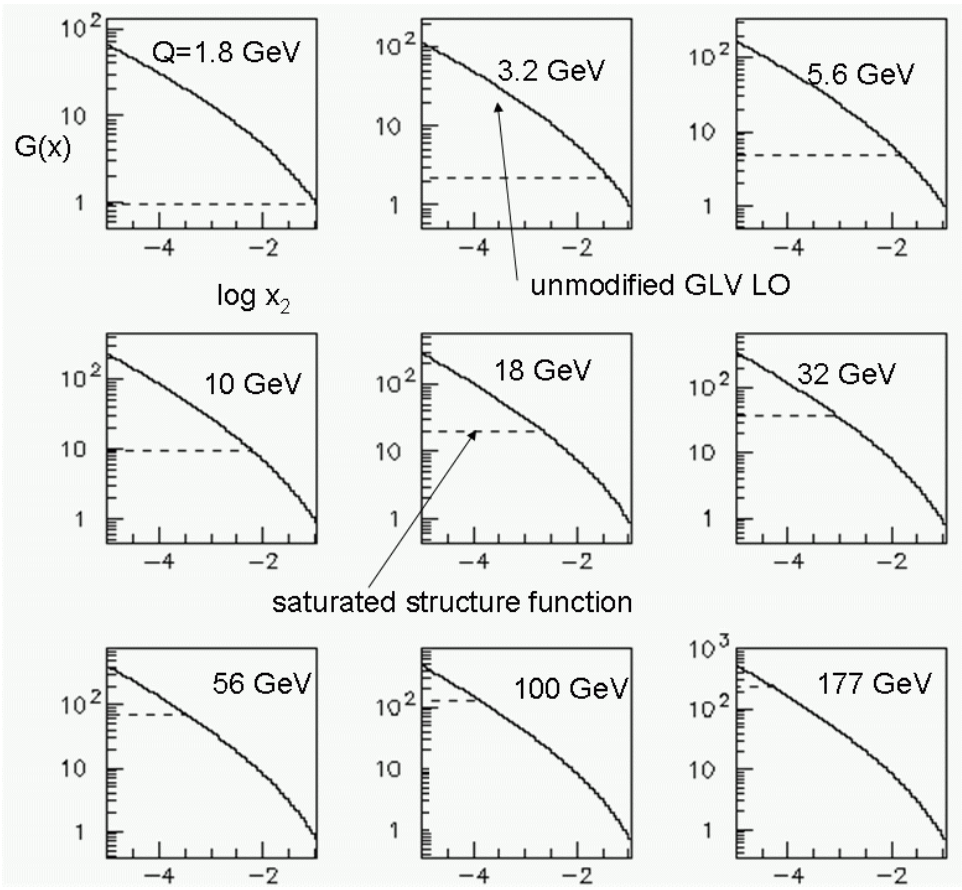

FIG. 28 figure caption

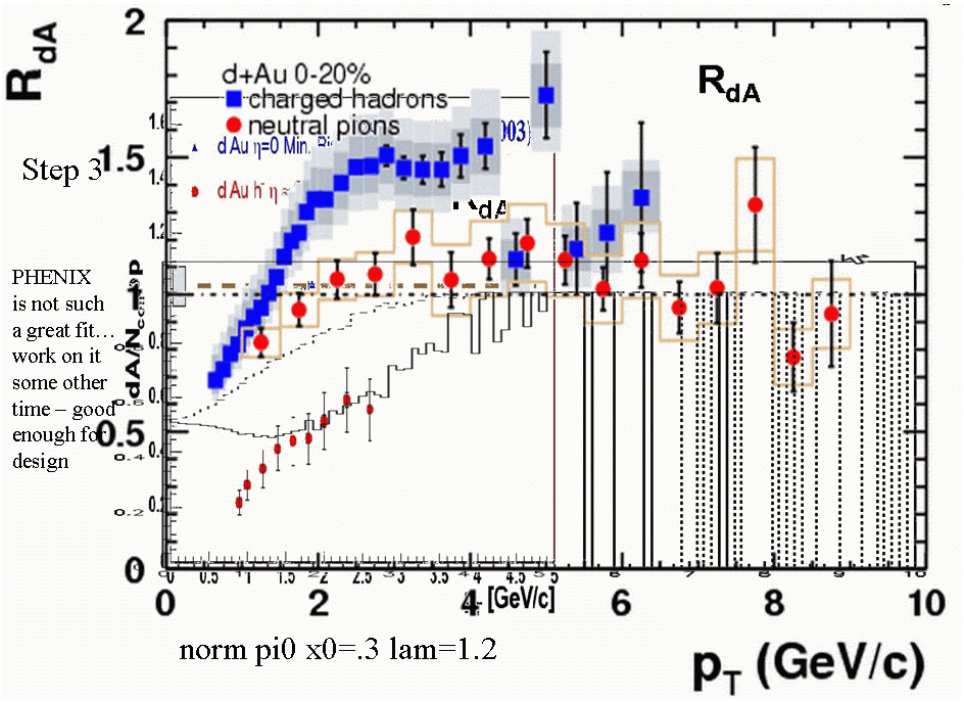

FIG. 29 figure caption

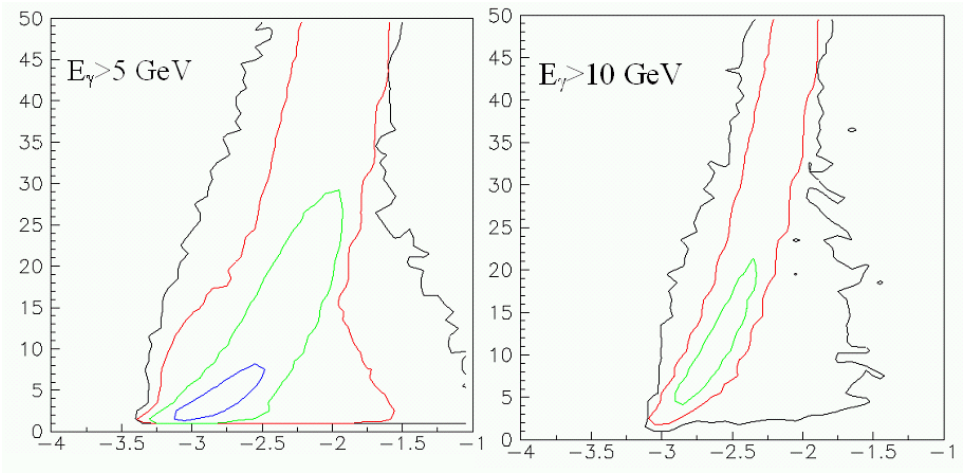

FIG. 30 figure caption

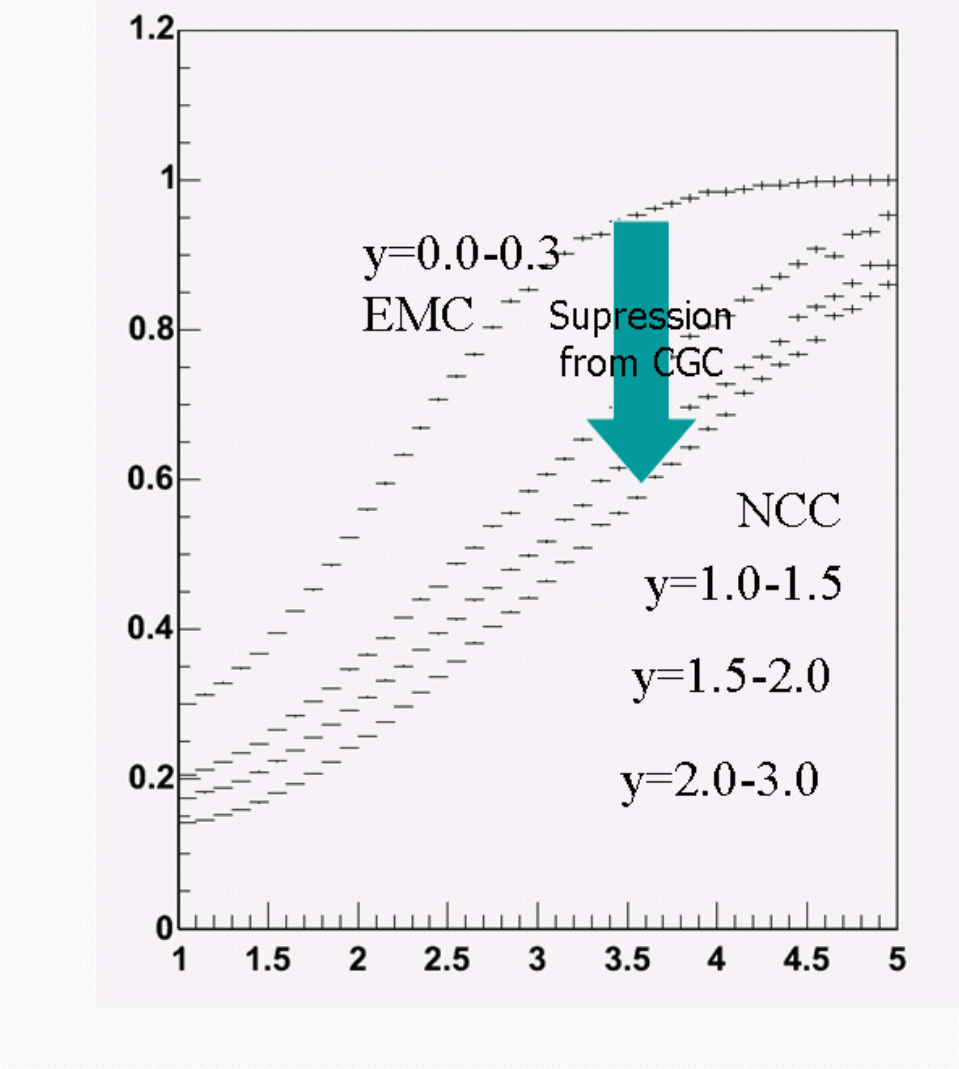

FIG. 31 figure caption

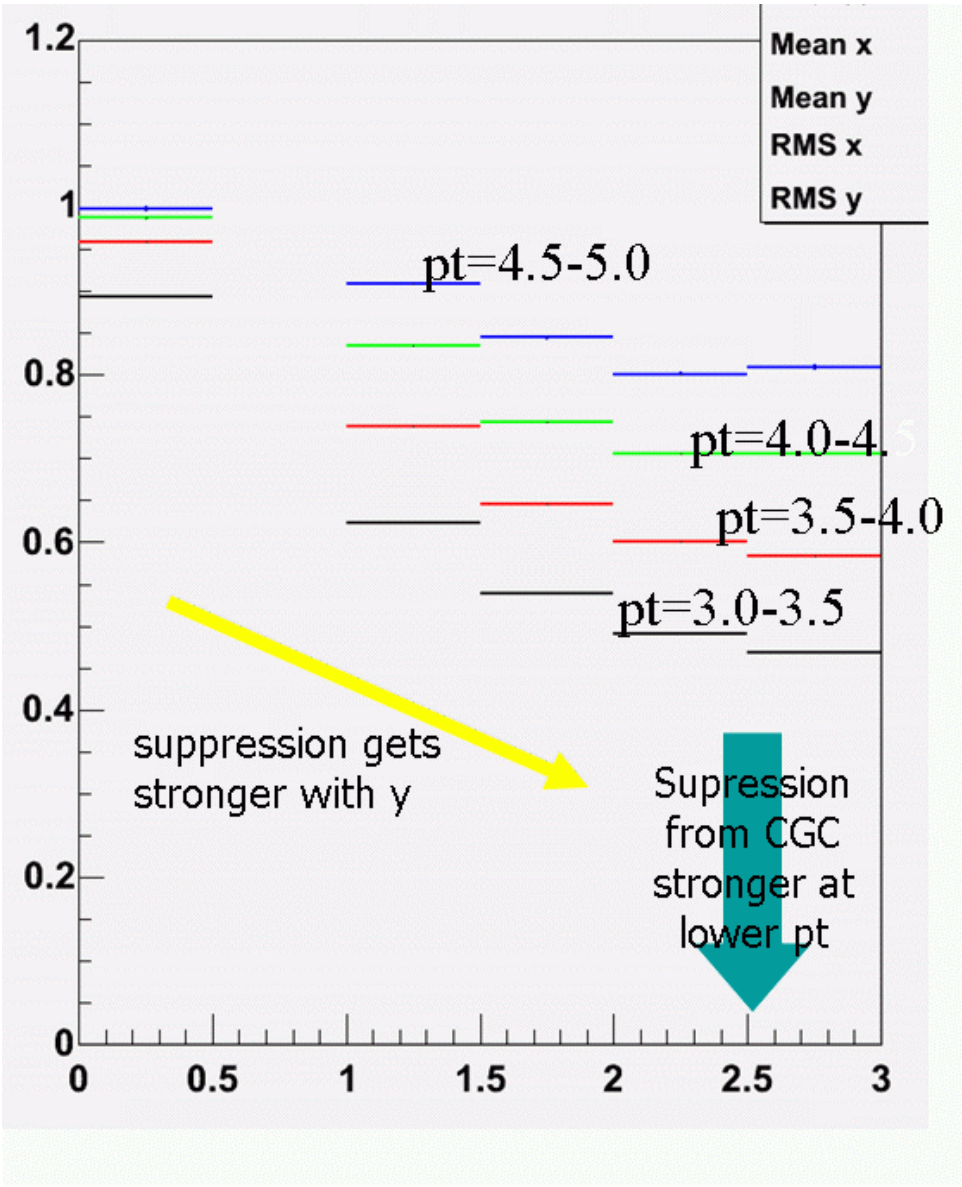

FIG. 32 figure caption

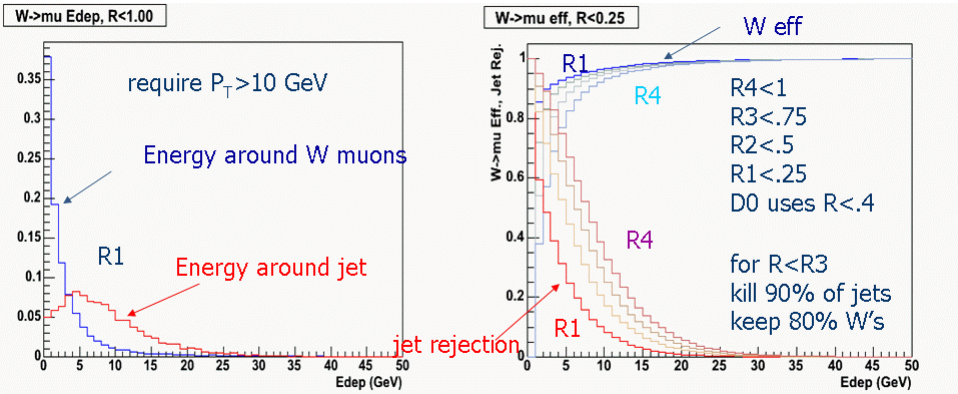

FIG. 33 figure caption

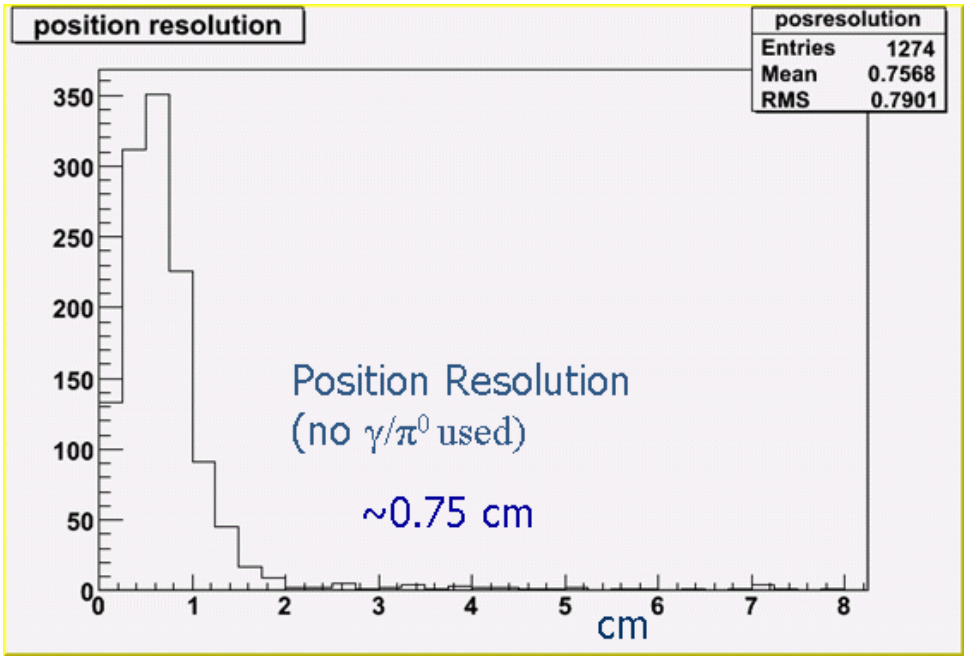

FIG. 34 figure caption

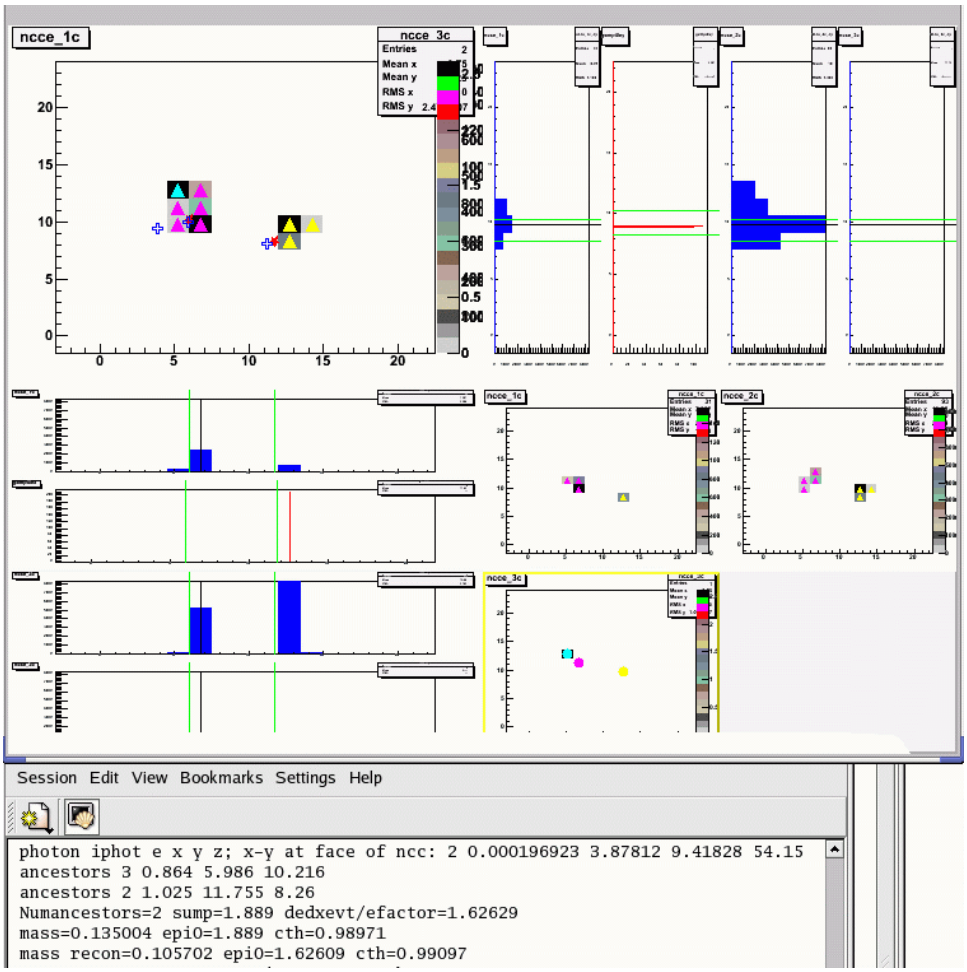

FIG. 35 figure caption

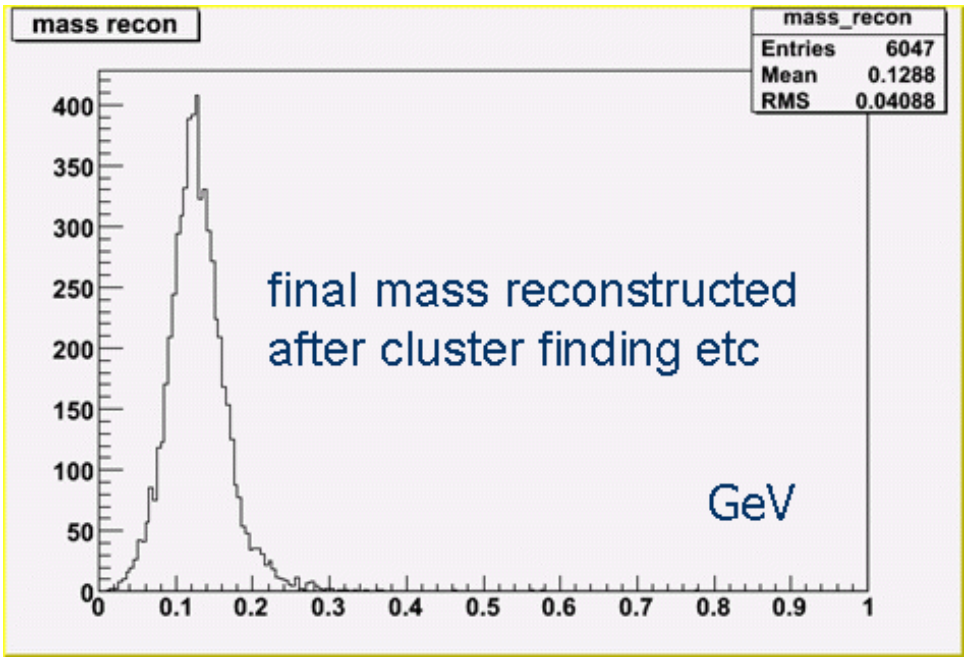

FIG. 36 figure caption

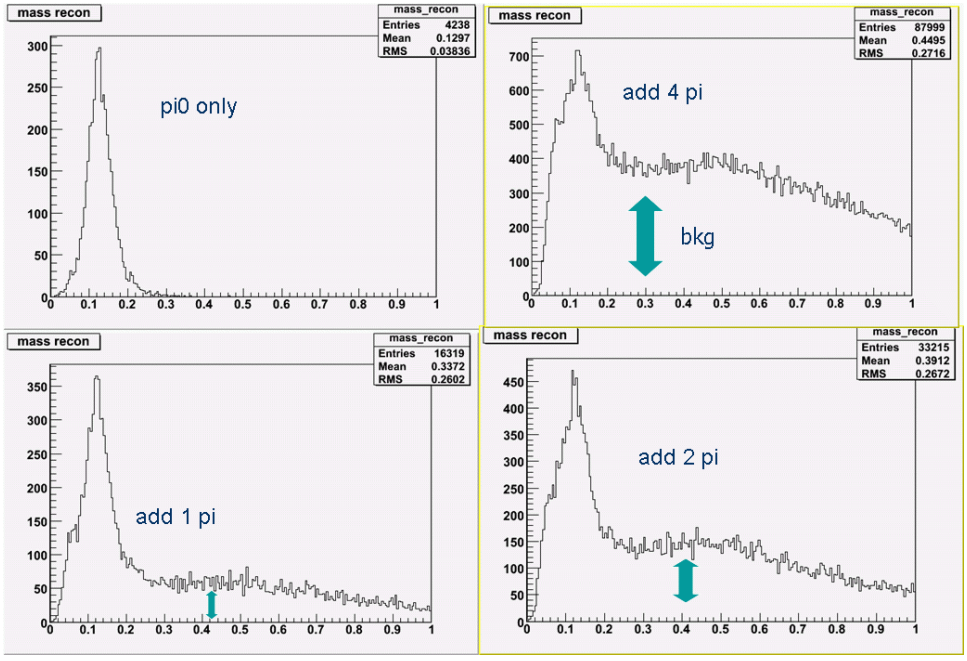

FIG. 37 figure caption

F. Simulation study of reaction plane with NCC

The NCC detector is defined and installed in PISA geant simulation to replace the entire nosecone. Using the given geometry, a single particle simulation with charged and neutral pion was performed to prepare a mapping file, which covers full phase space (rapidity, p_T, phi) with uniform distribution first. The mapping file is then used in the 2^{nd} step of simulation, which include realistic multiplicity (charge pion and pi0) and flow (v2) depending on pT and rapidity. Therefore, the back- grounds from other detector elements as well as NCC itself are included. The figure.1 shows overlay of several single track events.

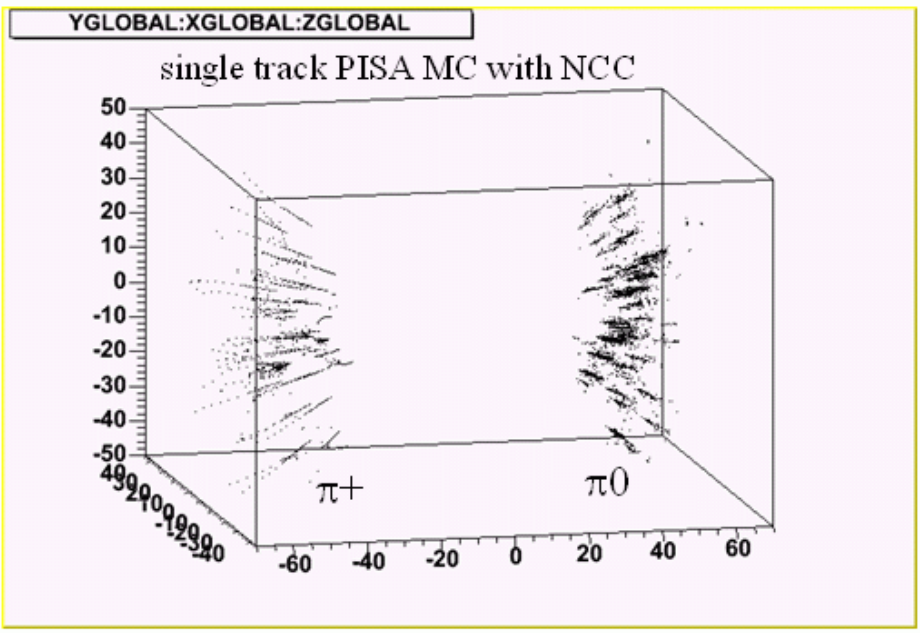

FIG. 38 figure caption

Input flow values and multiplicity used in the 2^{nd} step of simulation are shown in figure.2. The top 3 panels in the figure.3 show hit position in x-y on the NCC detector for 3 different z sectors, the first electro-magnetic sector (EM1) and the second electro-magnetic sector (EM2) after gamma/pi0 ID strip layer and the third hadronc sector (HAD). The radial hit distribution, azimuthal hit distribution with respect to the generated primary track and azimuthal hit distribution with respect to the simulated reaction plane orientation are shown in the bottom three panels in the figure.3.

The figure 4 shows the reaction plane distribution ($\Phi_{calc} - \Phi_{true}$) with different weighting methods described in the figure caption. The bottom panel shows the reaction plane

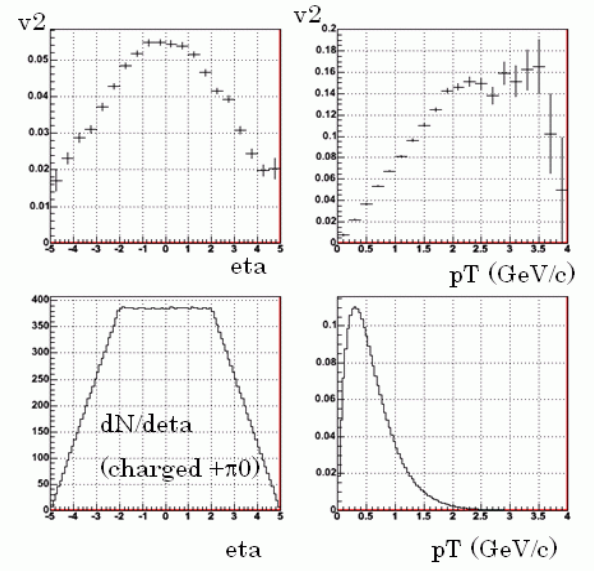

FIG. 39 figure caption

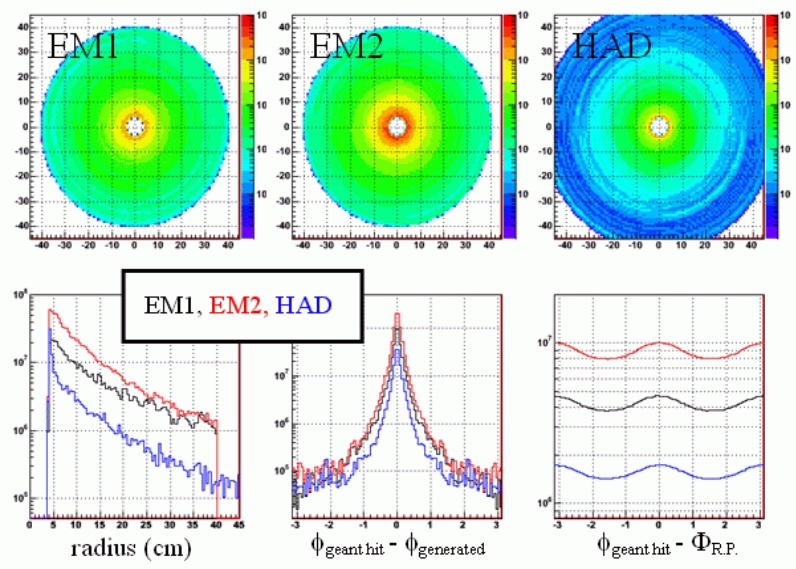

FIG. 40 figure caption

resolution with different cases, where the conditions marked with circle are described in the following. (1:black) BBC or central arm reaction plane resolution is about 0.4, (2:black) use all charged particles in NCC acceptance, (3:black) use all geant hits in NCC, (4:red) weighting all the geant hits with dE/dx, (5:green) v2 weighting according to eta dependence of v2 in addition to (4), (6:blue) z sector depending weight in addition to (5), (7:pink) 2 dimensional r, z weight in addition to (5). The resolution goes up from about 0.8 in the

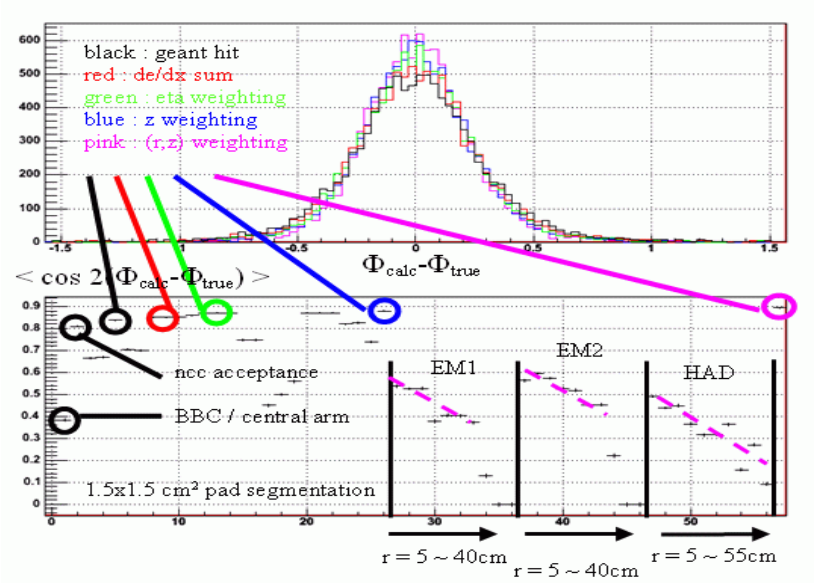

FIG. 41 figure caption

case (2) with charged particle alone to about 0.9 case (7) by including $\pi 0$ conversion, dE/dx weighting and optimizing the weight. The three regions in the bottom panel show the radial dependence of the reaction plane resolution for each z sector, the pink dashed lines show parameterized function of radial dependence of resolution, which is used to weight each reaction plane to get the best resolution in the case (7).

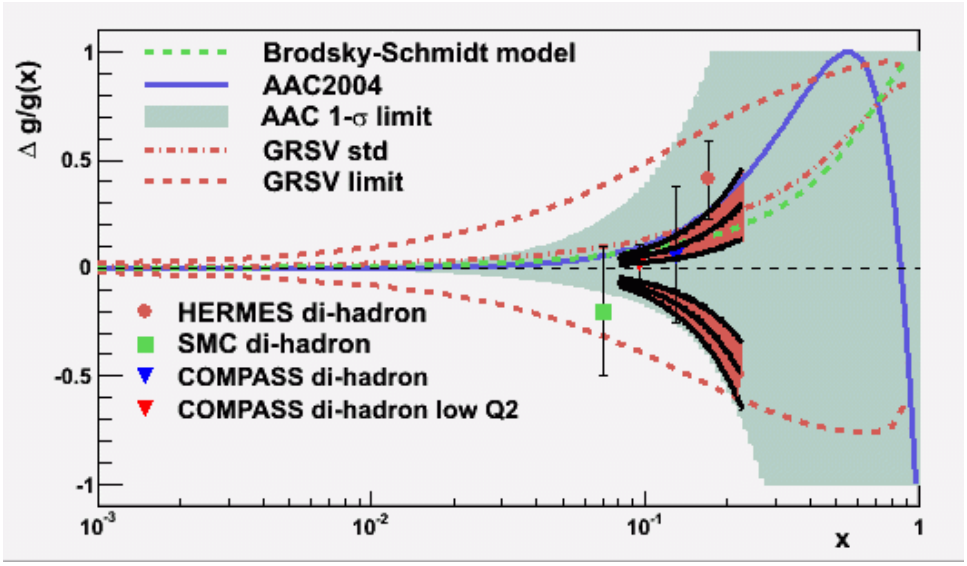

FIG. 42 figure caption

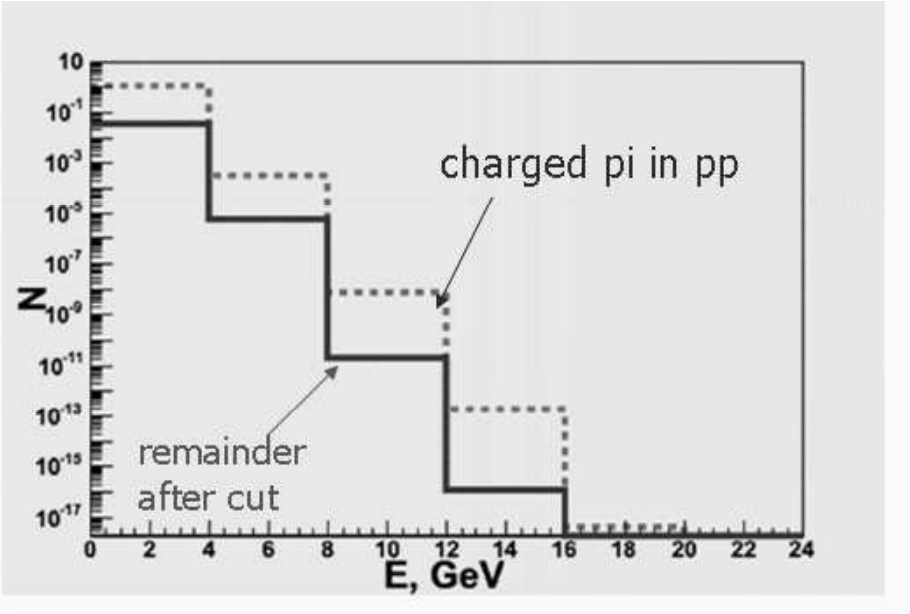

FIG. 43 figure caption

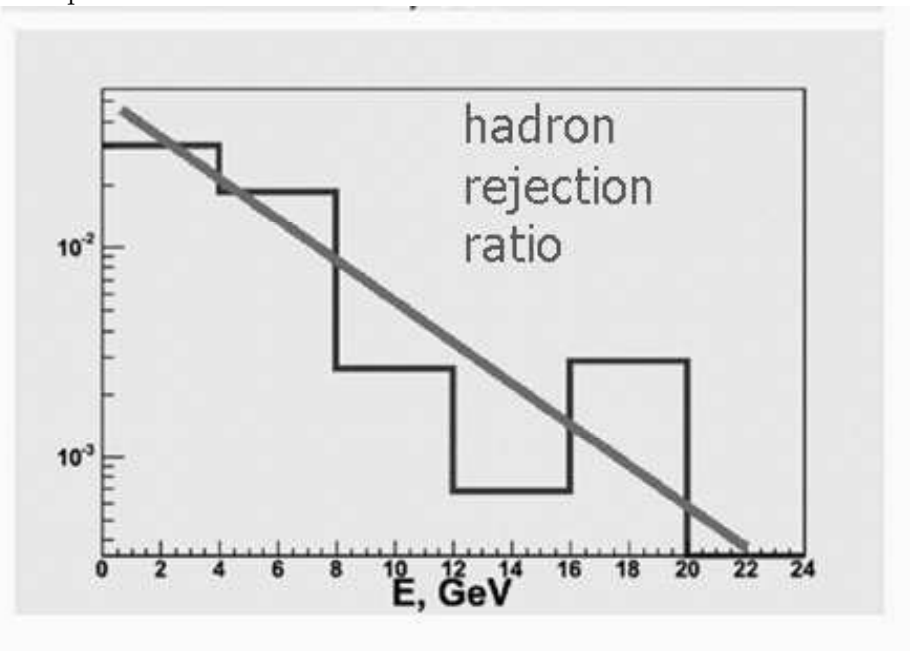

FIG. 44 figure caption

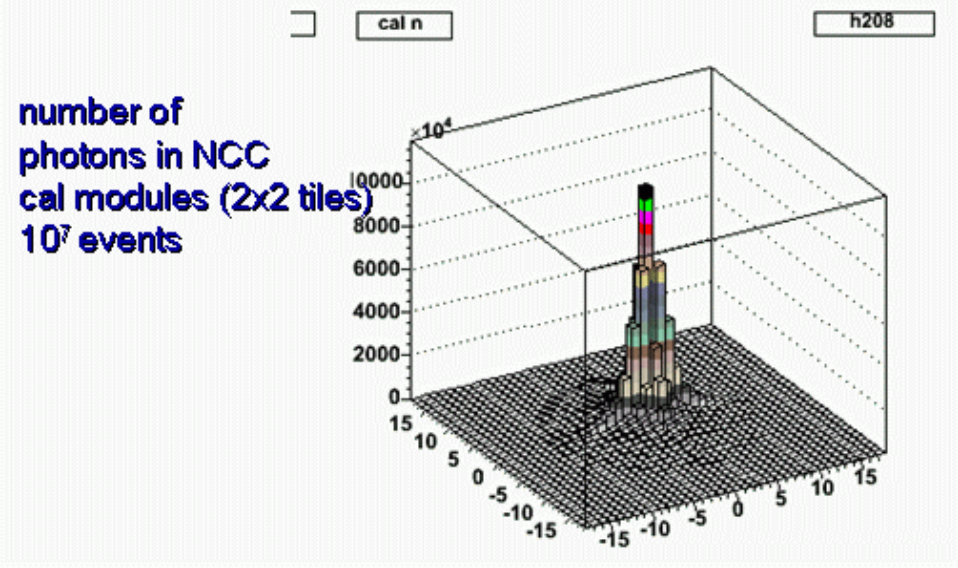

FIG. 45 figure caption

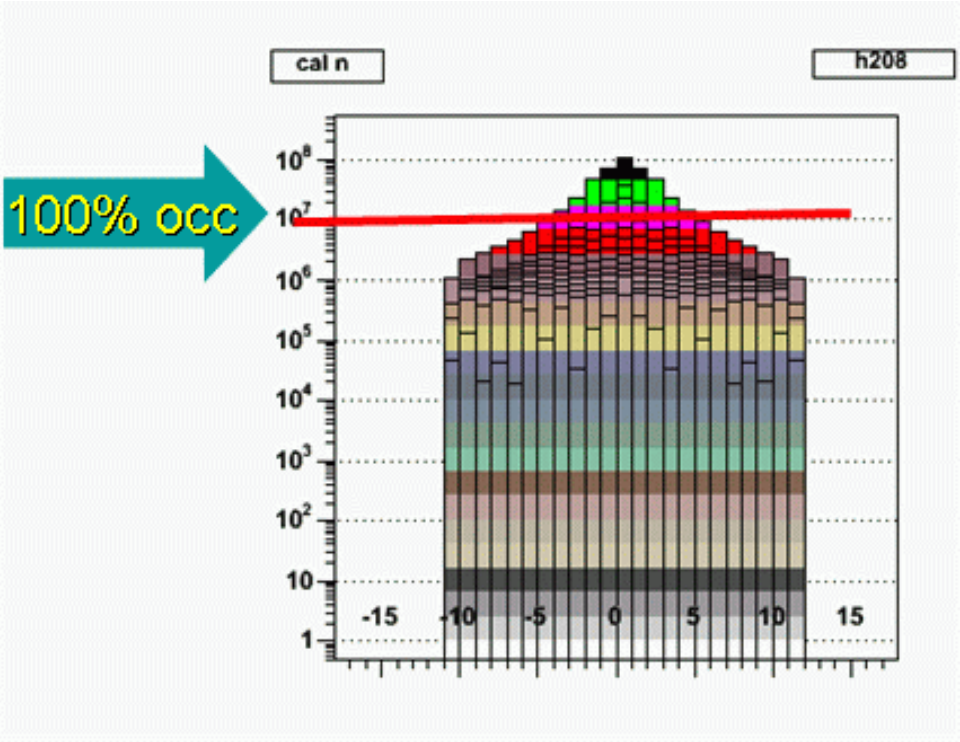

FIG. 46 figure caption

IV. THE DESIGN OF THE NOSECONE CALORIMETER

A. Overview

The PHENIX [1,2] detector (Fig. 47) is designed to perform a broad study of nucleus-nucleus (A-A), proton or deuteron nucleus (p-A or d-A), and proton-proton (p-p) collisions to investigate nuclear matter under extreme conditions and spin dependent structure functions. The needs of the heavy-ion and polarized-proton programs have produced a detector with unparalleled capabilities. PHENIX measures electrons muons, photons, and hadrons with excellent energy and momentum resolution. The PHENIX detector utilizes global detectors to characterize the collisions, a pair of central spectrometers at mid rapidity to measure electrons, hadrons, and photons, and a pair of forward spectrometers to measure muons. Each spectrometer has a geometric acceptance of about one steradian and excellent particle identification.

The proposed forward spectrometer upgrade will introduce new detector elements in the forward direction which will result in a ten-fold increase in rapidity coverage for charged hadrons and photons. This upgrade will provide us the access to the physics observables that are to date not accessible to PHENIX or available only indirectly with very limited accuracy. Forward production of inclusive jets, direct photons or Drell-Yan pairs at large xF in nucleon-ion collisions at RHIC will provide a new window for the observation of saturation phenomena expected at high parton number densities [3, 4]. In addition these upgrades will give greater coverage for the direct photon-jet measurements, critical to the measurement of the spin dependent structure functions, and photon decays of the charmonium states such as the $\chi\mathrm{C} \rightarrow \mathrm{J}/\psi + \gamma$ for the study of charmonium suppression in heavy ion collisions.

B. Upgrade Layout and NCC Configuration

Currently the PHENIX Forward (Muon) spectrometers (Fig. 47, bottom) are limited to identifying muons and measuring their momenta via the muon tracker (MuTr) and the muon identifier (MuID). The proposed upgrade to the forward spectrometers is shown diagrammatically in Fig. 48.

The three principal components to the upgrade are: 1) an enhanced muon trigger that processes signals from the R1-R3 trigger chambers which is able to recognize muons and

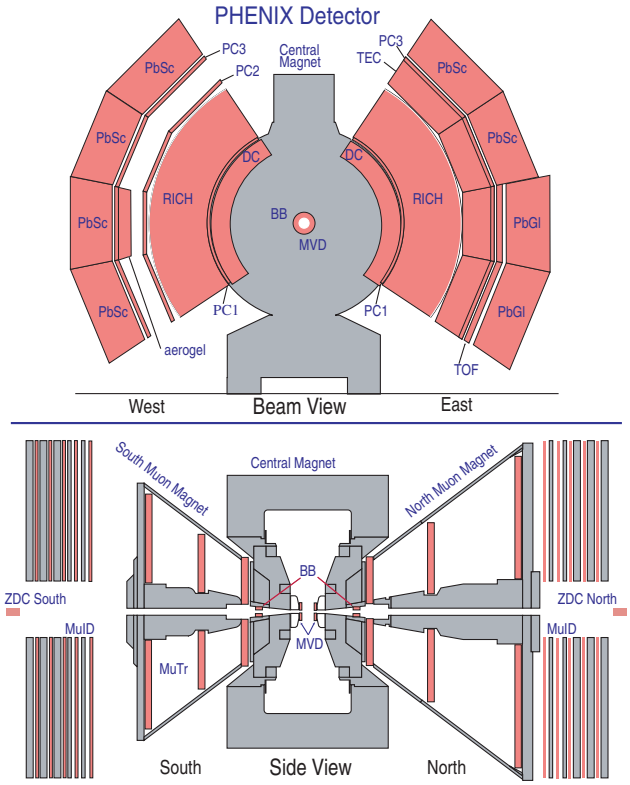

FIG. 47 A beam view (top) and side view (bottom) of the PHENIX detector in its most recent configuration. MVD - Multiplicity Vertex Detector; BB-Beam-Beam trigger counters; DC-Drift Chambers; RICH - ring imaging Cerenkov counters; PC-Pad Chambers; TEC - Time Expansion Chambers; PbSc/PbGl – Electromagnetic Calorimeters; MuTr/MuId -Muon Tracking and Muon Identification; ZDC - Zero Degree Calorimeters. There is an axial magnetic field in the central regions; the muon magnets produce a radial magnetic field.

impose cutoffs on the muon pointing and muon momenta at a RHIC rate of 10 MHz 2) a forward Si vertex detector for identifying secondary vertices (FSVT) and 3) a compact W-Si sampling calorimeter (NCC) built to identify and measure forward electromagnetic activity and provide jet identification and coarse jet energy measurements. It is this third component which is the subject of this Conceptual Design Report.Available real estate is shared between the Forward Silicon Tracking, the Central Silicon Vertexing System, Hadron Blind Cerenkov Detector and Nose Cone Calorimeter, the location of the latter is explicitly shown in the next picture (Fig. 49) presenting current PHENIX vision of the space allocation in the central region of upgraded PHENIX.

The NCC will occupy the space along the collision axis which is currently used by supplementary muon filters (NoseCones, one for each magnet pole) consisting of Cu disks 19

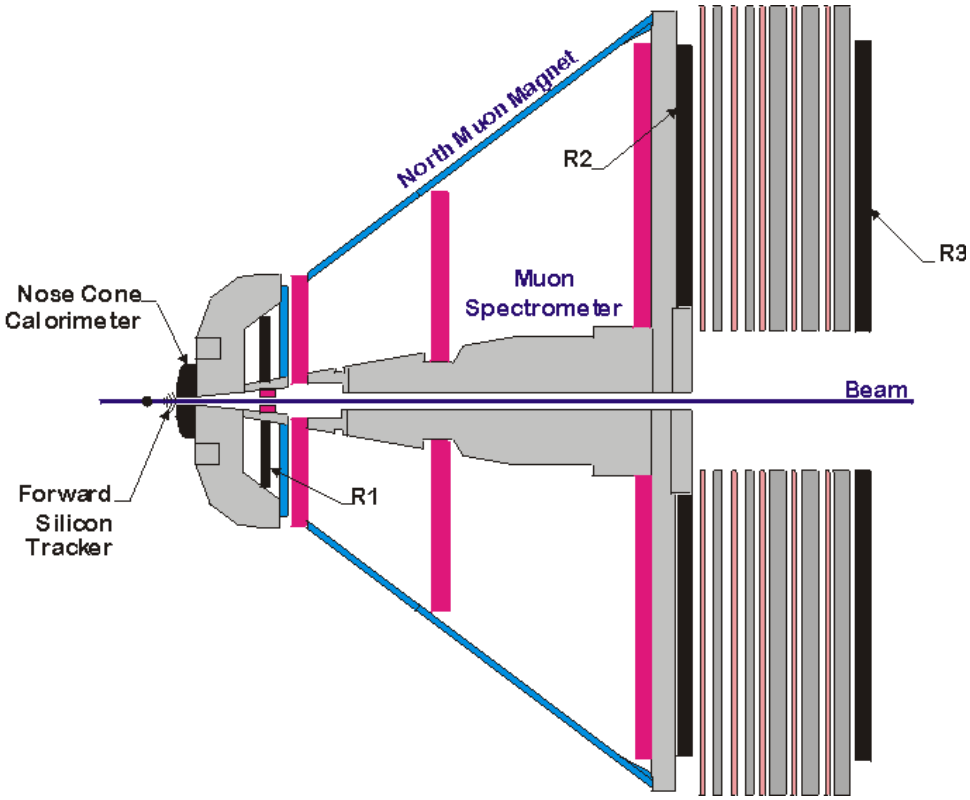

FIG. 48 Schematic rendering of the new PHENIX Forward Spectrometer. R1-R3 – resistive plate chambers built for triggering on muons.

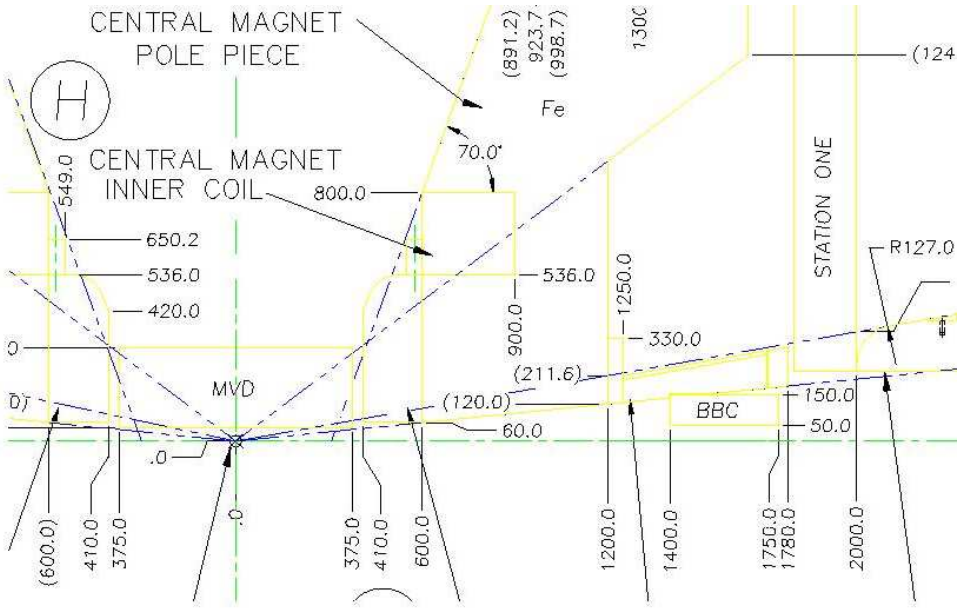

FIG. 49 Sharing of the space budget between new detectors in the central PHENIX region.

cm deep and $\sim$ 1m in diameter. The depth of the new calorimeter is chosen to fit within the envelope of the existing Cu Nose Cones. We propose to build two identical devices for the North and South Arms of PHENIX. 3-d rendering of the PHENIX central region with all new silicon-based sensing devices installed is presented in Fig. 50 below.

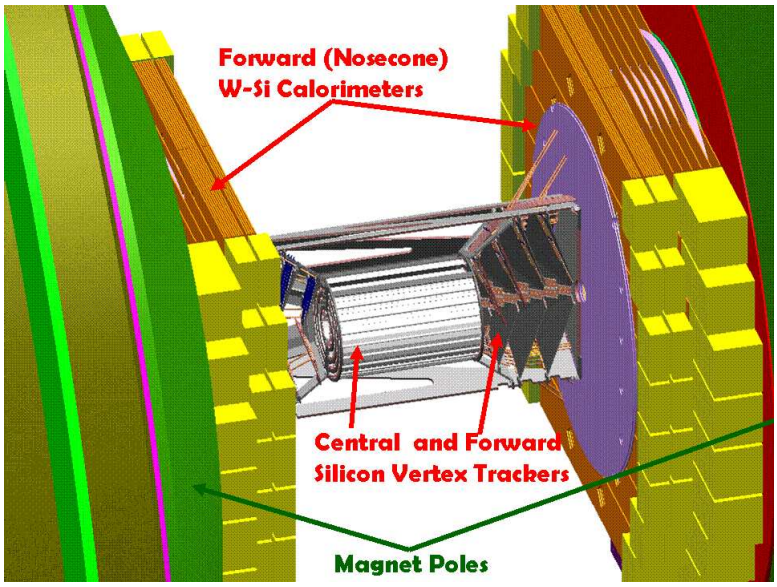

FIG. 50 3-d rendering of the new detectors employing silicon sensors in the central PHENIX region.

As a component of the PHENIX Forward Spectrometer the NCC will provide or contribute to the following:

1) precision measurements of individual electromagnetic showers;

2) $\gamma/\pi 0$ discrimination similar to the central PHENIX electromagnetic calorimeters;

3) photon/hadron discrimination;

4) jet finding , jet energy and impact position measurements;

5) data for fast triggering.

C. NCC Design considerations

The design considerations for the detector were defined as:

ability to measure electromagnetic showers with a precision comparable to the cumulative total of all systematic uncertainties characteristic to similar measurements with PHENIX central electromagnetic calorimeters (p0 effective mass resolution better then 20 MeV in the pT range above 5 GeV/c);

ability to discriminate between electromagnetic and hadronic showers in the calorimeter to the extent allowing extraction of the direct photon signal down to ∼5% of the p0 yield;

ability to reconstruct p0's via effective mass measurements and shower shape analysis to the pT extents allowed by the calorimeter acceptance and RHIC luminosity;

ability to measure shower impact vectors with resolution sufficient for efficient matching to charged tracks reconstructed by Forward Silicon Tracking;

ability to measure the total jet energy and jet vector with precision sufficient to reconstruct kinematics of the g-q hard scattering resulting in g-jet events with jets in the forward direction;

ability to measure energies inside the jet cone around high pT lepton candidates for isolation testing.

Satisfying these specifications requires a combination of highly segmented electromagnetic and hadronic compartments supplemented by high resolution position detectors located at the depth in the calorimeter sufficient to convert both photons from ?w decay with good probability (preshower detector) and measuring decay asymmetry so the efficiency of p0 reconstruction and p0 yield are correctly measured (shower maximum detector). The NCC's are located 40 cm from the nominal collision point on both north and south poles of the PHENIX central magnet and limited to the depth of 19 cm each. Building the instrumentation capable to attain required performance under constrains of PHENIX geometry requires densest known absorber material (tungsten) and the most versatile active media known to instrumentation in physics (silicon). Silicon provides for simplicity of the transverse segmentation, tungsten has a small Molier radius (9 mm) so the showers are very compact. Tungsten also has an excellent ratio of radiation and absorption lengths (Pb has even better ratio but is much to light compared to W) what is very important for em energy measurements in the presence of heavy hadronic background.

Numerous simulations have proven that even if we rely on the utmost technology in instrumentation satisfying the whole multitude of design goals can't be achieved unless reasonable compromises are made everywhere. These compromises also require priorities assigned to different performance goals. Based upon physics expectations priorities are given to particle identification (including resolving close showers) and electromagnetic energy measurements.

A few cm of tungsten will fully absorb the electromagnetic showers; hence a properly

structured 20 cm deep tungsten calorimeter can have both an electromagnetic segment and a shallow hadronic (leakage) segment. The W plate thickness and the total depth of absorber in the calorimeter are constrained by readout; it is our goal to reduce the readout space to about 2.5 mm per layer (0.5 mm silicon, 1.6 mm of pc-board, and clearance gaps).

The design of the NCC relies heavily on past experience in Si-W calorimetry [5,6,7] it is technologically challenging and nontraditional for it can't rely on momentum measurements in upstream tracking for any of particle identification purposes (in principle the integral Bdl is sufficient to identify the charge of impinging charged particle in the pT range below 20 GeV/c).

Such a calorimeter covering an area ∼0.7 m2 with towers comparable in size to molier radius will have ∼3000 silicon pixels per readout layer. A number of ongoing R&D projects aimed to build readout for the W-Si calorimeters able to digitize signals from every pixel in every sampling layers are currently ongoing mostly within the scope of preparing the experimentation for the future electron-positron linear collider. The solutions are mostly on the drawing board and prohibitively expensive. To reduce cost and complexity we decided on a solution when geometrically matching pixels from a number of sequential silicon sampling layers are ganged together and connected to the input of a single amplification/digitization circuit.

This solution allows to reduce the number of channels in the detector by x 6 (see below), to use signal amplification solutions developed at BNL Instrumentation Department for earlier projects and to solve the problem of compatibility between new detector and existing mechanical infrastructure in efficient manner.

This document is still not a final technical detector design, some of the parameters being an educated guesses based on limited simulation studies and published documents. An essential features of our design are "as good as fiscally feasible" shower shape measurements and the spatial separation of energy depositions due to photons from those due to charged and neutral hadrons reaching the calorimeter. Very limited real estate available to calorimeter naturally suggests the same lateral granularity all through the calorimeter depth easily achievable with alternating tungsten and silicon layers.

A long and painful optimization process resulted in choosing the calorimeters built of 18 pad-structured sampling layers and two layers of 2-d position sensitive pixilated strips (preshower and shower max) which will serve as a very efficient photon-p0 identifier dis-

criminating between individual electromagnetic showers and overlapping photons from high momenta p0's. The particle identification capabilities are due to longitudinal shower shape measurements in three sequential longitudinal segments (the first two are fine sampling and the last serving as a coarse leakage segment) and independent lateral shower shape measurements in three longitudinal segments and two high resolution position sensitive layers.

We have chose 3 mm W plates for the fist two fine sections based upon the following simple considerations.

In general the radial shower profile which is the main source of data to discriminate single vs multiple showers has a pronounced central core surrounded by halo. The central core effectively disappears beyond shower maximum. The radial profile integrated over the whole shower depth in different materials is shown in the Fig. 51.

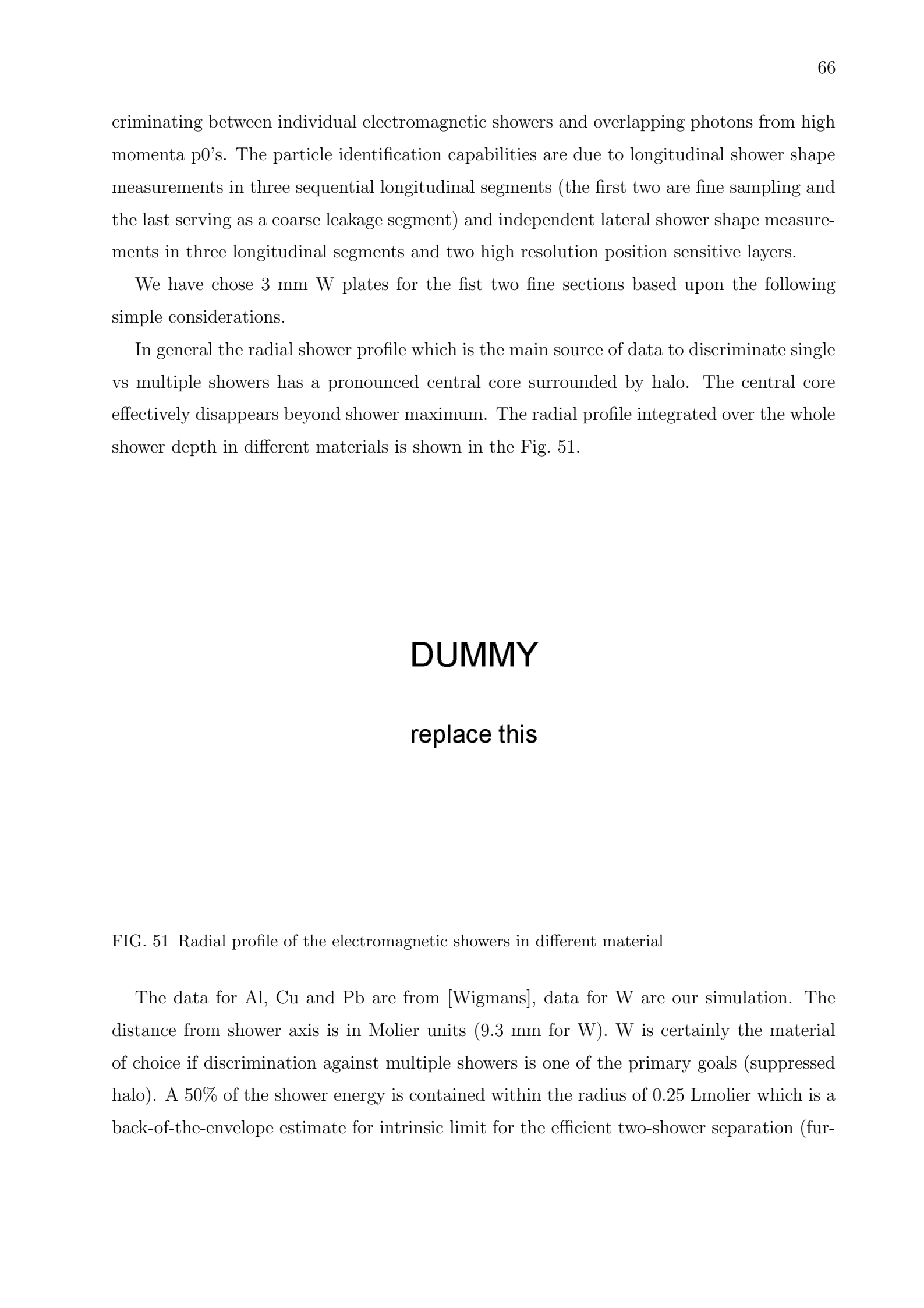

FIG. 51 Radial profile of the electromagnetic showers in different material

The data for Al, Cu and Pb are from [Wigmans], data for W are our simulation. The distance from shower axis is in Molier units (9.3 mm for W). W is certainly the material of choice if discrimination against multiple showers is one of the primary goals (suppressed halo). A 50% of the shower energy is contained within the radius of 0.25 Lmolier which is a back-of-the-envelope estimate for intrinsic limit for the efficient two-shower separation (fur-

ther improvements are hampered by fluctuations in the number of particles in the shower). The symmetrically decaying 30 GeV/c p0 will have two photons in calorimeter at a distance of the order of 5 mm (depending on the production kinematics) thus setting the upper limit to Molier radius for NCC equal to 20 mm. Technology sets a lower limit to the thickness of readout layers (carrier boards, silicon sensors, interconnects, protection) close to 2.5 mm. To keep Molier radius below 20 mm the thickness of W plates in the fine sections of calorimeter must be equal or above the same 2.5 mm value.

As it is always with energy measurements in multi-GeV range the energy resolution is driven by the sampling fluctuations, the latter (see [Wigmans]) can be reasonably well described with the following simple formula:

$$\frac{\sigma}{\sqrt{E}} = c\sqrt{d/fsampl},$$

where the thickness d of the active layers is in [mm] and fsampl is the sampling fraction for MIP's. The collection of the data presented in the Fig. 52 exacted from the same reference agree well to this parametrization (within 10%) with coefficient c $\approx$ 2.7%.

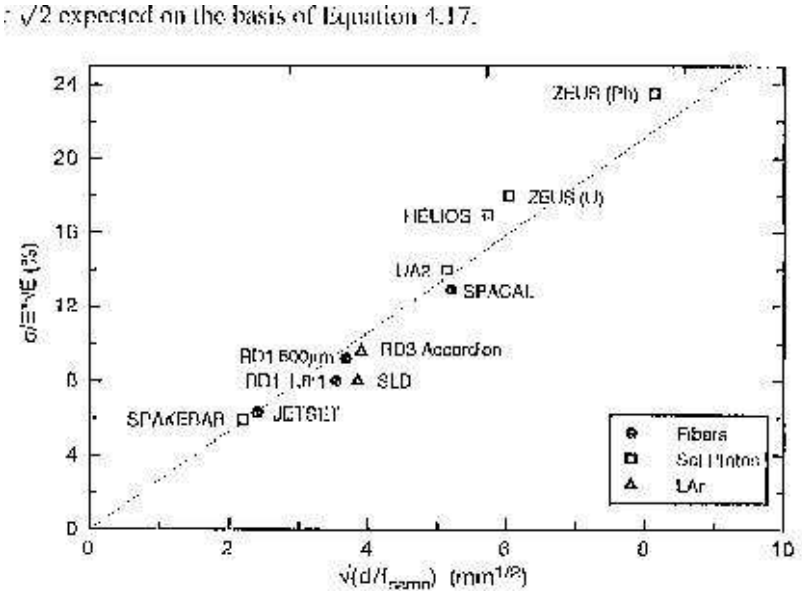

FIG. 52 Compilation of data on energy resolution of the sampling electromagnetic calorimeters [Wigmans].

The calorimeter built of 2.5 mm W plates and 2.5 mm readout layers (525 mm Si sensors) will sample approximately 2.9% of energy left in the calorimeter by minimum ionizing

particles resulting in the energy resolution close to

$$\frac{\sigma}{E} \simeq \frac{25\%}{\sqrt{E}}.$$

The NCC is supposed to discriminate electromagnetic and hadronic showers based upon shower shape measurements only. To make this approach effective it must retain its declared energy resolution towards the limit set by physics (requires reasonable longitudinal containment within fine sections for electromagnetic showers) and a total shower energy measurement (including hadronic showers) well downstream of the total depth required to contain electromagnetic showers. We propose to build electromagnetic segments of 3mm W/2.5 mm readout sampling cells. 12 sampling cells combined with 2 Lrad upstream converter comprise close to 12 Lrad electromagnetic calorimeter with energy resolution $\sim 27\%/\sqrt{E}$ sufficiently deep to contain at least 90% of the electromagnetic shower energy. Two layers of precision position sensitive silicon detectors will be located downstream of converter and between two fine sections (at approximately a shower max depth) to discriminate single vs multiple photons and to measure decay asymmetry. A single calorimeter tower thus structured is sketched in Fig. 53.

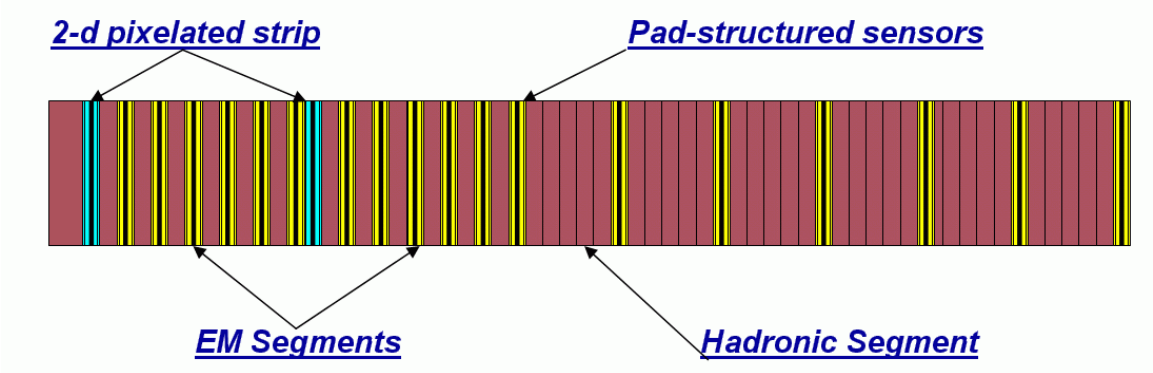

FIG. 53 Longitudinal structure of a single calorimeter tower.

The relative shallowness of the electromagnetic segments also serves to suppress the hadronic contribution to the energy seen in the electromagnetic calorimeter. Thus the third leakage segment serves the dual purposes of a hadronic energy identifier and shower tail catcher. The leakage section is structured following the pattern used in the fine electromagnetic sections: six sampling cells of a lateral size identical to that in em sections. It will (1) assist the energy measurements of photons at the extreme upper end of the spectrum);

(2) serve as an effective em/hadronic discriminator tool; and (3) assist with low grade jet energy measurements .t Leakage section will use all remaining available longitudinal space within 19 cm real estate currently reserved for calorimeters. Subtracting the space needed for 2 Lrad converter, two 5 mm thick layers of position sensitive detectors and twelve 5.5 mm sampling cells which comprise electromagnetic calorimeter the space left for leakage compartment is equal to 10.7 cm. (6 cells of 15 mm W and 2.5 mm Si readout layers).

The total depth of calorimeter seen by particles at normal incidence is ∼42 Lrad or 1.6 absorption length. A short summary of the calorimeter design features is in the Table II (all counts are for a single calorimeter unit).

1. NCC Performance Considerations

Simulation

Shower containment and energy resolution

Shower identification and hadron rejection

P0 reconstruction

Prompt lepton isolation

Jet finding and reconstruction

The four panels in the Fig. 54 illustrate different aspects of the NCC design and performance directly related to the PHENIX experimental goals. The top right panel is the NCC photon energy resolution (in GeV) plotted as function of $\sqrt{E}$. The resolution is a linear function of $\sqrt{E}$ with a 20% slope up to the energies of a few tens of GeV and slightly degraded compared to this function when energy leakage to the coarse hadronic compartment becomes substantial.

Most of the electromagnetic energy stays in the electromagnetic compartments, the depth and position of those compartments with respect to shower profile are chosen to insure the linear dependence of the energy deposited in the downstream electromagnetic compartment on the momentum of the impinging photon. (A trigger on electromagnetic energy can be based upon hits in the first compartment only).. Comparable lateral and longitudinal dimensions of the individual sub towers in electromagnetic and hadronic compartments allow for independent position measurements in every compartment and provide some degree of pointing capabilities. Geometrically very shallow subtowers help to minimize the underlying

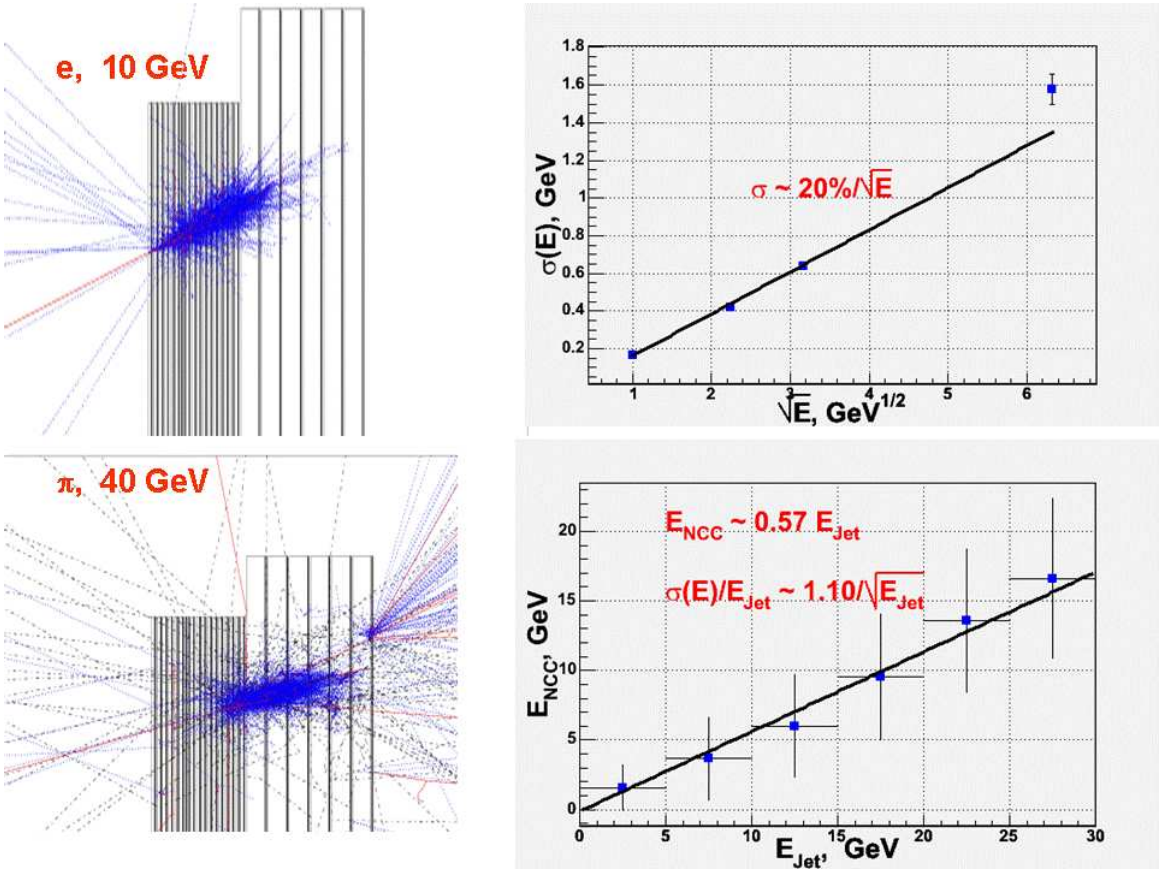

FIG. 54 caption

event contribution to the measured shower energy and improve two shower separation at extreme impact angles.

Space constraints limit the total depth of calorimeter to less then 2 Labs resulting in a substantial leakage of hadronic energy into the iron of the magnet pole backing the NCC. Comparison between energies of simulated jets and those seen in NCC (sum of energies scaled by respective sampling fractions) presented in the bottom right panel in Fig. 54 shows that jet energy measurements in this calorimeter are certainly limited by fluctuations in the amount of energy lost from leakage section. Preliminary estimates predict a jet energy resolution of about $110\%/\sqrt{\mathrm{E}}$ Fig. 54. While jet energy measurements will have only limited validity, the fine lateral segmentation of the calorimeter will allow the measurement of the jet space vector with resolution fully satisfactory to reconstruct the kinematics of hard scattering.

It is worth noting that a tungsten calorimeter with a shallow electromagnetic compartment will have little hadronic energy deposited in that compartment. Electromagnetic showers within a jet cone identified by the energy pattern in the first two compartments will be

Parameter		Value	Comment
Distance from collision vertex		40 cm	
Radial coverage		50 cm	
Geometrical depth		$\sim$ 19 cm	
Absorber		W	42 Lrad or 1.6 Labs
Readout		Si pads (15x15 mm2) and pixeleted strips (.0.5x0.5 mm pixels grouped into 60 mm long strips)	
Calorimeter		EMC(12 sampling cells: 3mm W + 2.5 mm readout) longitudinally structured into two identical non-projective sections. Leakage(6 sampling cells: 15 mm W + 2.5 mm readout)	
Preshower detector (PS)		2 Lrad W converter followed by a stripixel layer (0.5 mm strips) with 2-d readout	
Shower max detector (SM)		In between two EM sections at $\sim$ 7 Lrad depth. Stripixel layer (0.5 mm strips) with 2-d readout	
Sensors		calorimeter	3192 (12 x 168 + 6 x 196)
		PS and SM detectors	336 (2 x 168)
Channel count		calorimeter	8152
		PS and SM detectors	86016 (672 SVX4 chips)
Multiple scattering in NCC combined with Fe magnet pole		133 MeV	To compare with 106 MeV in the existing configuration with Cu NoseCone
Expected EM energy resolution		$27\%/\sqrt{E}$	
Expected jet energy resolution		$100\%/\sqrt{E}$	
Two showers resolved at	in calorimeter	3 cm	
	in preshower	2 mm	
	in shower max.	4 mm	

TABLE II Nose Cone Calorimeter design featues

used to improve jet energy resolution and to study modifications to jet fragmentation in nuclear matter.

A difference in the shower penetration and longitudinal shower shape serve a basis for hadron suppression and allow the NCC to be used as standalone photon identifier Fig. 55.

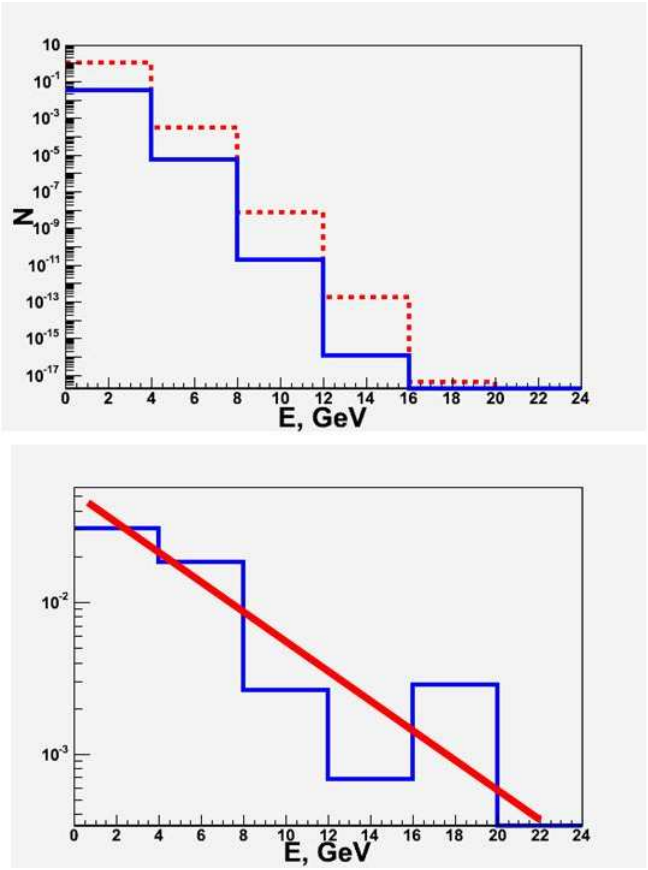

FIG. 55 Momentum spectrum of charged pions hitting the NCC in hard scattering pp events at $\sqrt{s}$=200 GeV simulated with PYTHIA (top panel – dotted histogram) and the energy spectrum of hadronic showers passing the shower shape test applicable to electromagnetic showers (top panel – solid histogram). Testing is based solely upon longitudinal shower shape. The ratio of the two histograms indicating the level of suppression of charged hadrons using this method is shown in the panel at the bottom.

The momentum spectrum of hadrons in this picture (bottom histogram) was normalized to the average hadron multiplicity in NCC. Consequently the solid histogram on the top panel can be interpreted as an expected per event multiplicity of fake electromagnetic showers. This value is to be compared to the corresponding numbers for direct photons. The latter can be estimated from PHENIX published data on $\pi 0$ and direct photon production

in pp interactions at 200 GeV [8,9]. In the pT range above 6 GeV/c where direct photon yield exceeds 10% of the $\pi 0$ yield ($\sim$5% of the charge hadron yield) fake electromagnetic showers are less then 1% of the total hadronic yield corresponding to direct photon to fake electromagnetic showers ratio better then 10%.

Since the NCC is located only 40cm from the nominal collision vertex, the job of separating single isolated photons from overlapping photons from $\pi 0$ decays is extremely challenging. The NCC design incorporates a $\gamma/\pi 0$ identifier built of Si strips 0.5 mm wide. Simulations show that two shower separation will be possible down to the impact point separation $\sim$2 mm corresponding to $\pi 0$ momenta $\sim$ 15 GeV. We will explore all potential algorithms for reducing the $\pi 0$ background to single photons such as independent handling of data in all three longitudinal sections to control the lateral shower shape. However we do not expect further significant improvements to two shower separation unless the granularity is substantially increased.

2. NCC Dynamic range considerations

In NCC the energies of the showering particles will be shared between thee segments of the calorimeter. In principle this sharing is uneven, most of the electromagnetic energy will be deposited in the second, most of hadronic energy in the third or leakage section. Accounting for fluctuations and lateral energy sharing it is sufficient to set the upper limit of dynamic range per tower per section close to $\sim$ 60% of the W mass to cover the whole range of physics topics we are planning to study in pp-interactions at a 1 TeV collision energy.

Since the NCC is close to the production vertex, the calorimeter will need to work in at high occupancy, especially in central Au-Au collisions. The calculations were made assuming that any shower in the calorimeter would always fire a base matrix of 3x3 towers and 3 neighboring strips in the SMD. The strips and towers were assumed to be of a similar surface area ($\sim$200 mm2) what is grossly exaggerated for the SMD version as per this proposal. The resulting radial (from the beam) dependence of the probability for strips in the SMD and towers in the calorimeter to see event related energy is plotted in Fig. 56 below.

In pp collisions, conditions similar to those in the central calorimeter are reached at a radial distance of 10 cm hence the entire calorimeter area will have a reasonable occupancy.

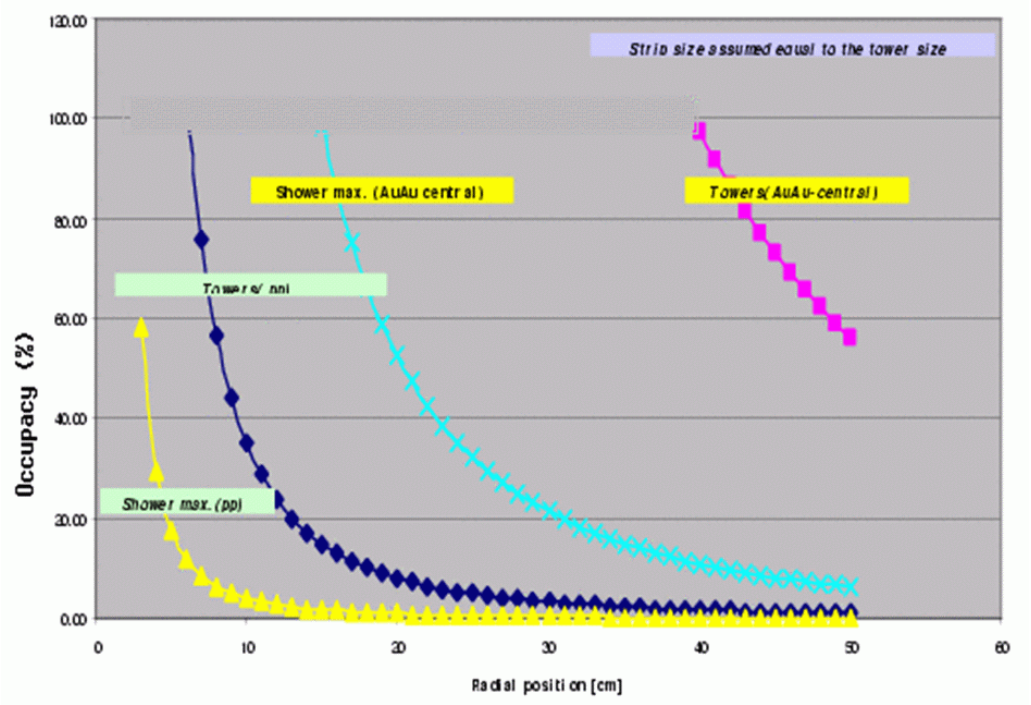

FIG. 56 Probability for Tower in NCC and strip in SMD to be fired (occupancy) in pp and AuAu collisions in PHENIX as function of the distance from the beam pipe.

The beam pipe assumed to be 4 cm in diameter. Running conditions are certainly less favorable in AuAu collisions where the calorimeter will be heavily occupied by the showers due to soft secondary particles. The SMD occupancy still stays relatively low for cluster counting and impact point measurements in the calorimeter allowing jet finding based upon hit occupancy even in the events of highest multiplicity. Energy measurements in AuAu collisions will be strongly affected by the pileup from underlying events resulting in higher threshold values and additional inefficiencies. Similar problems are seen in the present central calorimeters. Jet measurements are certainly the most challenging part of NCC program. Multiple approaches such as threshold selected hit counting, energy profiling and energy flow should be tried. The next figure (Fig. 57) is a crude example of what to expect in pp collisions.

Depending on the rapidity, a 4 GeV/c transverse momentum jet in the NCC acceptance window will have a total energy of 8 GeV to 80 GeV. It will be seen in the calorimeter with very little pileup contribution up to ∼2.5 units of rapidity and will start merging with the underlying event only at rapidity ∼3. In pp collisions a dense relatively shallow calorimeter will see high pt jets as easily identifiable, narrow peaks in the energy profile. Due to the

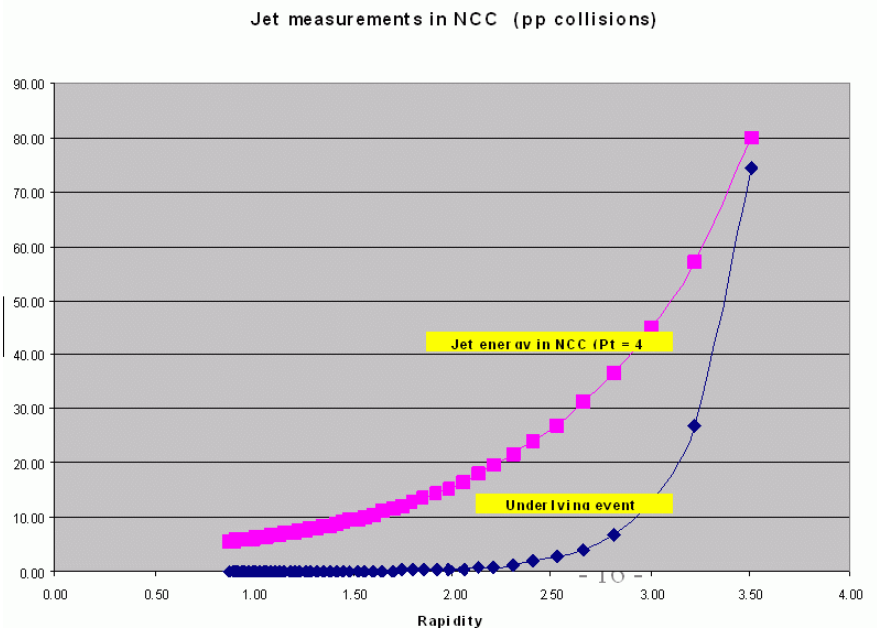

FIG. 57 Effect of the underlying event on the jet measurements in the Nose Cone Calorimeter in pp collisions at RHIC.

background from underlying events in Au-Au collisions, there will be more smearing to the energy profile which will move the threshold for identifiable jets to somewhat higher transverse momenta.

D. NCC Mechanical design

A modular NCC design emerged as an outcome of a study of a different approaches to mechanically structuring future detector is illustrated in Fig. 58.

The calorimeter is designed of "bricks", two kinds of bricks (see Fig. 59) used to build two quasi-independent calorimeters: shallow electromagnetic and coarse hadronic (leakage). All bricks are single sensor wide, there are three standards for the brick length in electromagnetic and hadronic sections (7/6/5 sensors in hadronic, 6/5/4 sensors in electromagnetic sections). Readout-wise the electromagnetic bricks are much more demanding compared to hadronic. Electromagnetic brick will house converter, preshower detector, shower max detector and two electromagnetic segments, hadronic brick will consist of a single hadronic segment. Each brick has a W plate facing upstream and Cu skin locking it on all other sides except one for connections to external electronics boards.

When assembled bricks will form two vertical walls, small locking pins will be used to

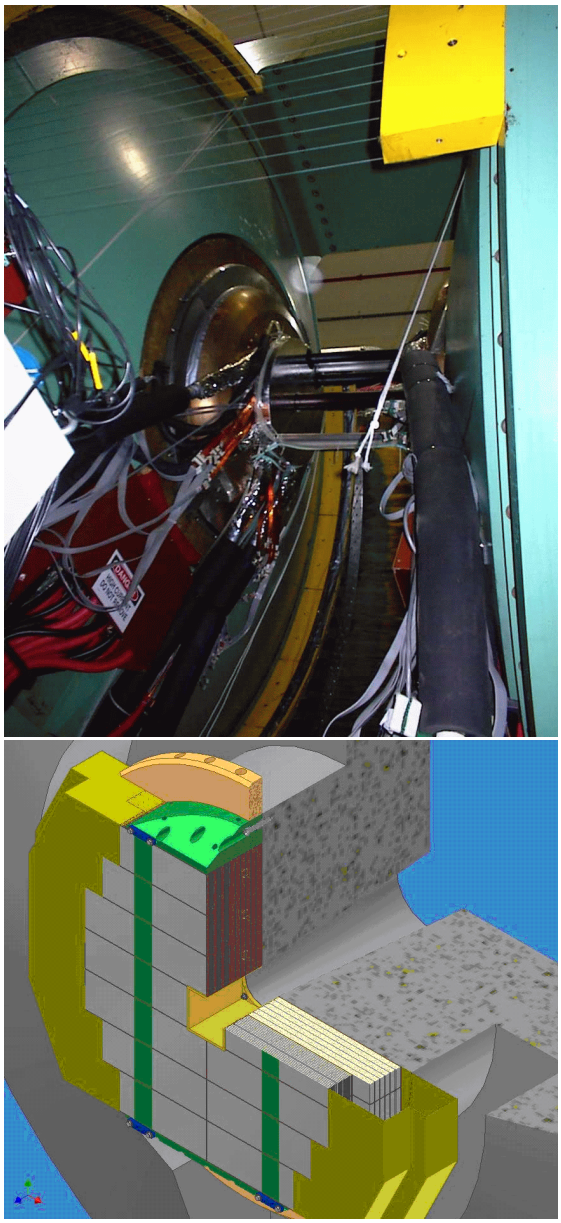

FIG. 58 PHENIX Nose Cone (left panel). Nose Cone Calorimeter (right panel). Boxes upstream are with electromagnetic segments, downstream boxes are leakage segment. Air plenums housing preamplifiers are also shown.

maintain the geometry. For mechanical reasons the two walls will have the same size vertically (giving up some of the hadronic acceptance), horizontally hadronic wall is two sensors wider compared to electromagnetic wall. This geometry allows to minimize the cost while keeping all light rays from the nominal collision point to the currently existing brass cones within calorimeter structure. Calorimeter walls are supported by two (bottom and top) shelfs and thin pretensioned front braces (strips of stainless steel or kevlar) preventing walls

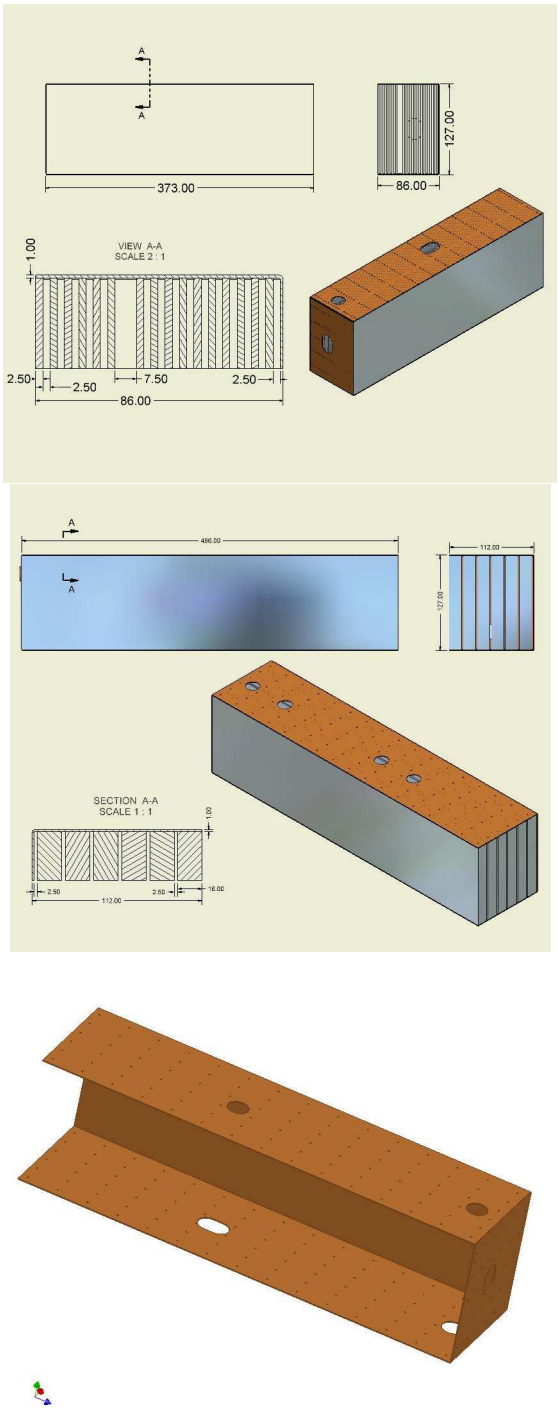

FIG. 59 NCC building bricks. Left – electromagnetic. Wide gaps indicate locations for preshower and shower max detectors. Center – hadronic (leakage). Cu skin for the electromagnetic brick is shown on the right.

from buckling out.

1. NCC Silicon Sensors

The main requirements for the silicon detectors in the calorimeter are reliability, precise shower energy measurements via charge measurements in silicon, precise tracking measurements, and radiation hardness. The solution to the problem is arranged using multilayered device built of pad-structured layers organized into towers in readout and strip-structured layers (pixelated strips in our case) to track individual charged particles and resolve close showers. The pad size chosen for NCC is 1.5x1.5 cm2, the strip size is 0.5x60 mm2, all silicon detectors in NCC are 6x6 cm2 diced of 4" wafers 525 mm (pad structured) and 600 mm (stripixels) thick. Critical to the success of the experiment will be reliable operation of these sensors in a radiation environment. The estimates based upon total energy flow simulation predict the total fluence of 100 kRad (in Si) or about 3*1012 equivalent neutrons per cm2 over the period of 10 years (assuming pp interactions at 200 GeV with luminosity ∼2 1032 s-1cm-2). For a pad size of the order of a few cm2 and 300 mkm sensor thickness, published data predict the leakage current of the order of 5 – 10 mkA per pad. Handling this value of current definitely requires decoupling capacitances being present between pads and preamplifiers,

For the operation of the detectors the control of leakage current is important not only because it leads o increased noise. It may also result in the increased bulk heat production in silicon which may lead to thermal runaway if the silicon detector is not cooled. In our design of sensors and selection of raw material we were guided by the experience and work done within the scope of D0 (FNAL) and ALICE (LHC) projects and recent published data from the research and development in the radiation hard silicon technology. In particular we followed few simple and well known rules:

single sided sensors from established vendors to insure higher yields and less trouble due to simplicity of the design. It is also well known that double sided sensors are the once suffering radiation damage;

minimal number of different sensor designs (only two in NCC case);

design to successful completion of he project using single vendor. Transfer the design to additional vendors when ready. This will speed production;

use short strips to reduce the number of ghosts hits otherwise creating pattern recognition hassle (we use 4" wafers only);

avoid double metalization. Reasons are not 100% clear, but we followed this recommendation too;

special designed guard ring structures. Such guard rings are important in order to keep breakdown voltage before and after irradiation as high as possible.

In short for the construction of the Nose Cone Calorimeters we will use the single–sided single-metal p+ on n-bulk silicon devices. We also to have an integrated polysilicon resistors on the sensors to simplify the test procedures (sensor can be fully depleted using two lines only) and to minimize the real estate used by external RC chains to DC couple detectors to readout electronics (crucial in the strip sensors). Two kinds of sensors are used to construct NCC's : pad structured and pixilated strips. They both will be described in more details below. The pad-structured sensors has many prototypes, this technology is well tested and we already have three established vendors ready to manufacture the 6x6 cm2 pad-structured sensors using common design files (corrected for specifics of technology). The pixilated strips (stripixels) are novel detectors developed at BNL and currently selected as a base design for silicon sensor for the PHENIX central silicon tracker. The design chosen by PHENIX are interleaved stripixel detector where each pixel is divided into two parts: X-cell (or pixel) and Y-cell. X-strips and Y-strips connect X-cells and Y-cells, respectively, in a strip detector readout scheme. In this detector two dimensional (2D) position sensitivity is achieved with single-sided processing. A short summary of sensor parameters is given in Table III.

Both sensors have been prototyped at ELMA (Russia) and are currently investigated.

2. Pad-structured sensors and pad-structured readout layers

The calorimetric energy measurements are based upon ionization charge left by shower particles in the layers of pad structured silicon sensors. We are also considering using signals from preshower detector to compensate for the energy loss in the first 2 Lrad of W used to convert photons. The pad structured Si layers (18 in total) interleaved with W plates 3 mm (in electromagnetic) and 15 mm (in hadronic) segments are built of 6x6 cm2 silicon detectors subdivided into 16 identical square cross section pads (diods).

Test pad-structured DC coupled silicon sensors optimized for radiation hardness following

Specifications	Pad-structured sensors	Stripixel sensors
Wafer thickness	525 mm	600 mm
Depletion voltage	100-120 V	130 – 155 V
Diod capacitance	37 - 41 pF	
Bias voltage	Full dep. V + 20V	Full dep. V + 20V
Leakage current	< 300nA total, <20nA/pad	< 1?A total
Junktion breakdown	> 300V	> 300V
Implant area	15 x 15 mm2	TBD
Al area	15.02 x 15.02 mm2	15-60 mm prototyped. Decisi pending.
Polysilicon bias resistor	1 m?	1 m?
Interpad (strip) capacitance	< 2pF (pad-pad) or < 8 pF (pad-all neighbors)	TBD
Maximum heat dissipation from the bulk material	< 50 ?W	< 100 ?W
Heat dissipation from on-the-sensor electronics	-	TBD

TABLE III Sensor parameters

the prescriptions above were recently produced at ELMA foundry in Moscow suburb and delivered to our collaborators laboratory at MSU. The actual sensor picture together with the guard-ring structure are shown in Fig. 60.

5k?, 300 mm thick FZ- wafers from Wacker (Germany) available at MSU were used for this submission. In total 30 sensors were produced, IV and CV measurements at MSU resulted in 25 sensors accepted and 5 sensors rejected (large leakage currents). Results of the depletion voltage (CV) and leakage current (IV) measurements are shown in Fig. 61.

We are very pleased with an outcome of this work, both yield and performance are satisfactory, good sensors were used to build a proof-of-principle NCC prototype recently tested in the test beam in Protvino, Russia (IHEP). The design of the test sensors was largely influenced by preexisting experience at MSU (pad-structured sensors for CALICE

W-Si calorimeter prototype). In parallel we considered a number of options varying between two extremes illustrated in Fig. 62 (with decoupling RC networks on and off sensors).

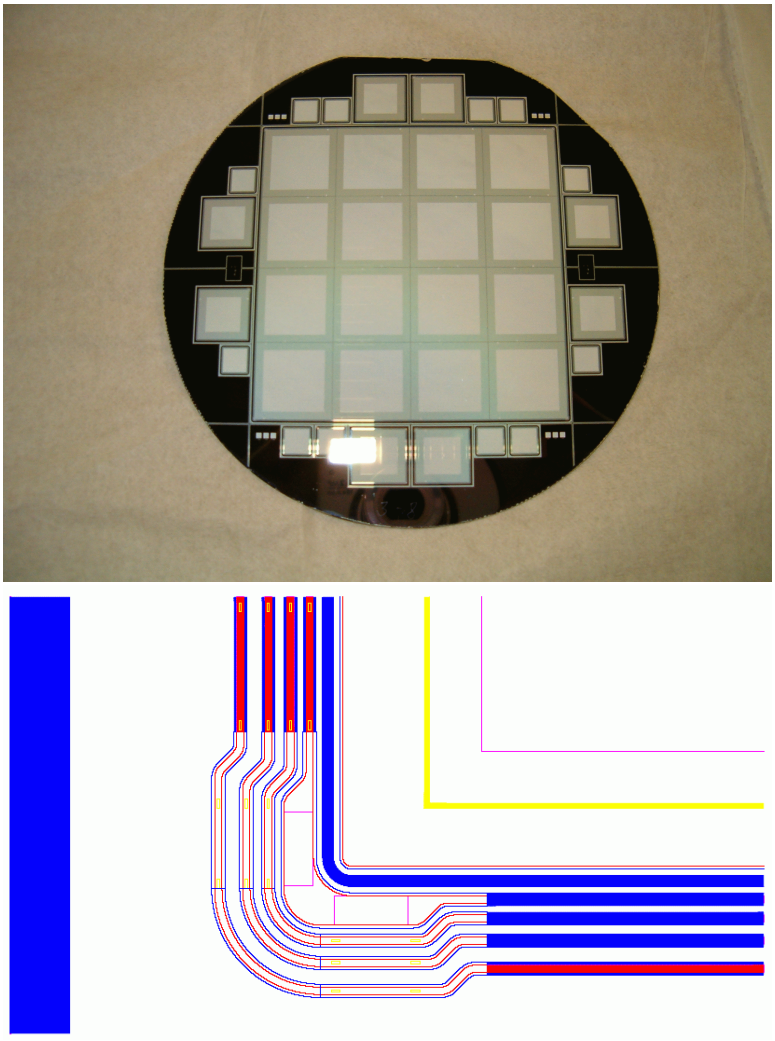

FIG. 60 NCC Silicon sensor. Undiced wafer is shown. Active area is subdivided into 16 readout pads 1.5x1.5 cm2 each. On the right is the structure of the guard rings. The complexity of he design is to prevent voltage breakdowns after radiation exposure.

The sensors with built-in RC networks are probably the only option for detectors planning to digitize signals from individual pixels. Unfortunately this technology routinely results in increased cost and reduced yield associated with extra steps required to grow large capacitances on pad surfaces. In case of PHENIX NCC where individual pixels are ganged together to allow a single preamplifier to handle analog sum of the pixel currents the advantages of AC coupled design are not obvious at all, it may result in ineffective spending of resources. Our project was recently reviewed by the unofficial panel of Si detector experts at SiDet

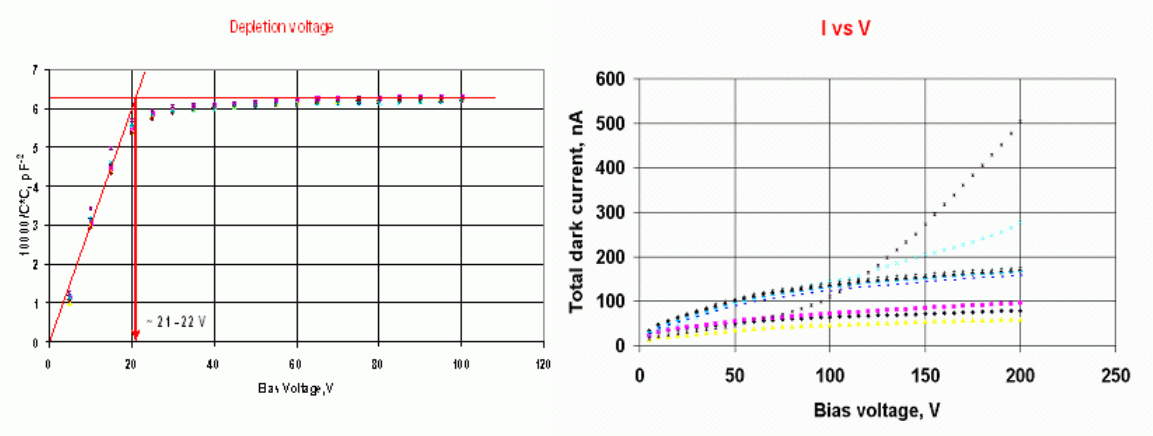

FIG. 61 CV and IV measurement data for the test batch of 30 PHENIX NCC pad-structured sensors produced at ELMA in Russia.

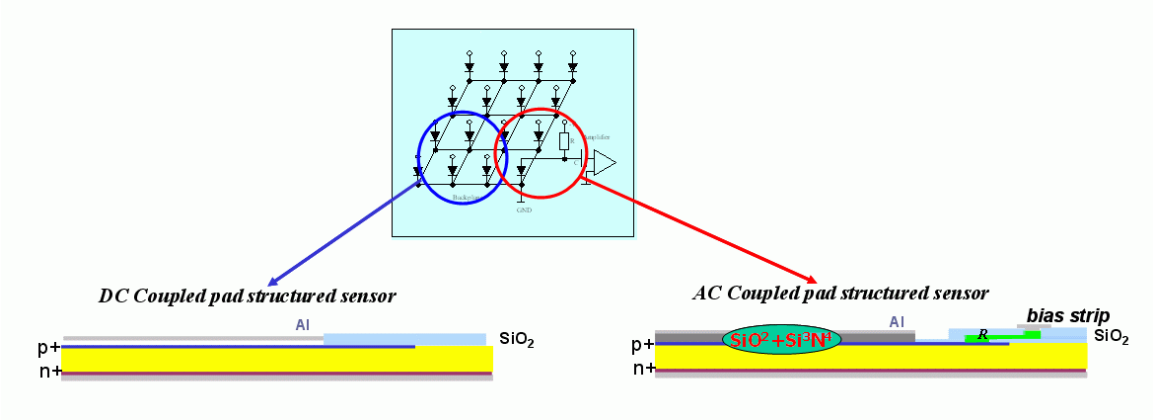

FIG. 62 Two extreme designs for the pad-structured Si sensors. DC on the left and AC on the right.

Laboratory at FNAL, the recommendation which we accepted was to retain the polysilicon resistors on the sensors and to use external decoupling capacitances. Modified design is now available to ELMA (Russia), ON Semiconductors (Czech Republic) and SENS (Korea) foundries, we expect new sensors for evaluation and system prototype construction delivered first trimester of the next year.

The sensors will be mounted on the sensor carrier pc boards, Sensors, carrier boards and interconnects (see Fig. 63) form readout unit the latter installed in the gap between W plates, its positioning is defined by the locking pins on the side opposite to sensors.

The interplate gap reserved for readout unit is 2.5 mm thick. 0.5 mm of this space is silicon, ∼1.2 mm is FR4 (motherboard), 0.2 mm is the FR4 interconnect, another 0.2 mm is

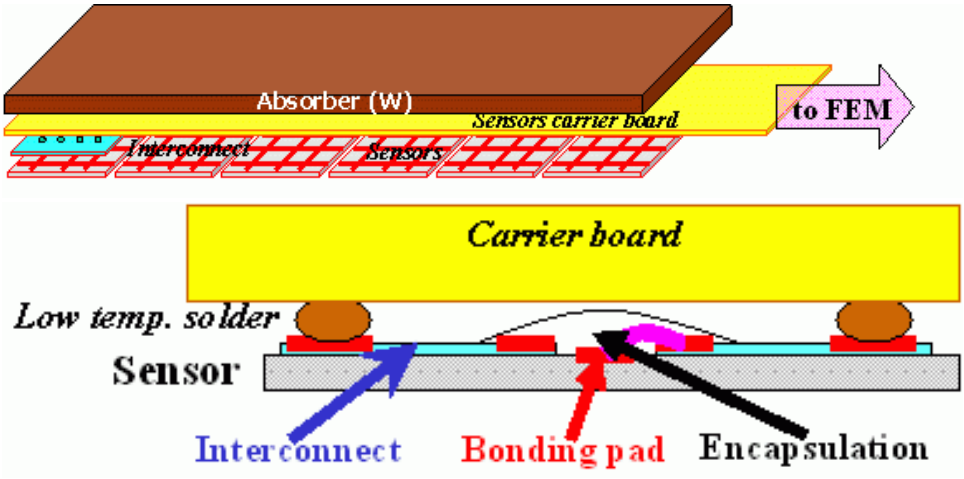

FIG. 63 NCC Readout unit structure. Details of the sensor installation scheme are in the bottom part of the picture.

the FR4 spacer required to control the height of low temperature solder between interconnect board and carrier board. Remaining ∼0.4 mm gap is to insure that no pressure is applied to the surface of Si sensors what otherwise may result in increased noise due to piezoelectric effect.

This particular design which may still undergo further modifications is chosen because of a premise of repairablility for assembled readout unit. Soldering points are connected to the bonding pads via traces what allows to locate them around center of the interconnect board. If sensor fails it will take heating just the central area of the sensor to remove the sensor with interconnect board from the carrier board. New sensor assembly will then be installed (soldering points will require cleaning and new dose of paste).

The NCC will use four different standards for the readout units: all single sensor wide with the number of sensors varying between 3 and 7.

E. Stripixel sensors and stripixel readout layers

One of the major tasks NCC will need to complete is to study direct photon production in events with correlated photon-jet in the final state resulting from Compton scattering of soft gluon on a quark. This is probably he most revered process as concerns our ability to access the partonic evolution in the initial state leading to sQGP formation. The background to this process are the double-jet final states with one jet fragmenting into leading p0 faking single photon due to shower overlaps. In the detector built of composite material with

Molier radius rM ∼18 mm and characteristic slope of the shower core ∼0.2 rM = 4 mm, the clear separation of the maxima due to two photons with close energies is possible down to a similar value of ?∼0.2 rM.

The problem arises when attempting to prove that observed maxima do really due to independent showers and not to the shower fluctuations. The separation is too small compared to the average shower radius at the same energy to make meaningful qualitative testing based even on the most detailed lateral shower shape measurements. The following strategy is adopted for NCC to deal with fluctuations. We are installing two layers of identical 2-d position sensitive detectors (0.5 mm pitch) in the calorimeter at two depths: 2 Lrad and 7 Lrad. The first layer (preshower) installed downstream of 2 Lrad W converter is a hit counting layer where position resolution is limited by the strip width to ∼150 mm, the second (shower max) layer will serve to measure decay asymmetry (if two showers are expected) through the shower shape analysis at a depth where the shower expands to rM radius. The algorithm will first try to find all showers in the calorimeter, for every shower it will look for hits in the preshower layer to find those candidates to be close overlaps, the candidates will be checked for consistency with the picture in the shower max layer where the deconvolution will finally be made assuming that contribution of individual photons is proportional to the peak energy values as measured in shower max detector. Simulation have shown that this approach may work well to ?0 energies above 30 GeV (effectively to the limit set by integrated luminosity we can hope for). We have chosen a novel detector of interleaved pixilated strips ("stripixel") developed at BNL and already in use for the Central Silicon Tracker in PHENIX. This novel detector generates X-Y two dimensional position sensitivity with single-sided processing and readout . Fig. 64 is an illustration of the concept. Comb shaped structure with 250 ?m prongs cover the pixel area 500x500 mm2. Prongs are interleaved with similar prongs from two overlapping pixels on the right and on the left.

Alternate combs are connected either in X direction (forming strip measuring Y coordinate) or in Y direction (for X measurement).Pitch between prongs belonging to different strips is chosen comparable to charge diffusion to insure uniform charge sharing. While it is easy to predict that an optimal pitch for 525?m wafer must be in the range of 15 mm, it may still be affected by the comb geometry and needs prototyping and infrared laser or beam testing before the project commits itself to one particular value. Another critical issue are interpixel connections and crosstalk, the latter depend on the total length of the strip

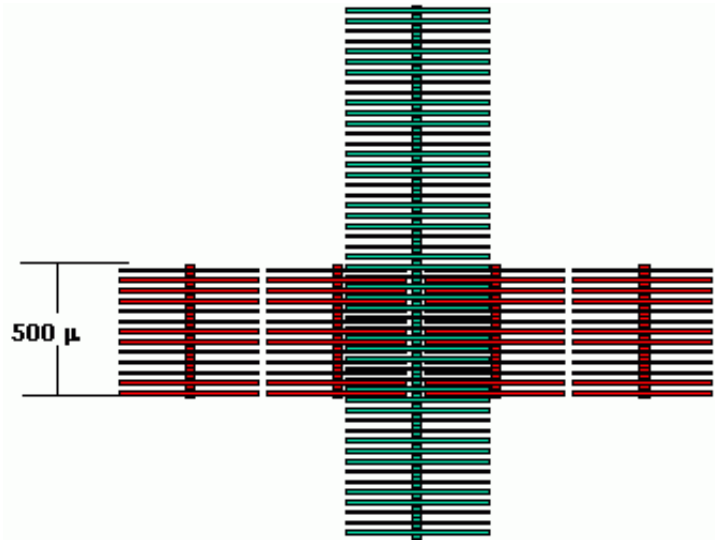

FIG. 64 Design of the detector with interleaved pixilated strips with 2-d position sensitivity. Ionization charge produced by charged particles in Si is shared between X and Y oriented strips.

edge which in turn is correlated to the pitch. While PHENIX Central Tracker employs the double metal technology for interpixel interconnects, it may be of advantage to the Forward Calorimeters to use a different technology with better promise for radiation hardness. The n+ implants create conductive regions in the bulk silicon separated from Al with a layer of SiO2.

To test different versions of the comb structure BNL Instrumentation (Zheng Li) produced the design for the 6x6 cm2 test stripixel sensor with bands of X and Y strips 20-strips wide (short strips crossing the bands are all connected together to simplify crosstalk measurements). Sensor has 5 stripixel configurations prototyped, all strips are connected to bonding pads via local pitch adaptor (Fig. 65).

Measurements of depletion voltages using on-sensor test structures have shown that wafer processing was done satisfactorily (Fig. 66). Test sensors are expected to be fully functional and fit for further testing.

The readout system for the stripixel silicon detectors will be based on the SVX4 chipo and the existing PHENIX data acquisition system. Strips are connected to DCM's through hybrids with RC network and SVX4 chips daisy chained and followed by interface board with sequencer which are in turn connected to DCM's. The hybrids will be glued directly onto the sensors with a common of the sensor glued to carri board. A very preliminary design of the hybrid is shown in Fig. 67 with a carrier board and sensor.

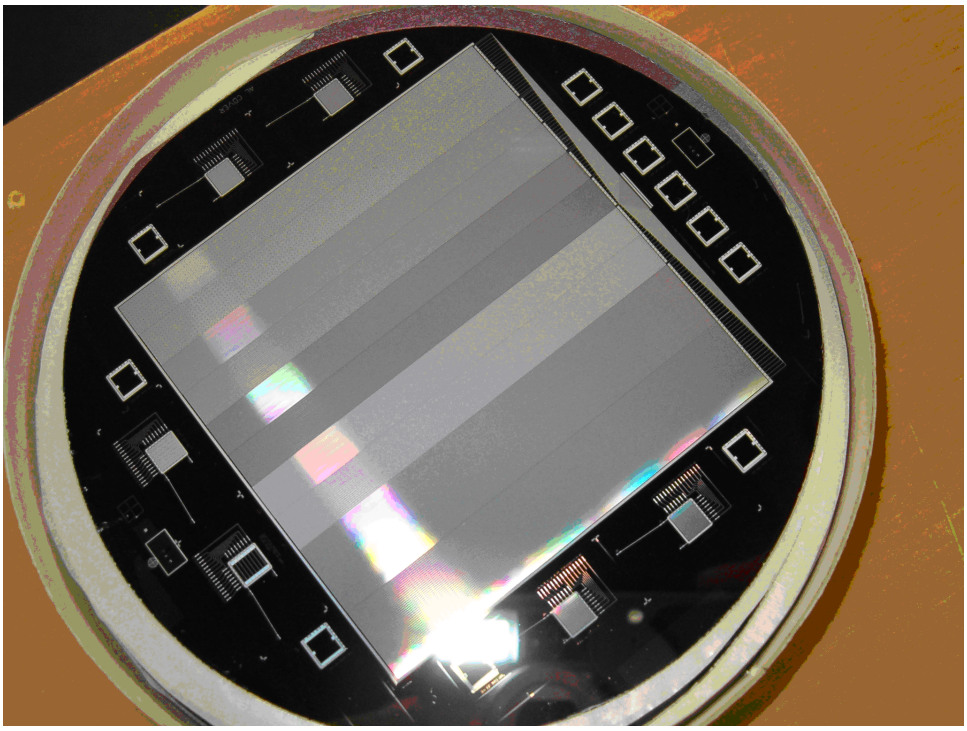

FIG. 65 Si wafer with stripixel test structure designed in BNL Instrumentation Department and produced by ELMA in Russia.

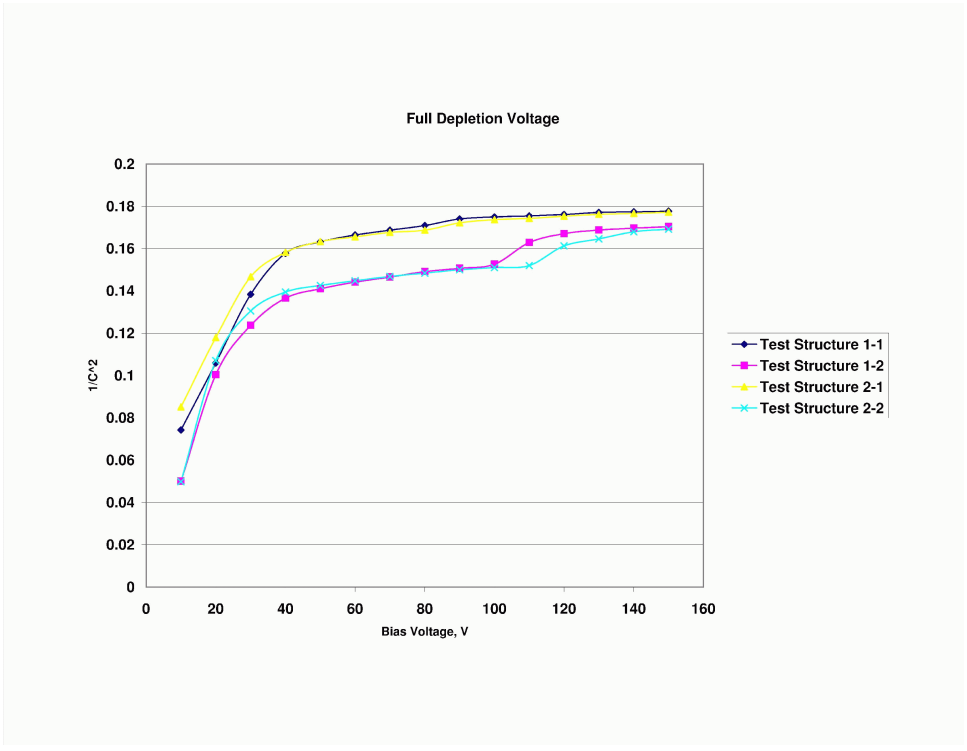

FIG. 66 Preliminary results of depletion voltage measurements on a test structures on the new stripixel sensor for the PHENIX NCC.

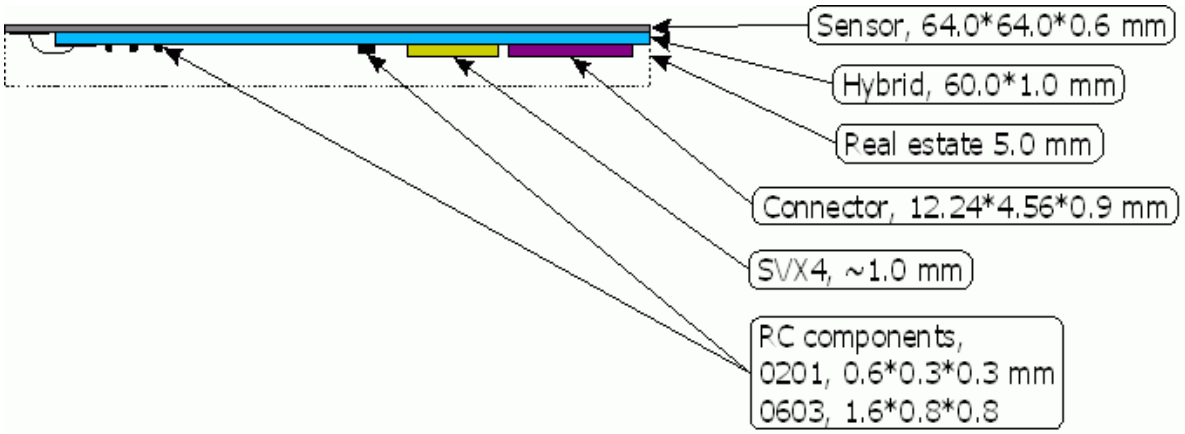

FIG. 67 Design of the interconnect (hybrid) with external RC network and SVX4's for the NCC stripixel layer.

F. NCC Electronics

1. NCC ANALOG SIGNAL PROCESSING

For readout purposes the calorimeter is longitudinally segmented into two fine and one coarse sections (two electromagnetic and one shallow hadronic compartments) and two 2-D sensitive coordinate section. In total the silicon tungsten calorimeter as it was described above will have close to 60 000 silicon pixels and 80 000 strips. This calls for a compact, economical readout.

Depending on the location in the calorimeter the readout unit will deliver between 48 and 112 signal lines to the preamplifier board. Following the declared intent to minimize the number of individually designed components in the detector, we are planning to use the same design of the adapter board everywhere with only live channels populated.

We will sum up all depth-sequenced pixels in each longitudinal segments of the calorimeter. A simple passive (on the resistors) summation scheme will be implemented on the outskirts of the detector (signals from individual pixels are sent to the summer via traces on carrier board). Rather modest goals for the electromagnetic energy resolution as set in this proposal allow us to disregard the potential contribution to resolution due to the spread in the gains between individual channels. Summed signals are amplified using hybrid trancere-sistance amplifiers developed at BNL for ATLAS liquid argon calorimeter. Modifications to the existing design will include polarity change for all transistors (to work for positive swing signals) and adding differential drivers to drive the signals over twisted pairs cables to the

digital signal processing plant. Block diagram of the analog signal processing plant is shown in Fig. 68.

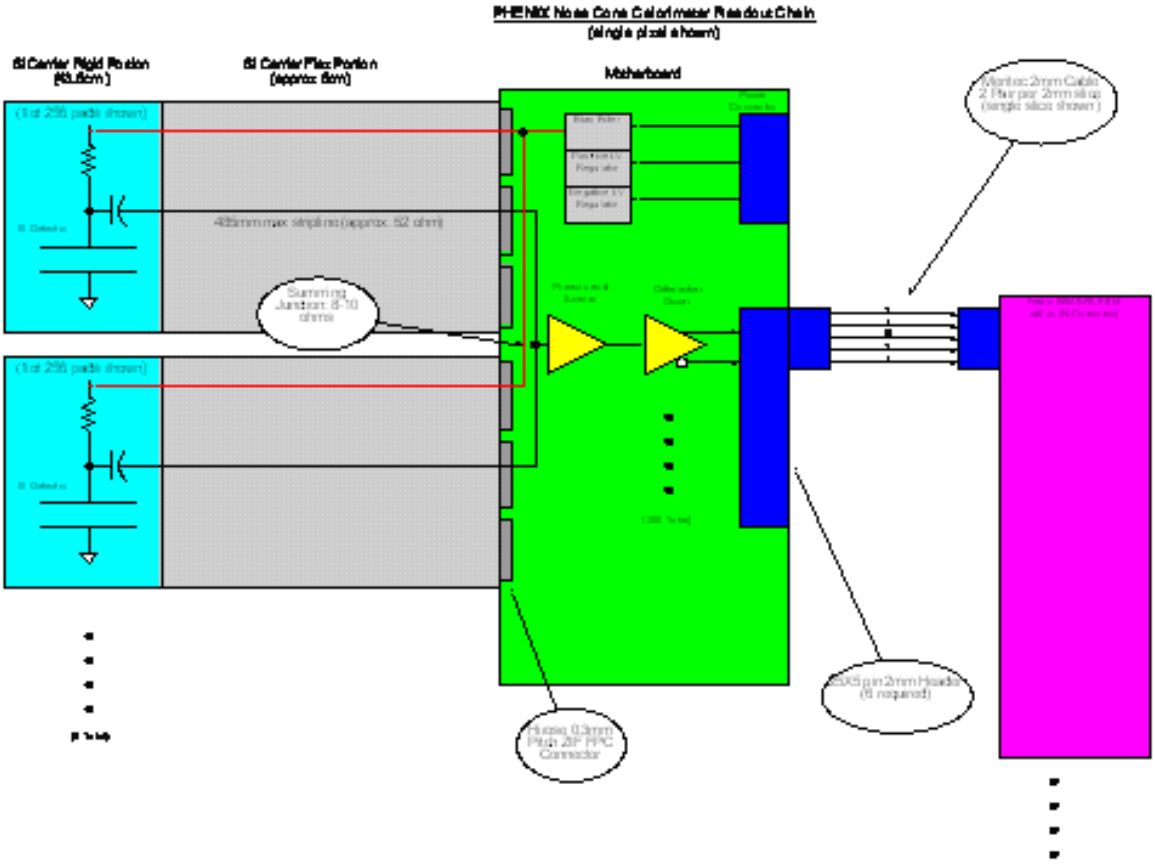

FIG. 68 NCC analog signal processing block-diagram

2. NCC DIGITAL SIGNAL PROCESSING

G. NCC BASED EVENT TRIGGERING

In order to pursue it's rare-event physics program the PHENIX experiment requires high luminosity from the RHIC accelerator and highly selective Level-1 and Level-2 trigger systems. In particular, the Level-1 trigger system is limited to a maximum rate of 12.5kHz by the readout rate of the detector front-end electronics. This will require an overall event rejection of up to ∼1000 when RHIC reaches its goal of ten times design luminosity for protons in future runs. Since we anticipate the parallel acquisition of several rare event channels, the rejection for an individual trigger channel must be larger by a factor 5-10.

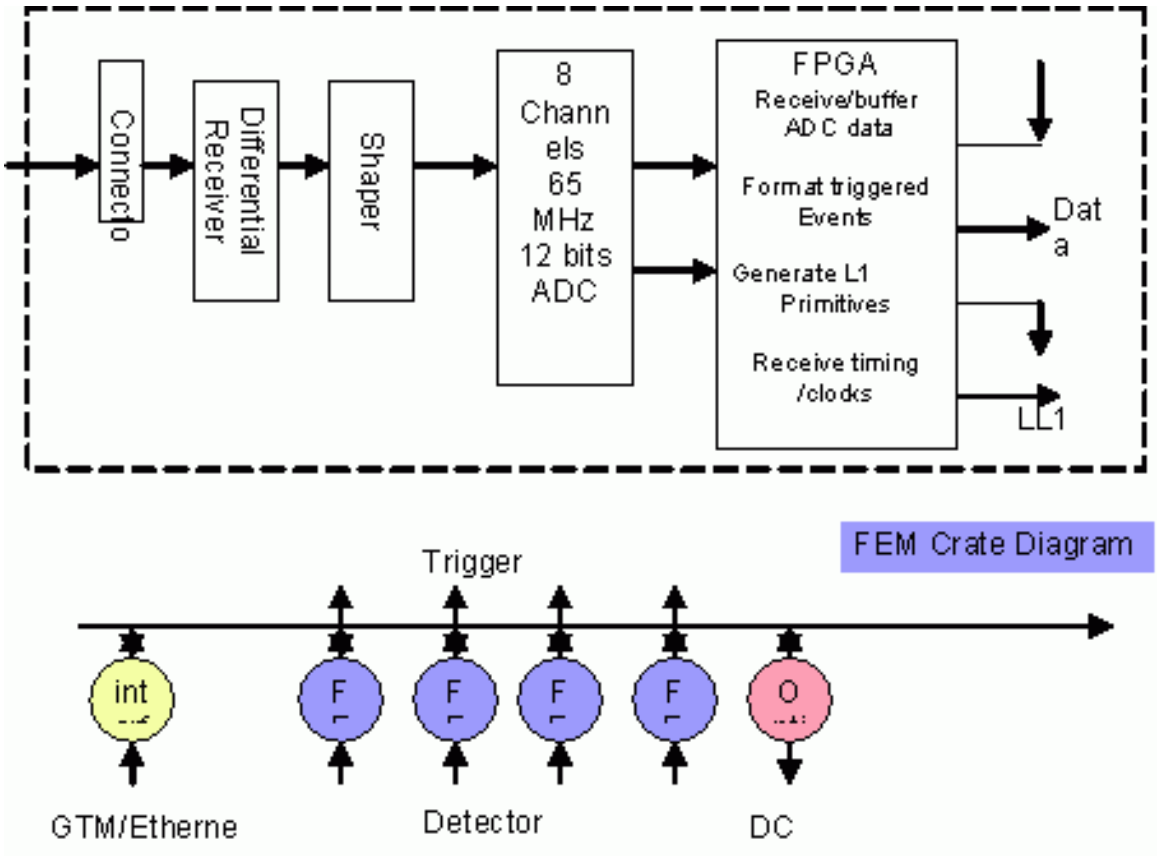

FIG. 69 Digital signal processing in NCC

The PHENIX Level-1 trigger is fully pipelined and provides an event decision in less than 4.2μs (40 RHIC clock ticks).

The PHENIX Level-1 Trigger is a parallel, pipelined trigger system designed to provide a highly configurable trigger capable of meeting the demands of the PHENIX physics program. The Level-1 Trigger consists of two separate subsystems. The Local Level-1 (LL1) systems communicate directly with the participating detector systems. The input data from these detector systems is processed by the LL1 algorithms to produce a set of reduced-bit input primitive data for each RHIC beam crossing. The Global Level-1 system receives and combines this data to provide a trigger decision. In addition, busy signals (both global and trigger) are managed by GL1. The PHENIX detector system readout is divided into two sets of elements: granules and partitions. A granule is the smallest detector element that communicates with the PHENIX timing and control system via a Granule Timing Module (GTM). The GTMs distribute the local 9.4Mhz RHIC beam clock as well as control bits and event accepts to the granule. A partition is an administrative configuration of granules

that share both busy signals and Level-1 triggers.

In this PHENIX upgrade the nosecone calorimeter (NCC) LL1 primitive system will generate primitive information on the jet axis, as well as single and multiple high energy clusters. A possible muon tracker LL1 system will generate primitive information on the momentum of high pT tracks.

The MuID LL1 system is based on a generic, configurable LL1 trigger board designed and built by Iowa State University. The Generic Local Level-1 hardware (GenLL1) was designed to address a number of difficulties faced in extending the original design concepts for LL1 systems to address the full range of PHENIX trigger needs. First, the hardware had to be re-programmable to allow not only quick corrections to the trigger logic, but modifications of the trigger system as the PHENIX physics program evolved. This also had the added advantage of lowering development costs and allowing quicker prototyping of new trigger systems. Second, the new hardware had to be able to manage a data throughput of $\sim$20Gb/s in order to be able to handle large data volume detectors (such as the Muon Identifier) without prohibitive cross-stitching between multiple boards (and crates of boards). Finally, in order to keep power consumption and heat load on the board within reasonable limits the GenLL1 design was required to use the next generation of HP GLINK receiver/transmitter logic (the HDMP 1032/1034), which runs at 3.3V. Smaller format transceivers (Agilent HFBR 5912) were also required in order to be able to handle up to twenty fiber inputs on a single 9U VME board. A complete description of the GenLL1 hardware can be found elsewhere.

In order to maximize the trigger rejection at Level-1 it will be necessary to combine trigger information from all of the forward Level-1 systems. In order to accomplish this, a new regional trigger processor will then take the complex trigger primitive information from the nosecone calorimeters, muon tracker systems and muon identifiers, combine the individual detector LL1 primitives, make trigger decisions and send them to GL-1. A block diagram of the data flow is shown in Fig. 70. In order to pass data between the regional trigger processor and the LL1 systems efficiently it may be possible locate all the Level-1 trigger systems in a single crate and make use of a high-speed 16-bit data bus that is already available in the GenLL1 design to transfer the trigger primitives.

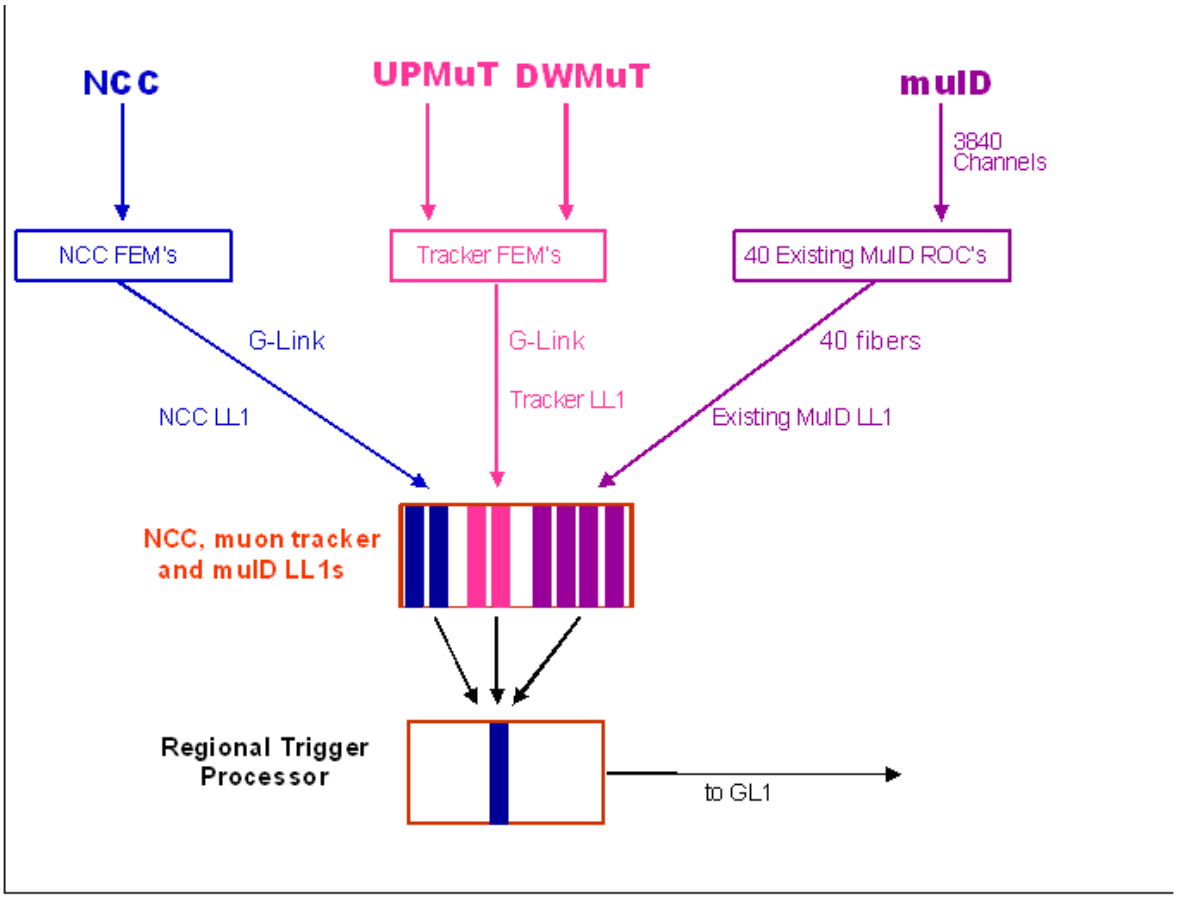

FIG. 70 Block diagram of the combined forward PHENIX Level-1 trigger system showing the nosecone calorimeter, NCC, trigger muon tracker stations and the existing MuID LL1 system for a single PHENIX muon arm. In order to combine the primitives of the various trigger systems a regional trigger processor will combine the trigger information before sending primitives to Global Level-1.

1. The NCC Level-1 Trigger System

The nosecone calorimeter (NCC) will use a Local Level-1 (LL1) trigger to select events via with a high pT photon or jet in the calorimeter acceptance. As is typical of PHENIX LL1 systems the processing will consist of a set of pipelined stages. First, a set of primitive data will be digitized on the front-end modules (FEMs). Second, this data will be transferred to an LL1 system, and finally the bit-reduced trigger information is sent from the LL1 system to the PHENIX Global Level-1 trigger system; possibly via a new regional trigger processor to combine level 1 information from the different forward detector systems.

The NCC system consists of over 10k channels of analog data per nosecone spread over

three layers in depth. The FEMs will combine calorimeter towers into non-overlapping 2x2 trigger tiles, digitize the output, and pass the LL1 system an 8-bit ADC value per trigger tile. The 8 bits per channel will allow a ∼400 MeV least count with a full range of 100 GeV, and will result in an aggregate bandwidth of 200Gbit/s per nosecone into the LL1 system, roughly a factor of 5x larger than the data processing capacity of the existing MuID LL1 system.

Because of the large data volume and tight space constraints on the detector FEMs we are considering the possibility of transferring the data over high-speed serial links into an LL1 system located in the detector hall, as opposed to other LL1 systems that transmit their data over optical fiber links to LL1 electronics in the PHENIX rack room. The advantage of this approach would be that with serial links we could concentrate the entire NCC LL1 data stream into a smaller number of LL1 modules, simplifying the data cross-stitching required for jet cluster trigger algorithms. This would only be possible by using high-speed copper serial links between the detector FEMs and the LL1 electronics which are inherently short-range, requiring the LL1 electronics to be located in the detector hall.

The LL1 system would process the NCC 2x2 data to provide a set of photon triggers and jet cluster triggers based on the 2x2 trigger tiles, where both sets of algorithms would operate both laterally and using the depth information in the NCC to provide clean photon triggers. Detailed simulations of the performance of the NCC LL1 system are underway. The reduced bit output of the NCC LL1 trigger, in the form of a set of bits indicating satisfied algorithms, would be transmitted to the GL1 system over optical fiber.

The NCC will participate in a local-level-1 trigger (LL1) to select events with a high pT photon or jet in the calorimeter acceptance. The processing will consist of a set of pipelined stages. First, primitive data will be built of bit-reduced digitized measurements. Second, this data will be transferred to a LL1 system, and finally, further bit-reduced trigger information will be sent to the global-level-1 trigger (GL1), via a new regional trigger processor combining level-1 information from the different forward detector systems.

The single NCC system consists of about 8k channels of analog data per nosecone, spread over three layers in depth. The local processing units will combine calorimeter towers into non-overlapping 2x2 trigger tiles and pass the LL1 system an 8-bit ADC value per trigger tile. The 8 bits per channel will allow a ∼400 MeV least count with a full range of 100 GeV, and will result in an aggregate bandwidth of 200 Gbit/s per nosecone into the LL1 system;

this is roughly a factor of 5 times larger than the data processing capacity of the existing PHENIX LL1 system.

We are considering the transfer of data over high-speed serial links into an LL1 system located in the detector hall as opposed to other LL1 systems that transmit their data over optical fiber links to LL1 electronics in the PHENIX rack room. The advantage of this approach would be that with serial links we could concentrate the entire NCC LL1 data stream into a smaller number of LL1 modules simplifying the data cross-stitching required for jet cluster trigger algorithms. This would only be possible by using high-speed copper serial links between the detector front end readout modules and the LL1 electronics which are inherently short-range - thus requiring the LL1 electronics to be located in the detector hall.

The LL1 system would provide a set of photon triggers and jet cluster triggers based on the 2x2 trigger tiles where both sets of algorithms would use information from neighboring trigger tiles and the NCC depth information to provide clean photon triggers. Detailed simulations of the performance of the NCC LL1 system are underway. The reduced bit output of the NCC LL1 trigger, in the form of a set of bits indicating satisfied algorithms, would be transmitted to the GL1 system over optical fiber.

H. NCC PROTOTYPING AND TESTING (R&D)

With the help of institutional contributions it was possible to maintain a small, but well focused, effort over the past two years to explore technologies for silicon detectors suitable for PHENIX NCC. These investigations were organized around well defined goal of construction proof-of-principle prototype and testing it in the particle beam. Results of these investigations are the basis of the present proposal. The outcome and corresponding technology choices, which are the pad-structured DC coupled silicon sensor, pixilated strip sensor with 2-D sensitivity, pad structured readout units, hybrids and FEM's for pad-structured and stripixel sensor readout through SVX4, have been discussed in section 4. More recently the R&D effort has shifted towards finalizing technology choices as required by construction project. In part this is possible due to the support PHENIX received following a request to BNL management for generic R&D funds.

We converged on the pad-structured sensor design but we are still in he evaluation stage

as concerns the stripixel sensor (prototype sensor was recently delivered from foundry in Russia). The completion of R&D work on DC coupled pad-structured sensors allows to proceed with he final design of the readout units for the sampling cell and layout for the preamplifier boards.

We closely follow the development of the digital signal processing plant for HBD which is functionally identical to what is proposed for NCC and SVX4 based readout currently under development for the two outer layers of the PHENIX SVT. We are planning to use the outcome of those projects in NCC with minimal modifications.

The key issues still to be resolved are the noise (capacitative and pick-up) in the detector operating with ganged sequential pads and optimization of the stripixel sensor design. The solution to the noise issue requires extremely careful design with large care taken of grounding the detector components and readout electronics. We enlisted help from D0 silicon group at FNAL for the next step in the detector design and will rely on their expertise in large silicon systems and detector mechanics.

We continue stripixel sensor development in parallel with helping NUCLON to implement single sided stip detectors of a similar geometry which we consider a backup solution. We plan to make the final technology choice in the first half of 2006.

For many parts of the NCC, the technology choices have been made, and R&D is focusing on prototyping the designs. We need to pursue and complete these topics over the next year to start EDIA and construction of the NCC in FY07. Generic R&D funding through both RIKEN and from the DOE (at a level of $150k) will be required to complete these tasks. In detail the projects are:

- Implementing polysilocon resistors on padstructured sensors
- Finalizing design for the stripixel sensors
- Finalizing design of the readout units for both kind of sensors;
- Generating layout for the preamplifier summer boards;
- Finalizing conversion of ATLAS preamps to PHENIX specification. Implementing new version of amplifier with hybrid technology;
- Finalizing detector mechanical design;

- Building system prototype (single brick) and accessing the noise performance.

V. PROJECT MANAGEMENT AND RESPONSIBILITIES

The organization and management of the proposed effort is embedded in the management structure of the PHENIX experiment, which is part of the BNL RHIC project. The new organization must satisfy a number of requirements including a clear interface to the existing RHIC and PHENIX management structure, clear roles and responsibilities within the existing PHENIX subsystem structure. Particular attention has to be paid to the fact that a significant portion of the project is supported by foreign contributions. Clear deliverables, responsibilities for deliverables and the accountabilities of the participating funding Agencies have to be defined. These responsibilities will be formalized in memoranda of understanding (MOU's) between PHENIX and the participating institutions. In this section, we outline our proposed management organization and delineate responsibilities within the project.

A. Project background

The proposed project is part of a detailed upgrades program to enhance the physics capabilities of PHENIX over the next 8 years. Realizing this plan will enable PHENIX to remain competitive well beyond the turn on of LHC expected for 2008, as well as advance our understanding of QCD by fully exploiting the unique spin physics capabilities of RHIC. The plan covers a broad range of measurements in AA, pA, and pp and its goal is to provide key measurements which currently can either not be addressed at RHIC or only with limited accuracy. The development of the PHENIX upgrade program started in response to the recent NSAC long-range plan, which was developed in 2000.

In the fall of 2004 an LOI for an upgrade of the Forward region of PHENIX was written and presented to the PHENIX management. This LOI included the NCC, and a trigger for the muon spectrometer which is being funded by the NSF. This LOI was reviewed at a joint meeting of the PHENIX detector council (DC) and executive council (DC). Following their recommendations PHENIX management (PM) endorsed both projects and the group was charged with preparing a proposal (CDR) for presentation to the DOE through BNL.

B. The management plan for the NCC

1. PHENIX management structure

The NCC project is part of the PHENIX project and as such integrated into the PHENIX management structure as described by the PHENIX bylaws. The PHENIX Detector Council (DC) will advise PHENIX management on the design, construction, and integration of the NCC. The DC is co-chaired by the operations manager (E.O'Brien) and the upgrades manager (A.Drees). The NCC subsystem manager will serve as a member of the DC. PHENIX subsystem leadership

We expect that the proposed NCC project will be funded through two agencies, the DOE Office of Nuclear Physics (DOE-NP) and the RIKEN Institute. A successful completion of the NCC will require close collaboration and well-defined responsibilities and scope of the contributions of both agencies in terms of deliverables. The deliverables and foreign contributions are outlined below. Within PHENIX, the responsibility for the NCC subsystem will be shared by the subsystem leader, Richard Seto (UCR) and his two deputies, Itaru Nakagava (RIKEN) and Edouard Kistenev (BNL). The subsystem leader reports to PHENIX PM and will represent the NCC in the PHENIX DC.

Simultaneously, E.Kistenev will serve as the DOE contract project manager (CPM), and will have the fiscal and construction responsibility for the DOE funded deliverables as outlined in this proposal. This involves appropriate planning, budgeting, and reporting. I.Nakagava will serve as RIKEN counterpart and have similar responsibilities for the RIKEN funded deliverables.

2. Role of BNL

Because we expect that all DOE funding for this effort will be directed through the BNL Physics Department, BNL line management will have ultimate fiscal and management responsibility for the construction of the NCC and for its subsequent operation.

Fig. 71 Management chart of the NCC project. The fiscal responsibilities for the individual tasks are specified in bold letters. The institutions participating in each task are given in italic. In PHENIX the DAQ is a separate subsystem and therefore not connected to the NCC management.

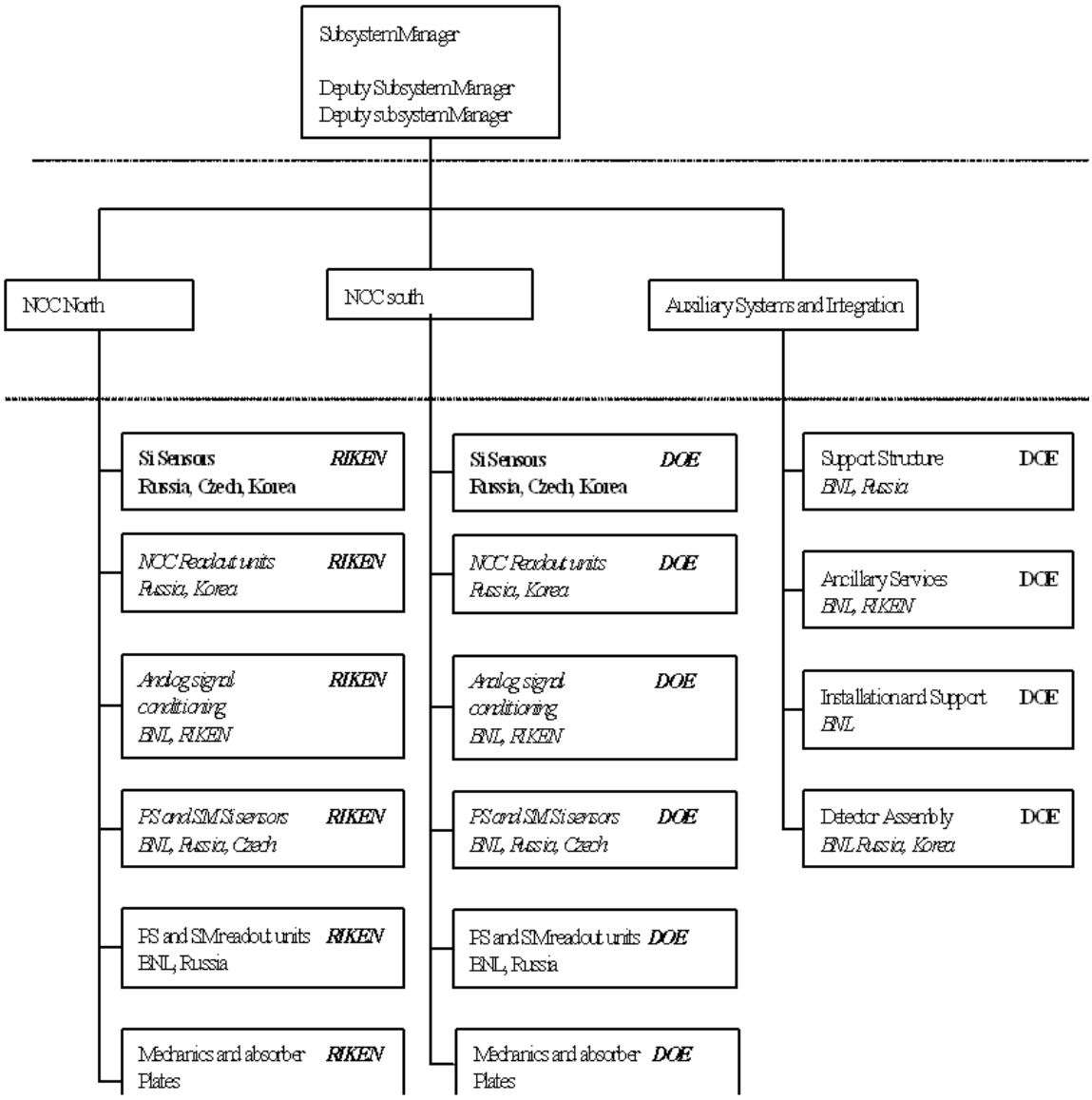

FIG. 71 Management chart of the NCC project. The fiscal responsibilities for the individual tasks are specified in bold letters. The institutions participating in each task are shown. In PHENIX the DAQ is a separate subsystem and therefore not connected to the NCC management.

3. Specification of deliverables

The NCC is divided into subprojects, which themselves are divided into tasks. The tasks closely relate to deliverables, which need to be completed before the NCC construction project can be considered complete. The proposed fiscal responsibility for each deliverable, either RIKEN or DOE, is indicated in brackets. Expected institutional involvement is listed

together with the fiscal responsibilities. The present and future involvement of individual institutions is discussed in more detail in the next section.

North/South Calorimeters

- Silicon pad-structured sensors designed and implemented to the specification (DOE)
- Silicon strip sensors designed and implemented to the specification (RIKEN)
- Silicon pad sensors for the South Calorimeter produced (RIKEN)
- Silicon pad sensors for the North Calorimeter produced (DOE)
- Readout units and Front-end modules for the calorimeter designed (DOE)
- Readout units for PS and SM detectors designed (RIKEN)
- Readout units and FE modules for South Calorimeter produced, assembled and tested (RIKEN)
- Readout units and FE modules for North Calorimeter produced, assembled and tested (DOE)
- Support structure and absorber plates for South Calorimeter produced (RIKEN)
- Support structure and absorber plates for North Calorimeter produced (DOE)
- South Calorimeter bricks assembled and tested (RIKEN)
- North Calorimeter bricks assembled and tested (DOE)

DAQ system

- Data collection modules for calorimeters and position detector (PS and SM) manufactured and tested (DOE)

Auxiliary Systems and Integration

- System support requirements specified, including heat loads, power distribution, mechanical tolerances and ground scheme (DOE)
- Mechanical support structure designed (DOE)

- Ancillary systems operational, including power distribution and cooling system (DOE)
- Calorimeter bricks mounted in mechanical support (DOE)
- Commissioning of full detector system (DOE)
- Full system test in PHENIX (DOE)
- Integration into PHENIX DAQ system (DOE)

C. 6.3 Institutional involvement

Currently about 20 institutions with a total of 60 collaborators are involved in the NCC project. The different institutions bring in diverse research background, physics interests and expertise, which form a broad base to carry out the proposed project. All groups have taken on specific responsibilities and will actively participate in the NCC project. Matching their expertise these group will be involved in construction, installation, commissioning, operation, and data analysis. Formal commitments of the involved institutions will be specified in MoU's. At this early stage of the project naturally some groups have been actively involved and launched R&D through institutional contributions while others have joined the project only recently. In the following we will briefly discuss the different groups, their expertise and their potential involvement. University of California at Riverside and the RIKEN BNL Research Center have made major contributions to this proposal and will specify their specific responsibilities in the future. The BNL Instrumentation Division and EWHA University in Japan join the NCC project because of their interest in the technological development, but are not members of the PHENIX collaboration.

1. Brookhaven National Laboratory, Chemistry Department (BNL CHEM)

Mark Baker and his group bring in broad experience with silicon detector technology. In addition to management and physics experience, each group member brings specific technical skills that will be important for the successful construction, installation, commissioning and operation of a silicon detector in the RHIC environment.
Rachid Nouicer is one of the two primary silicon experts active on PHOBOS, having participated in the construction, installation, and commissioning of the detector. Andrei Sukhanov

is an expert in data acquisition (real-time programming, firmware programming, triggering, electronics etc.).

The group will take a major responsibility for the Preshower and Shower max Detectors of NCC and in collaboration with BNL Instrumentation Department will lead the effort to develop the strip sensors and related readout for NCC.

2. Brookhaven National Laboratory, Instrumentation Division (BNL ID)

BNL's Instrumentation Division's Silicon Detector Development and Processing Laboratory (SDDPL) will be involved in the development of silicon strip detectors for PHENIX Upgrades. The activity will include detector simulation, design, and processing of prototype detectors. SDDPL will also be involved in laser scan tests of those prototypes, these tests will be carried out in close collaboration with the BNL Physics Department and RIKEN-BNL Research Center. Zheng Li, the group leader of SDDL, will be involved in these activities.

BNL Instrumentation Department proposed the solution based upon hybrid amplifiers earlier developed for ATLAS experiment at CERN to serve as a basis for the analog signal processing for NCC. The further activities will involve modification to the schematics for the amplifiers to work with positive polarity signals, compactification of the layout, testing and participation in production. S.Rescia will be involved with this part of the Project, V.Radeca will provide advise and guidance.

3. Brookhaven National Laboratory, Physics Department (BNL PHY)

The PHENIX Group from the BNL Physics Department provides infrastructure and technical support as part of Systems Engineering and Integration (SE&I) for the entire PHENIX experiment. It has a staff of mechanical and electrical engineers and a group of experienced technicians who are intimately familiar with the detector, and work closely with the BNL Collider-Accelerator Department for operations and any modifications to its present design. They designed much of the infrastructure for the baseline detector, including racks, cable trays, electrical power, cooling, access, safety systems and numerous other services, and carried out the installation of all of the present subsystem detectors. This group will now be closely involved with the design of the infrastructure and support for the PHENIX

Forward Calorimeters, and with its installation into PHENIX.

The BNL PHENIX group also has primary responsibility for a number of major subsystems. These include Electronics Facilities and Infrastructure (EF&I), Online Computing Systems (ONCS) and Offline Computing. These groups will participate in the electronic integration and readout of the NCC detector into the PHENIX data acquisition system, and will be involved with track reconstruction and offline data analysis.

The BNL PHENIX group will also serve a host institution for the project, will provide the lab space for the final detector assembly and testing .....

4. University of California, Riverside (UCR)

The group at UCR has taken primary responsibility for Simulations and Software Vasily, Dzordzhadze as well a project management (R. Seto). A post-doc is provided for NCC work in the UCR grant.

5. Iowa State University (ISU)

The group at ISU has primary responsibility for the Level-1 trigger for PHENIX. As such they are the ideal group to take charge of the NCC trigger design, electronics, and implementation (J.Lajoie).

D. Foreign Contributions

The group at Yonsei University together with Ewha University have become involved in the work on Silicon pads. I. Park and his group at Ewha has built the Silicon detector for the CREAM balloon project working together with industrial partners SENS Technology - a small company specializing in Silicon detectors. The group will begin prototyping the pad detectors made on 8" wafers - a major development since this would significantly reduce the cost.

VI. BUDGETS AND SCHEDULE

A. Total estimated cost (TEC)

The costs and schedule for the NCC project have been developed using engineering estimates, vendor quotes and experience from the construction of the silicon detectors from participating Institutions. The proposed project is based on a cost sharing between the DOE Office of Nuclear Physics and the RIKEN Institute of Japan. Responsibilities for specific deliverables have been discussed in the previous chapter. RIKEN funding will start in ..... and we expect that it will continue at a level of approximately \$1M per year for the next three years. In addition, RIKEN provides substantial manpower (equivalent to $\sim$ \$1M) through in house contributions. The total estimated costs for the proposed DOE construction project is \$7 M including an average contingency of 30%. We have implemented a work breakdown structure (WBS), which is the basis for the following more details on the cost estimate and schedule.

1. Fiscal Responsibilities

Table IV summarizes the mapping of the major construction tasks onto the proposed fiscal responsibility as discussed in the previous section. Completion of some of these tasks will require collaboration and expertise from institutions funded through the DOE as well as from foreign institutions. In order to proceed with the project in a timely manner and to bring technologies ready as soon as possible, R&D and prototype cycles for some of the major tasks have already been started based on institutional funding. For example, the first round prototyping of the pad-structured and pixilated strip sensors was funded jointly by UCR and BNL R&D funds and by RIKEN to advance with the project, while the fiscal responsibility will reside with the DOE (pad-structured sensors) and RIKEN (strip sensors).

2. Contingency Analysis

In order to estimate the necessary contingency we have taken the following approach:

- For all tasks that require the production of prototypes, contingency is taken to be 100% of the cost of one extra design plus prototype cycle.

- For all testing, assembly, and installation tasks, we assume that the contingency is 50% of the costs.
- For purchases based on vendor information, 25% of the cost is included as contingency.
- For all other purchases, the contingency is 50% of the costs.

3. Overhead Estimate

For the overhead we assume a 17.5% rate for MST at BNL as is the current practice for capital construction project at BNL, e.g. US-ATLAS at BNL. This 17.5% overhead is listed separately in our budget tables. Also listed as overhead are 9% for funds that are transferred from BNL to other institutions. The additional overhead charged by local institution is not listed separately. However, these costs are included in the budget tables. In particular, all manpower costs are fully burdened costs, including all overheads.

4. Budget

Table V summarizes the estimated costs for the NCC project and shows the split between the two funding agencies. For those items for which we seek funding through the DOE, a detailed cost-breakdown is given in Table VI.

B. Schedule

The following plots summarize the construction schedule to complete the NCC detector upgrade for PHENIX. The overall schedule is shown in Fig. 72. It assumes start of the DOE construction project in FY07. The schedule implies that construction dollars from RIKEN are available 2007 through 2009 and that the DOE construction funds become available in FY08.

Fig. 52 gives the funding profile for the DOE project. In this schedule the South Calorimeter in summer 2009 and the North Calorimeter in summer 2010. The proposed schedule assumes that $100k of R&D funds will be available from the DOE for the NCC project for FY06.

TABLE IV Map of construction tasks and WBS numbers onto the proposed fiscal responsibilities.

WBS	Construction Task	DOE	RIKEN
1.1	***NCC***		
1.1.1	***Design***	X	
1.1.2	***Prototyping***	X	X
1.1.3	**NCC South**		
1.1.3.1	***Calorimeter***		X
1.1.3.1.1	Absorber plates		X
1.1.3.1.2	Pad structured sensors		X
1.1.3.1.3	Carrier boards		X
1.1.3.1.4	Interconnect boards		X
1.1.3.1.5	Stock components (connectors etc)		X
1.1.3.1.6	Front-end modules		X
1.1.3.1.7	Support structure		X
1.1.3.2	***PS and SM layers***		
1.1.3.2.1	Strip sensors		X
1.1.3.2.2	Carrier boards		X
1.1.3.2.3	Hybrids		X
1.1.3.2.4	SVX4		X
1.1.3.2.5	Front-end modules		X
1.1.4	**NCC North**		
1.1.4.1	***Calorimeter***		
1.1.4.1.1	Absorber plates	X	
1.1.4.1.2	Pad structured sensors	X	
1.1.4.1.3	Carrier boards	X	
1.1.4.1.4	Interconnect boards	X	
1.1.4.1.5	Stock components (connectors etc)	X	
1.1.4.1.6	Front-end modules	X	
1.1.4.1.7	Support structure	X	
1.1.4.2	***PS and SM layers***		
1.1.4.2.1	Strip sensors	X	
1.1.4.2.2	Carrier boards	X	
1.1.4.2.3	Hybrids	X	

TABLE V Overview of the total estimated cost for the NCC project

WBS	**Name**	**DOE**	**RIKEN**	**Total**
1.1.1	Design	70 000		70,000
1.1.2	Prototyping	200 000	150 000	50,000
1.1.3	South Calorimeter		3 000 000	3,000,000
1.1.4	North Calorimeter	3 000 000	0	3 000 000
1.2	DAQ	400 000	0	400 000
1.3	ANCILLARY SYSTEMS & INTEGRATION	300 000	0	500 000
1	Total	3 970 000	3 150 000	7 120 000

References

Adcox, K., *et al.* (PHENIX), 2002, Phys. Rev. Lett. **88**, 022301.

Adcox, K., *et al.* (PHENIX), 2003, Phys. Lett. **B561**, 82.

Adler, S. S. (PHENIX), 2003, (to be published) eprint nucl-ex/0308006.

Adler, S. S., *et al.* (PHENIX), 2003a, Phys. Rev. Lett. **91**, 072303.

Adler, S. S., *et al.* (PHENIX), 2003b, Phys. Rev. Lett. **91**, 172301.

Adler, S. S., *et al.* (PHENIX), 2003c, Phys. Rev. Lett. **91**, 072301.

Baier, R., Y. L. Dokshitzer, A. H. Mueller, and D. Schiff, 1998, Phys. Rev. **C58**, 1706.

Baier, R., Y. L. Dokshitzer, S. Peigne, and D. Schiff, 1995, Phys. Lett. **B345**, 277.

Bjorken, J. D., 1982, fERMILAB-PUB-82-059-THY.

Gyulassy, M., P. Levai, and I. Vitev, 2000, Phys. Rev. Lett. **85**, 5535.

Gyulassy, M., P. Levai, and I. Vitev, 2001, Nucl. Phys. **B594**, 371.

Gyulassy, M., and M. Plumer, 1990, Phys. Lett. **B243**, 432.

Wang, E., and X.-N. Wang, 2002, Phys. Rev. Lett. **89**, 162301.

Wang, X.-N., and M. Gyulassy, 1992, Phys. Rev. Lett. **68**, 1480.

Wang, X.-N., M. Gyulassy, and M. Plumer, 1995, Phys. Rev. **D51**, 3436.

TABLE VI DUMMY Cost breakdown for tasks to be funded through the DOE. Tasks which do not show a cost correspond to deliverables for which the RIKEN Institute will take fiscal responsibility.

WBS	**Name DUMMY!!!!**	**Fixed Costs (Parts)**	**Labor**	**DOE Cor**
5.11.1.1	**STRIP**			
5.11.1.1.1	Strip ROC Card SVX4	235,000	307,000	542,000
5.11.1.1.2	Strip Sensor			
5.11.1.1.3	Integration of ROC Card & Sensor	0	23,000	23,000
5.11.1.1.4	Strip bus	20,000	80,000	100,000
5.11.1.1.5	Strip pilot	30,000	313,000	343,000
5.11.1.1.6	Assembly and Testing of Strip	220,000	120,000	340,000
5.11.1.1.7	Services, LV, racks etc	56,000	10,000	66,000
	Totals:	561,000	853,000	1,414,000
5.11.1.2	**PIXEL**			
5.11.1.2.1	Pixel Sensors			
5.11.1.2.2	Pixel ROC			
5.11.1.2.3	Pixel Hybrid			
5.11.1.2.4	Pixel Bus			
	Pixel Pilot FPGA	96,000	52,250	148,250
5.11.1.2.6	Pixel Systems Test (Hybrid+Pilot)			
5.11.1.2.7	Pixel FEM	63,000	77,000	140,000
5.11.1.2.8	Pixel Assembly and Test			
5.11.1.2.9	Services, LV, racks etc	40,000	0	40,000
	Totals:	199,000	129,250	328,250
5.11.2	**DAQ**			
5.11.2.1	Strip DCM	165,000	30,000	195,000
5.11.2.2	Pixel DCM	45,000	30,000	75,000
	Totals:	210,000	60,000	270,000
5.11.3	**ANCILLARY SYSTEMS & INTEGRATION**			
5.11.3.1	Specifications	0	67,500	67,500
5.11.3.2	Mechanical Structure	367,000	333,000	700,000
5.11.3.3	Infrastructure	90,000	550,000	640,000

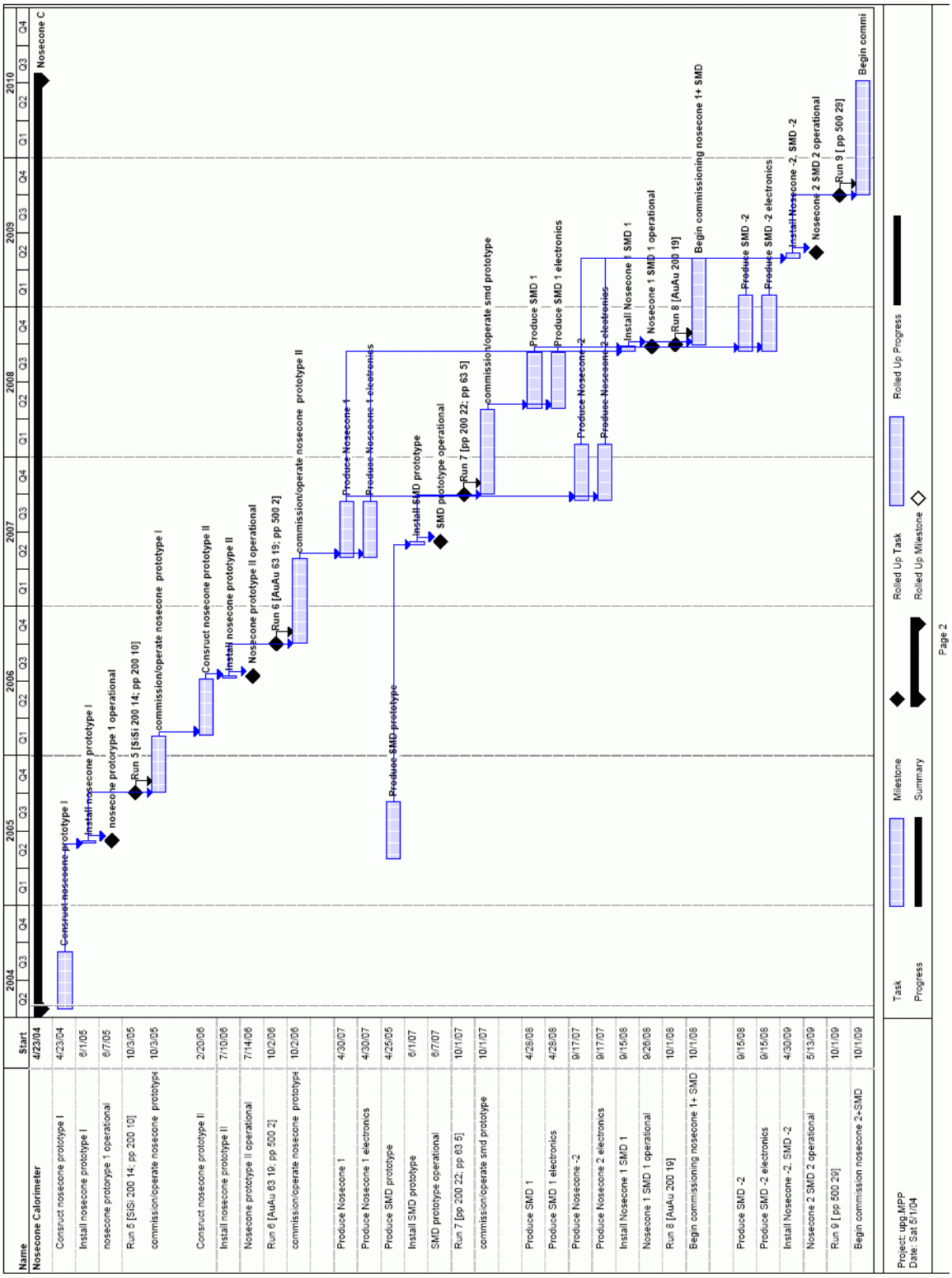

FIG. 72 The overall schedule for the NCC Project.

DUMMY

replace this

FIG. 73 The schedule for the South Forward Calorimeter DUMMY PICTURE

DUMMY

replace this

FIG. 75 The schedule for the auxiliary systems and infrastructure DUMMY FIGURE

DUMMY

replace this

FIG. 76 DOE budget profile for the NCC.

Outline Here is a general Outline. I will keep it up to date: RKS Nov 2

1. Executive Summary (RKS)
2. Physics Overview
   (a) Heavy Ion Physics
      i. Gamma-jet (John L-Stefane)
      ii. Chic (Jamie)
      iii. charm (Jamie)
   (b) pA collisions and the CGC (Jen-Chieh+R. Seto)
      i. direct photons
      ii. dileptons
      iii. hadrons
      iv. jets
   (c) Spin Structure of the nucleon
      i. Delta G Gamma-jet (Ken)
      ii. W (Mickey/Ken)
      iii. Transversity (Mickey)
   (d) Nucleon structure - probably same as the pA section (Jen-Chieh/Mark Strikman)
3. Physics Measurements with the NCC (RKS)
   (a) Performance
      i. pi^0
      ii. Photons
      iii. Electrons
      iv. Jets
   (b) Physics reach
      i. Heavy Ion Physics
      ii. Spin Structure

iii. Nucleon Structure

(c) Physics reach with the all Upgrades

4. The design of the NCC (EK)

(a) Overview

(b) The Calorimeter

(c) EM compartment

(d) Hadronic compartment

(e) Gamma π^0 detector

(f) Electronics

(g) Mechanics and Cooling

(h) Integration

(i) Triggering

5. R and D (EK)

6. Project Management and Responsibilities (RKS)

(a) Overview

(b) Management Structure

(c) Responsibilities

7. Budget and Schedule (RKS, EK)

(a) Total Estimated Cost (TEC)

(b) Contingency Analysis

(c) Overhead

(d) Budget

(e) Fiscal Responsibilities

(f) Schedule

8. Appendices

Folks who have agreed so far to be readers of various sections:

- Raju Venugopalan (pA - saturation)
- Ahbay - spin, and pA
- Ed Kinney - Spin
- Mark Strickman - nucleon strucutre
- Atsushi - lots of it (design etc)
- Matthias - lots of it.
- Ken -
-